AD_____

EERO TECHNICAL REPORT NO. 39

A REVISED EMPIRICAL APPROACH TO AIRBLAST PREDICTION

AD 742673

CHARLES M. SNELL

and

DENNIS L. OLTMANS

DDC
RECEIVED
MAY 31 1972
B

Reproduced by
NATIONAL TECHNICAL
INFORMATION SERVICE
Springfield, Va 22151

U. S. ARMY ENGINEER WATERWAYS EXPERIMENT STATION
EXPLOSIVE EXCAVATION RESEARCH OFFICE
Livermore, California

November 1971

Approved for public release; distribution unlimited.

Destroy this report when no longer needed.
Do not return it to the originator.

The findings in this report are not to be construed as an official Department of the Army position unless so designated by other authorized documents.

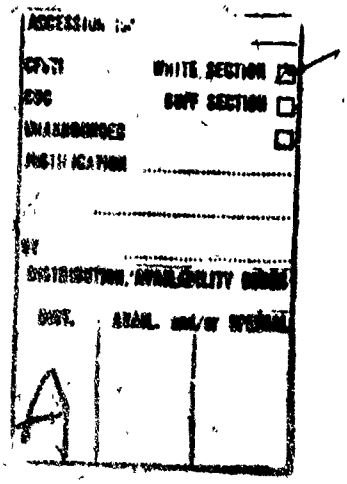

Printed in USA. Available from Defense Documentation Center,
Cameron Station, Alexandria, Virginia 22314 or
National Technical Information Service,
US Department of Commerce,
Springfield, Virginia 22151

Unclassified
Security Classification

DOCUMENT CONTROL DATA - R & D

(Security classification of title, body of abstract and indexing annotation must be entered when the overall report is classified)

1. ORIGINATING ACTIVITY (Corporate author) U. S. Army Engineer Waterways Experiment Station Explosive Excavation Research Office	2a. REPORT SECURITY CLASSIFICATION 2b. GROUP

3. REPORT TITLE

A Revised Empirical Approach to Airblast Prediction

4. DESCRIPTIVE NOTES (Type of report and inclusive dates)
Final Report

5. AUTHOR(S) (First name, middle initial, last name)

Charles M. Snell and Dennis L. Oltmans

6. REPORT DATE	7a. TOTAL NO. OF PAGES	7b. NO. OF REFS
November 1971	119	36

8a. CONTRACT OR GRANT NO. b. PROJECT NO. c. d.	9a. ORIGINATOR'S REPORT NUMBER(S) EERO/TR-39 9b. OTHER REPORT NO(S) (Any other numbers that may be assigned this report)

10. DISTRIBUTION STATEMENT

Approved for public release; distribution unlimited

11. SUPPLEMENTARY NOTES	12. SPONSORING MILITARY ACTIVITY

13. ABSTRACT

Airblast from buried chemical and nuclear detonations has been under systematic investigation for two decades. There now exists a sizable body of information collected during field experiments conducted over the years. The report contains a summary compilation of the available data for all significant large-yield events and synthesizes these data into an empirical prediction method.

Since the airblast from buried detonations approaches a consistent attenuation at the longer ranges of interest for safety predictions, a purely empirical "transmission factor" analysis based on consistent longer range data from subsurface detonations is used. Transmission factors are established as functions of scaled depth of burst for a variety of media and types of explosives. These are used to predict both ground-shock and gas-vent airblast from single- and row-charge detonations. A new approach to predicting the close range overpressures is also discussed. A summary of airblast from surface bursts is included.

The empirical prediction method presented is well-founded for those types of events which have been extensively investigated. Its chief weakness lies in the prediction of dissimilar events (different yields, explosive types, or media) for which there is insufficient data.

DD FORM 1 NOV 68 1473

Unclassified
Security Classification

Unclassified
Security Classification

14. KEY WORDS	LINK A		LINK B		LINK C	
	ROLE	WT	ROLE	WT	ROLE	WT
Airblast Overpressures						
Airblast Prediction						
U erground Explosions						
Explosive Excavation						
Explosive Engineering						

Security Classification

TID-4500, UC-35

EERO TECHNICAL REPORT NO. 39
A REVISED EMPIRICAL APPROACH TO AIRBLAST PREDICTION

CHARLES M. SNELL
and
DENNIS L. OLTMANS

U. S. ARMY ENGINEER WATERWAYS EXPERIMENT STATION
EXPLOSIVE EXCAVATION RESEARCH OFFICE
Livermore, California

MS. date: November 1971

Foreword

The Explosive Excavation Research Office is embarked on a program of research in topical areas critical to the overall technology titled "explosive excavation." Some of these topical areas relate to the prediction of safety-related effects. This work was funded by the Office of the Chief of Engineers (OCE), appropriation 96X3121, General Investigations. Effort is being expended in these areas to review all pertinent measured data and all current prediction methods in use, and to make an attempt to advance the state-of-the-art. This report and a companion report, EERO TR-40, "Prediction of Ground-Shock-Induced Airblast Overpressures for Subsurface Explosions From Peak Vertical Spall Velocity," provide the basis for, and present improved methods of, making airblast overpressure predictions for surface and underground chemical and nuclear detonations. Critical review and comment are invited. An additional report, EERO TR-7, in preparation, will develop a simplified prediction system which integrates and is based on the systems presented in this report, EERO TR-39, and its companion report, EERO TR-40.

Abstract

Airblast from buried chemical and nuclear detonations has been under systematic investigation for two decades. There now exists a sizable body of information collected during field experiments conducted over the years. The report contains a summary compilation of the available data for all significant large-yield events and synthesizes these data into an empirical prediction method.

Since the airblast from buried detonations approaches a consistent attenuation at the longer ranges of interest for safety predictions, a purely empirical "transmission factor" analysis based on consistent longer range data from subsurface detonations is used. Transmission factors are established as functions of scaled depth of burst for a variety of media and types of explosives. These are used to predict both ground-shock and gas-vent airblast from single- and row-charge detonations. A new approach to predicting the close range overpressures is also discussed. A summary of airblast from surface bursts is included.

The empirical prediction method presented is well-founded for those types of events which have been extensively investigated. Its chief weakness lies in the prediction of dissimilar events (different yields, explosive types, or media) for which there are insufficient data.

Acknowledgments

Grateful acknowledgment is expressed to L. J. Vortman and J. W. Reed of the Sandia Laboratories who have recorded and published the major portion of the airblast data available on underground nuclear and chemical explosive detonations. Parts of this report are derived from their work. We also wish to thank D. N. Montan, Lawrence Livermore Laboratory, for providing otherwise unavailable data.

The authors wish to acknowledge the assistance provided by Edward J. Leahy, who offered many helpful comments and suggestions. Appreciation is expressed to Mrs. Helen Sarles for long and faithful work in typing and retyping various parts of this report.

The Directors of the Explosive Excavation Research Office during the preparation of this report were COL William E. Vandenberg and LTC Robert L. LaFrenz. Mr. Walter Day was Deputy Director (Civil Program).

Contents

FIGURES

FIGURES (continued)

TABLES

TABLES

TABLES

Nomenclature

DOB = Depth of burst of a given experiment (in ft)

dob = Scaled depth of burst of a given experiment (in $ft/kt^{1/3}$)

f_{max} = Maximum value of transmission factor at any range for a given experiment; f_{max} may be the maximum value of $f(R_s)$ justifiable on the basis of a best fit to the scaled observed overpressures, or it may be the largest value of f for any scaled observed point.

$f(R_s)$ = Transmission factor at a given scaled range; the ratio of the scaled overpressure at the range R_s to the standard $R_s^{-1.2}$ line overpressure at that range:

$$f(R_s) = \frac{\Delta P_s \text{ (observed, scaled overpressure at } R_s)}{\Delta P_s \text{ (standard } R_s^{-1.2} \text{ line at } R_s)}$$

n = Number of charges in a row or square array

P_0 = Approximate ambient pressure for a given experiment (in mbar)

ΔP = True overpressure at a given range (in mbar or psi)

ΔP_s = Scaled overpressure, scaled to an ambient pressure of 1000 mbar (in mbar)

R = True range from surface ground zero (in ft)

R_s = Scaled range from surface ground zero, scaled to a yield of 1.0 kt and a pressure of 1000 mbar (in $ft/kt^{1/3}$)

$R_s^{-1.2}$ Line = The standard overpressure line; a straight line in a log-log plot of ΔP_s vs R_s, of the slope of $R_s^{-1.2}$, passing through the point R_s = 9000 $ft/kt^{1/3}$, ΔP_s = 25.5 mbar

S = Scaled spacing between charges in a row or array

$$\frac{\text{Spacing in ft}}{[\text{W of a single charge (in kt)}]^{1/3}} \text{ (in } ft/kt^{1/3})$$

$\underline{S}$ = Slant range from the explosion point to a point at the ground surface (in ft)

SGZ = Surface Ground Zero, location of the ground surface directly above shot point

W = Total yield of a single-charge detonation (in kt)

EERO TECHNICAL REPORT NO. 39
A REVISED EMPIRICAL APPROACH TO AIRBLAST PREDICTION

Section 1

Introduction

PURPOSE

Airblast overpressures from the use of buried explosives for excavation purposes can cause structural damage at close-in ranges and window pane damage for a considerable distance from a detonation. To evaluate the safety aspects of a proposed detonation, predictions of airblast overpressures as a function of range from the detonation area must be made. It is the purpose of this report to develop and to demonstrate an empirical technique for predicting airblast overpressures based on all currently available experimental data for large-yield events.

PRINCIPAL AIRBLAST CONSTITUENTS

Studies have shown that airblast from buried charges has two principal constituents: the ground-shock-induced overpressure pulse, and the gas-vent-induced pulse. The larger of these two pulses will determine the peak (maximum) airblast overpressure, which is the damage mechanism of interest. The gas-vent pulse is always dominant at shallow depths of burial, but the ground-shock pulse is often larger for deeply buried events, particularly those in strong rock or saturated media. The two pulses arise from quite different physical mechanisms. Ground-shock overpressure results from what is called the ground-piston effect; the rising surface of the earth mound above the explosion point directly pulses the overlying air. This pulse travels outward in all directions, transmitted with the sonic velocity in air. The amplitude of the ground-shock-induced pulse is determined by the peak vertical spall velocity of the rising mound. The gas-vent pulse is produced much later in the explosion history. As the mound grows and finally begins to break up, the gas bubble in the explosion cavity vents to the surrounding atmosphere. Venting usually occurs at many points near the crown of the mound. The excess pressure of the gas bubble is quickly relieved, producing a strong venting pulse. If the explosion is completely contained, or if the gas bubble has dropped to ambient pressure before venting occurs, no gas-vent pulse will be observed. The gas-vent pulse will dominate for near-surface detonations, but it is quickly suppressed with increasing depth of burial. The gas-vent pulse is comparatively weak for nuclear detonations in strong dry rock, and when the

depth of burst is selected to maximize crater dimensions (optimum depth) the ground-shock pulse will usually be larger.

The physical mechanisms involved for nuclear detonations in media with moisture content appreciably exceeding 1% by weight are somewhat more complex. These detonations vaporize much water and produce higher pressures during the cavity history. As a result, gas-vent overpressure is usually dominant for such nuclear detonations, at least from the surface to optimum depth of burst.

SECONDARY AIRBLAST CONSTITUENTS

In addition to the primary blast wave constituents, there may be additional pulses of lower amplitude. The earliest arriving is the ground-transmitted ground-shock-induced pulse (as opposed to the air-transmitted pulse, above). This pulse is due to the direct coupling between the vertical ground motion at a point and the overlying air. It is transmitted with sonic velocity in the medium, and drops off rapidly away from surface ground zero (SGZ). The high rate of attenuation is due to the rapid decrease of vertical ground velocity away from SGZ. It has been shown that the vertical component of ground surface velocity decreases as $\underline{S}^{-2}$ or faster, where $\underline{S}$ is the true slant range from the shot point to the point on the ground surface. Obviously, the ground-transmitted pulse will be observable only by the closest airblast measurement gages. It cannot be clearly identified beyond about two crater radii. For example, with gage records from the Cabriolet nuclear experiment[1] which gave accurate pulse arrival times, it was possible to calculate transmission velocities and thus distinguish air transmission from ground transmission. It was found that ground-transmitted pulse arrivals disappeared by a range of 375 ft from SGZ. This distance corresponded to 2.1 crater radii, or 2.2 times the depth of burst.

As the ground-transmitted pulse fades, another early-arriving pressure increase begins to appear. This is the surface Rayleigh-wave-induced pulse. The Rayleigh wave is propagated along the surface with a mean velocity slower than the sonic velocity in the medium, but faster than that in air. Its associated vertical component of ground motion also gives rise to an overpressure pulse. The pressure peaks in the Rayleigh wave train often attenuate more slowly than $\underline{S}^{-2}$.

After the domina t ground-shock and gas-vent pulses, there are characteristic negative excursions of overpressure (i.e., the overpressure, ΔP, temporarily

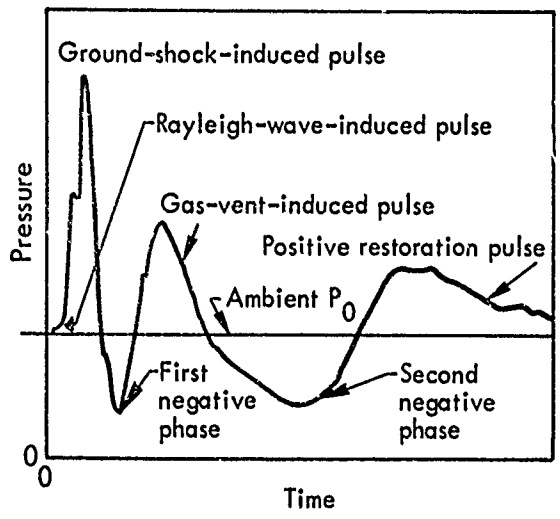

Fig. 1. Tracing showing a typical intermediate-range airblast overpressure pulse for a kiloton-size nuclear device at optimum depth of burst in strong dry rock.

decreases below ambient pressure). These negative excursions are usually smaller in amplitude than the preceding positive pulse and longer in duration. They tend to have smooth contours without sharp peaks. The negative excursion after the ground-shock pulse may be prematurely terminated by the gas-vent pulse arrival.

An additional positive pulse is commonly observed after the last negative phase. This pulse is attributed to air rushing back to restore the atmosphere to ambient conditions and temporarily overshooting the ambient pressure.

All the above pulses are of smaller amplitude than the dominant gas-vent and ground-shock components. They are primarily of academic interest and not important to airblast safety considerations, but they will often be observed on airblast overpressure tracings. Figure 1 summarizes the appearance of an overpressure tracing for a typical nuclear cratering event in strong dry rock.

Section 2
Rationale of the Method

PRESENT PREDICTION METHODS

One way to study and to predict the airblast from a buried detonation is to compare it with overpressures produced by surface or free-air detonations. Popular analogs for comparison have included the IBM Problem M free-airburst calculation, the Kirkwood-Brinkley TNT surface burst curves, and the measured overpressure from actual surface burst experiments. The "transmission factor" or "suppression factor" can be easily calculated by comparing airblast from a buried detonation to the surface burst airblast at the same scaled range. The empirical transmission factor thus determined is a function of explosive type, medium, and scaled depth of burst. It may be conveniently used to predict airblast from future detonations under similar conditions.

The empirical approach described above is predicated on the assumption that a subsurface burst produces exactly the same effects as a surface burst of somewhat smaller yield. As Montan[2] has pointed out, this is a dangerous assumption. The physical mechanisms which transfer energy at the detonation

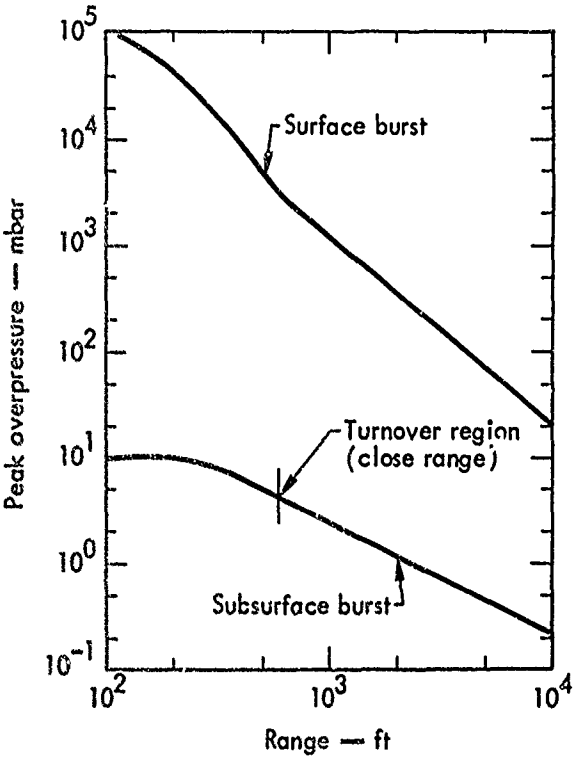

Fig. 2. Comparison of airblast overpressure as a function of range for 1.0-kt surface and subsurface detonations.

front into an airblast overpressure pulse differ greatly between surface and buried detonations. Facilely drawing a direct analogy between the two is difficult to justify. The overpressures produced by surface and subsurface bursts are indeed quite dissimilar at close ranges, as will be seen in Section 6. However, as one moves farther away, the detonation begins to look more like a simple acoustic point source of overpressure. Pressure contours assume a hemispherical "dome" shape and begin to follow near-acoustic propagation. Thus, there is some basis for comparing airblast at these long ranges, even though the sources are different. Figure 2 shows a comparative plot of overpressure as a function of range for a typical surface burst and a buried detonation.

REVISED EMPIRICAL PREDICTION METHOD

The revised method is a modification of present prediction techniques. The principal changes are: (1) a range-dependent transmission factor, $f(R_s)$, which is used for prediction of close-in airblast overpressures; (2) a maximum transmission factor, f_{max}, which is used to predict airblast overpressures beyond the range at which overpressure begins to propagate at a constant attenuation rate; and (3) both transmission factors are determined as ratios with respect to a standard $R_s^{-1.2}$ line, having an attenuation rate of $R_s^{-1.2}$ and passing through a point at $R_s = 9000$ ft/kt$^{1/3}$ where the overpressure, ΔP_s, is 25.5 mbar (all overpressures scaled to an ambient air pressure of 1000 mbar).

Both the range-dependent transmission factor, $f(R_s)$, and the maximum transmission factor, f_{max}, are derived from past experiments conducted with large-yield chemical and nuclear explosives. The range-dependent "f" is similar to the transmission factors currently in use, but it is taken relative to the $R_s^{-1.2}$ standard line:

$$f(R_s) = \frac{\Delta P_s \text{ (overpressure, buried event)}}{\Delta P_s \text{ (standard } R_s^{-1.2} \text{ line overpressure)}},$$

where all quantities are scaled to 1.0 kt at standard 1000-mbar pressure, and where both of the ΔP_s values are at the same scaled range R_s. The "maximum" transmission factor is determined at some range where the ΔP_s vs R_s plot has converged on a slope of $R_s^{-1.2}$. Beyond this range, the observed overpressures should parallel the $R_s^{-1.2}$ standard line, and the transmission factor should remain constant.

The maximum transmission factor, f_{max}, is then the largest value of $f(R_s)$ which can be reasonably justified on the basis of all observations for a given experiment. It may be the largest f-value indicated by a fitted line through all the observed points, or it may be the largest f-value for any of the individual observed points (some of the experiments had so few measurements that a fitted line was not justified).

The use of the standard $R_s^{-1.2}$ line for overpressure prediction has one important advantage over the use of the IBM Problem M curve or a surface burst curve. When the standard $R_s^{-1.2}$ line is

multiplied by the f_{max} for a specific situation and all quantities are properly scaled, a new $R^{-1.2}$ line will be obtained. This new line will give the correct overpressure at the range for which f_{max} was determined. It will overpredict at all closer ranges (where the true $f(R_s)$ is smaller), and will continue to predict correctly beyond the point at which f_{max} is determined if the propagated overpressure decays as $R^{-1.2}$.

BASIS FOR REVISED PREDICTION METHOD

Note that the use of "f" as a means of making predictions is not founded on assumed physical similarity between surface bursts and buried detonations. It is an empirical factor established from experimental measurements which will produce the desired results. The use of f_{max} is justified as long as two assumptions hold true: (1) the ΔP (buried detonation) curve becomes parallel to its comparison curve beyond some determinable scaled range; (2) the f-function is a unique-valued function of scaled depth of burst (dob) or some similar scaling dimension for all comparable experiments (same medium, explosive, and ambient propagation conditions).

The latter of the above two assumptions contains all physical complexities which an empirical approach does not fully analyze. The fraction of energy which finds its way into the distant shock wave hemisphere depends on the detailed manner in which energy transfer occurs. Even for a given set of physical conditions (given type of explosive charge and medium), the transfer process may be a complicated function of event geometry; i.e., a function of one or more dimensions of the system. Assumption (2) is equivalent to stating that the f-function, no matter how complex the physical processes which control it, must be directly related to some simple physical dimension of the system. This dimension must scale in a consistent way with yield. Any other geometrical parameters of the system which affect the transfer of energy must scale in the same way. The weakness of this basis is probably responsible for the few breakdowns of empirical prediction. In particular, gas-vent overpressures for large nuclear experiments may prove difficult to predict through the empirical approach. These overpressures may depend on physical parameters for which simple scaling does not apply: gravity and overburden effects which do not scale directly with yield, the time scale of gas bubble events, the cavity size history, and probably the cavity pressure history (time-dependent equation of state of the gas bubble). The latter parameter is also affected by medium moisture content and the resultant pressure boosting due to steam production. Empirical prediction of large nuclear events is rendered even more unsatisfactory by the paucity of data. A brief examination of such events is given in Appendix A.

Aside from this single shortcoming, the empirical method shows promise for predicting airblast overpressures from single-charge detonations. Row charges are discussed in Sections 7 and 8 and Appendix B. Successful application hinges on the answers to two questions: (1) At what scaled ranges do the ΔP curves for buried detonations become

substantially parallel to the standard $R_s^{-1.2}$ line? and (2) Are there sufficient data to determine the transmission factors for all cases of interest? These questions are discussed in the following paragraphs of this section. The experimental data to support the discussion are presented in subsequent sections of the report.

Most large-yield experiments have overpressure tracings which extend to a maximum range of 2000 to 20,000 scaled feet ($ft/kt^{1/3}$). Most of the well-observed nuclear experiments have data to at least 5000 scaled feet. These observations form a reasonably homogeneous body of data on which to base conclusions about the attenuation rate of overpressure. A log-log plot of ΔP vs scaled range shows that most of the overpressure curves have become straight lines by a range of 3000 $ft/kt^{1/3}$. The attenuation rates have converged on a value which should be valid at intermediate-to-long ranges. For the best observed recent nuclear experiments, a remarkably consistent attenuation rate of $R^{-1.2}$ is found. For ground-shock-induced overpressures, this rate seems to hold true beyond a range of 300 scaled feet (300 $ft/kt^{1/3}$). The situation with gas-vent overpressures is somewhat less clear, and the $R^{-1.2}$ attenuation rate does not hold until the range exceeds 400 to 1000 $ft/kt^{1/3}$. Close-in overpressures are comparatively small and would cause a fitted straight line to be too shallow (i.e., they would weight the line toward a slower attenuation rate). It is important to note that the intermediate range nuclear overpressure data are the best in existence—the accuracy is high, gage calibration is well-established at all ranges, and the data points for each experiment show very little scatter. In addition, the ground-shock pulse is the initial strong pulse and is dominant in most of these cases. For these reasons, the authors consider nuclear ground-shock-induced peak overpressures to be the best-established type of measurement, and thus the most accurate indicator of intermediate-range attenuation. Since these data indicate an attenuation rate of $R^{-1.2}$, the $R_s^{-1.2}$ standard line was selected for the empirical prediction method.

The chemical explosives data reveal a less encouraging picture in regard to attenuation rate. Several experiments[3-5] are consistent with an attenuation rate of $R^{-1.0}$. In some cases, the attenuation rate appears to be increasing slowly, even at scaled ranges $\approx$2000 to 3000 scaled feet ($ft/kt^{1/3}$). A rate of $R^{-1.2}$ is probably satisfactory at the outer limit of the measured points. The manner in which measured points converge on a slope of $R^{-1.2}$ is best seen in Fig. 3. This figure shows measured points for gas-vent and ground-shock overpressures, compared to prediction lines ($R^{-1.2}$ attenuation). The points seem to be converging fairly well on the prediction lines, as indicated. (Note that the figure is plotted in terms of true range R, not scaled range.)

Thus, an overpressure attenuation rate of $R^{-1.2}$ is compatible with the best available data. This rate appears reasonable, as will be seen in subsequent sections, for observed nuclear ground-shock overpressures (beyond 300 $ft/kt^{1/3}$), nuclear gas-vent overpressures (beyond

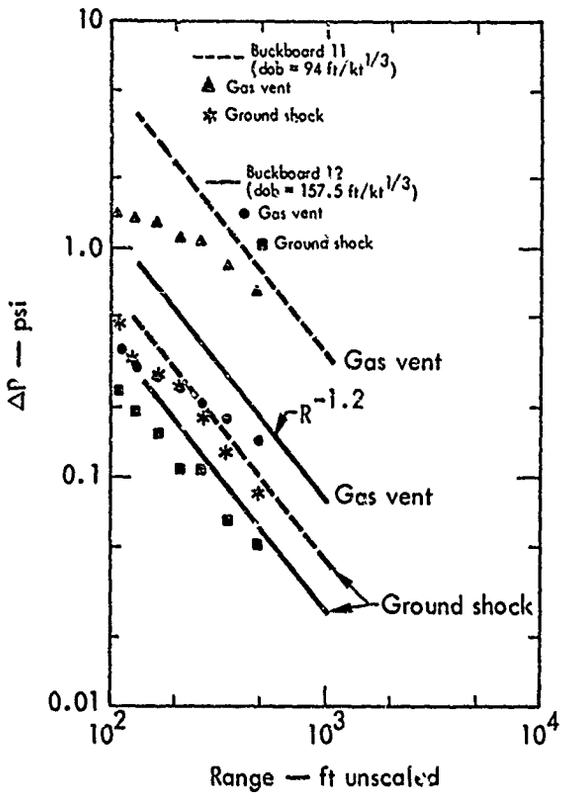

Fig. 3. Observed airblast overpressures compared to $R^{-1.2}$ lines, Buckboard 11 and 12—both 20-ton TNT detonations in basalt (Ref. 4).

400 to 1000 ft/kt$^{1/3}$), and chemical explosive overpressures (beyond relatively larger scaled ranges, sometimes as great as 2000 ft/kt$^{1/3}$).

By coincidence, the IBM Problem M line also has a slope close to $R^{-1.2}$ at 9000 scaled feet (it does not approach an $R^{-1.2}$ slope at closer ranges because of the relatively high nonacoustic close-in overpressures for a free-air burst). The IBM Problem M curve and the standard line used for this prediction system are identical at a scaled range of 9000 ft/kt$^{1/3}$, both in slope ($R^{-1.2}$) and in overpressure ($\Delta P = 25.5$ mbar for an ambient air pressure of 1000 mbar).

Table 1 presents a tabulation of overpressures at various ranges for the standard line. Comparable values for the IBM Problem M curve are discussed in Section 9 (surface and free-air bursts) and are listed in Appendix C.* For a scaled range not given in Table 1, the overpressure value on the standard $R_s^{-1.2}$ line may be calculated by:

$$\Delta P_{s_i}\,(\text{mbar}) = \Delta P_s \left(\frac{R_s}{R_{s_i}}\right)^{1.2},$$

Table 1. Approximate values of standard line overpressure ΔP_s as a function of scaled range R_s, assuming line of slope $R_s^{-1.2}$ through $\Delta P_s = 25.5$ mbar at $R_s = 9000$ ft/kt$^{1/3}$.

R_s(ft/kt$^{1/3}$)	ΔP_s(mbar)
10	89,500
30	24,000
80	7,400
100	5,650
300	1,510
400	1,070
500	816
600	658
700	546
1,000	357
1,500	219
2,000	155
3,000	95.4
5,000	51.6
6,000	41.5
8,000	29.4
10,000	22.5
15,000	13.8
20,000	9.8
9,000	25.5

*Table C31.

where ΔP_{s_i} and R_{s_i} are standard overpressure and range values at a point of interest and ΔP_s and R_s are standard overpressure and range values from the table.

Field measurements are expected to deviate from $R^{-1.2}$ attenuation. Thus, before examining the experimental data and applying the prediction method, some of the factors which cause attenuation to differ from $R^{-1.2}$ will be discussed. Several nonrepeatable effects may influence experimental airblast measurements[6]: (1) Winds may blow towards or away from the gage location (winds blowing from the gage toward SGZ reduce the overpressure). (2) Vertical meteorology, such as strong temperature gradients or inversions, may influence even close-in observations (overpressures are usually reduced if the temperature decreases with altitude; inversions or increasing temperature may increase the overpressure). (3) Gage response may be overranged or gages may be poorly calibrated at close-in distances. (4) Rounded wave crests may tend to shock up to a relatively higher peak overpressure at long ranges. Other factors, mentioned in the remainder of this paragraph, are common to all experiments, and are systematically discussed later in this paper. (5) The gas-vent pulse, which usually originates near the crest of the mound, is subject to mound shielding and diffraction down the sides of the mound. In other words, the close-in gages are relatively farther from the pulse source (mound crest), and the geometry of the situation tends to direct the pulse upward, away from the close-in gages. Thus, these gages "see" lower gas-vent overpressures than they otherwise would. (6) The ground-shock overpressures fall below the expected $R^{-1.2}$ line inside the radius of appreciable mound motion. This is because the more distant gages measure an overpressure pulse due to the combined effect of the entire rising mound, whereas the close gages resolve only the overpressure due to a small segment of the rising mound (the local or ground-transmitted pulse). The pulses from other parts of the mound arrive too late to combine with this initial pulse. This decline below expected ΔP's occurs only at very close ranges (inside the range of the ground-piston effect or range of appreciable surface motion). Normally, this region should not extend beyond $\approx$2 crater radii. There is, of course, a transition region between the ground-transmitted local pulse and the normal air-transmitted ground-shock-induced pulse. (7) One additional effect is observed only for row charges. At close ranges, the shock fronts from individual charges tend to arrive at different times; thus, the individual overpressure peaks do not combine (acoustic addition) as might be expected. Peak overpressure is considerably lower than would be predicted on the basis of adding the overpressures from each individual charge in the row. At longer ranges, however, the time separation between peaks is less, and the peaks begin to merge. Finally, the arrivals will be almost simultaneous, and the row will begin to look like a point source. This effect causes a low apparent attenuation rate close to the row (because the peaks continue to merge as range increases, gradually increasing the amount of energy in the peak overpressure front).

The peaks will ultimately attain a stable, semicombined waveform, and the attenuation rate will converge on the expected attenuation for a normal single-charge source. The overpressure peaks from small-charge row experiments combine efficiently at close ranges. However, the combination process may be slower and less efficient in the case of row experiments with large or widely separated charges. Indeed, the overpressure peaks achieve a stable form and airblast converges on normal $R^{-1.2}$ behavior only at the outer limit of available gage measurements. Therefore, to compare the overpressure from large-charge rows with standard single-charge overpressures, the most distant gage measurements must be used. Close-in overpressures might give a correct comparison at close ranges, but would underpredict further out (due to the lower attenuation rate for row charges). A detailed comparison of row-charge and single-charge overpressures is discussed in Section 7. Row-charge predictions are covered in Section 8 and Appendix B.

Section 3
Experimental Data

DATA SELECTION

In order to empirically predict overpressures, the results of past experiments must be analyzed. A transmission factor is wanted which will safely predict overpressures at all ranges relative to the $R_s^{-1.2}$ line. Therefore, the major problem concerns proper choice of data for the study of f_{max}. The range of interest in predicting for chemical explosive detonations is between 1 and 1000 tons.[7] For nuclear excavation, the interest extends to several megatons but available data limits the investigation to yields of 0.05 to 100 kt. The most relevant data obviously derive from tests in these yield ranges. Considerable information is also available from smaller chemical explosive experiments, 64 lb to 1 ton. Unfortunately, the results do not correlate well with large-yield shots. Small explosive charges frequently show nonrepeatable effects and differences due to small-scale local meteorology. In addition, there are problems with nonscaling over the rather large differences of yield. Since this is an empirical study, it has been decided to utilize larger yields (in the range of interest) for determining f_{max}. A comparison with Vortman's results (Ref. 1 and others) which emphasize small-charge experiments is also included. The section on row detonations uses small-charge experiments as a matter of necessity, as they comprise much of the available data. Certain dangers inherent in the approach are pointed out in Section 7.

TABULATION AND PLOTS OF DATA

Part of the purpose of this report is to compile a master list of available data on large-yield experiments. Each experiment has been scaled to a standard yield and ambient pressure for uniform comparison with the standard $R_s^{-1.2}$ line. Since previous investigators have scaled to a yield of 1.0 kt at an ambient pressure of 1000 mbar, these values will be used.

The scaling equations,[7] derived from Sachs energy scaling, follow:

Scaled ΔP_s:
(units: mbar)

$$\Delta P_s = \Delta P \frac{P_{standard}}{P_0} = \Delta P \frac{1000}{P_0},$$

where

ΔP = observed experimental overpressure (mbar)

$P_{standard}$ = standard ambient pressure = 1000 mbar

P_0 = observed experimental ambient pressure (mbar), obtained from meteorological data.

Scaled Range R_s:
(units: $ft/kt^{1/3}$)

$$R_s = R \left(\frac{W_{standard} \times P_0}{W \times P_{standard}} \right)^{1/3}$$

$$= R \left(\frac{1.0 \text{ kt} \times P_0}{W \times 1000} \right)^{1/3},$$

where

R = true range to the observed experimental overpressure = distance of gage from SGZ (in ft).

$W_{standard}$ = standard reference yield = 1.0 kt.

W = single-charge yield of the experimental detonation (in kt).

The data reduction procedure is as follows: first, the observed data points for each experiment are tabulated. Then these points are scaled to a yield of 1.0 kt at ambient pressure = 1000 mbar. The scaled values are plotted in log-log diagrams of ΔP_s vs R_s. If justified, a fitted curve is drawn through these points for each experiment. The f-value at any scaled range may then be calculated:

$$f(R_s) = \frac{\Delta P_s \text{ (fitted curve at } R_s)}{\Delta P_s \text{ (standard } R_s^{-1.2} \text{ line at } R_s)}.$$

Normally, f-values are calculated for several selected R_s values; each ΔP_s is read directly from the fitted curve. The largest of the tabulated f-values is f_{max}.

The original overpressure data derive from a number of different sources, as listed in the references. Most of these overpressures are final tabulated values given by the authors, but in some cases, early "unsmoothed" values have been used. In a few instances, the original tracings have been reduced. Several recent experiments have two (or more) measurements at each gage station. Either the mean values for the gages at each location or weighted mean values emphasizing the more sensitive gage or just the value from the more sensitive gage have been used (depending on the relative accuracy of the various results). A few questionable values have been rejected, but only in cases where there was ample reason for rejection. The measurements are tabulated in the following standard format (see Table 2 for sample table): at the top of the page, the name of the experiment is given, followed by yield (in kt or tons), explosive type, medium, moisture content by weight of the medium,* literature reference, depth of burst (in ft), scaled depth of burst ($ft/kt^{1/3}$), ambient pressure P_0 near SGZ (in mbar), and other notes of interest.

*Moisture content is classified as follows: Dry = water content less than or equal to 3% by weight for rock or 10% for soil. Wet = water content greater than the above values. Saturated = more than 90% of void space in the medium filled with water.

Table 2. Palanquin, 4.3-kt nuclear, rhyolite, dry (Ref. 8, 9).

DOB = 280 ft dob = 172.2 ft/kt$^{1/3}$ P_0 = 850 mbar

Observed data		Observed data scaled to 1.0 kt at P_0 = 1000 mbar		Data from fitted curve			
Distance (ft)	ΔP (psi)	$R_s\left(\frac{ft}{kt^{1/3}}\right)$	ΔP_s (mbar)	$R_s\left(\frac{ft}{kt^{1/3}}\right)$	ΔP_s (mbar)	$f(R_s)$	f/f_{max}
			A. Ground Shock				
21	0.62-0.74[a]	12.2	50.3-60	20	51	0.00133	0.195
328	0.248	191	20.1	80	29.1	0.00393	0.575
705	0.087	410	7.06	100	25.1	0.00445	0.651
1575	0.0193	917	1.567	200	14.6	0.00597	0.872
3280	0.0079	1910	0.642	300	19.9	0.00656	0.96
7380	0.0053	4295	0.4305	600	4.5	0.00684	1.0
				1500	2.36	0.00661	0.966
				5000	0.341	0.00661	0.966
			B. Gas Vent[b]				
328	0.073	191	5.93	200	5.55	0.00227	0.376
705	0.0307	410	2.49	300	3.60	0.00238	0.394
1575	0.0162	917	1.315	600	1.94	0.00295	0.489
3280	0.0049	1910	0.398	1000	1.24	0.00348	0.577
7380	0.0046	4295	0.3735	2000	0.68	0.00439	0.727
				5000	0.312	0.00603	1.0

[a]True ground-shock overpressure at 21 ft from SGZ; a later overpressure of 5.52 psi was observed at a time corresponding to an anomalous gas vent through a pipe near SGZ.

[b]Superimposed on negative phase.

The scaled depth of burst is calculated from:

$$dob = \frac{DOB\ (in\ ft)}{[Yield\ W\ (in\ kt)]^{1/3}}.$$

The table itself is divided horizontally into three sections. The first section lists the observed (unscaled) data points: first, the distance from SGZ, which is represented by R (in ft); then, the observed overpressure ΔP (in mbar or psi). The next section lists these data points scaled to 1.0 kt at 1000 mbar (R_s in ft/kt$^{1/3}$, ΔP_s in mbar). The third section gives points read from a fitted line through the scaled data. These fitted points are read off at even scaled ranges for convenience. The value of $f(R_s)$ at each fitted point is listed. In a few experiments, the ratio of $f(R_s)/f_{max}$ is tabulated, and this ratio will be discussed in Section 6. Note that the ground-shock and gas-vent overpressures are listed separately in each table.

The compilation for all large-yield experiments is given in Appendix C

(Tables C1 through C30) for convenient reference. Buried detonations, both nuclear and conventional, are listed in Tables C1 through C25. Tables C26 through C30 include a few surface bursts for use in surface event predictions (see Section 9).

For several experiments, the number of data points available is quite small. A fitted line was not considered justified in some of these cases. Therefore, there is no third section to the table; f-values are calculated for the individual scaled data points (not for a fitted line), and are listed in the second section of the table. Teapot ESS provides an example of such an experiment (see sample, Table 3). The largest of the data point f-values is accepted as an estimate of f_{max}. The f_{max} values thus obtained are approximate at best, and may apply only at scaled ranges close to the data point used.

There are other irregularities in a few of the tables. Sulky gas-vent overpressures, Table C1, are given as a range of uncertainty in some of the ΔP and f values. Scooter, Table C11, and Pre-Schooner II, Table C12, give additional data from aerial high-angle gages. Pre-Schooner II also gives θ, the angle from the vertical to the high-angle gage. The row-charge experiments (Dugout, Table C5, Buggy, Table C6, and Pre-Gondola II, Table C20, and III, Table C19) have all of the usual information, plus a conversion of f or of f_{max} to equivalent single-charge values (see Section 7).

Figures 4 to 11 show some of the scaled overpressure diagrams from which the fitted lines were derived. Figure 4 shows a plot of ΔP_s vs R_s for two typical nuclear experiments. Figures 5 to 11 are similar plots for nine chemical explosive experiments. All diagrams include the fitted lines and are scaled to 1.0-kt yield at an ambient pressure of 1000 mbar. Figure 12 shows a typical plot of $f(R_s)$ vs scaled range R_s, and the points at which f_{max} for ground-shock-induced and gas-vent overpressures were selected.

Table 3. Teapot ESS, 1.2-kt nuclear, alluvium, dry (Ref.10).
DOB = 67 ft dob = 63 ft/kt$^{1/3}$ P_0 = 860 mbar

Observed data		Observed data scaled to 1.0 kt at P_0 = 1000 mbar		
Distance (ft)	ΔP (psi)	$R_s\left(\frac{ft}{kt^{1/3}}\right)$	ΔP_s (mbar)	$f(R_s)$
		A. Ground Shock		
250	0.7 ?	224	56.2	0.0261
300	0.52 ?	268	41.7	0.0240
		B. Gas Vent		
250	14.4	224	1155	0.536
300	14.1	268	1131	0.652
400	11.3	358	907	0.740
600	6.14	537	493	0.653

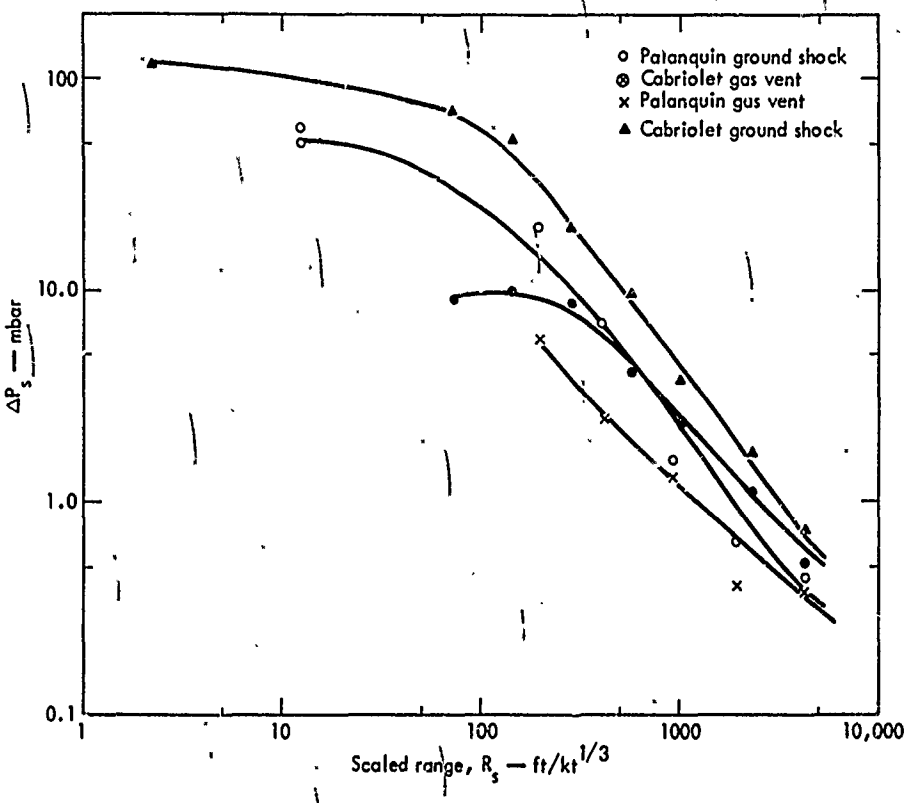

Fig. 4. Palanquin and Cabriolet (nuclear) observed overpressures (scaled to 1.0 kt at 1000 mbar).

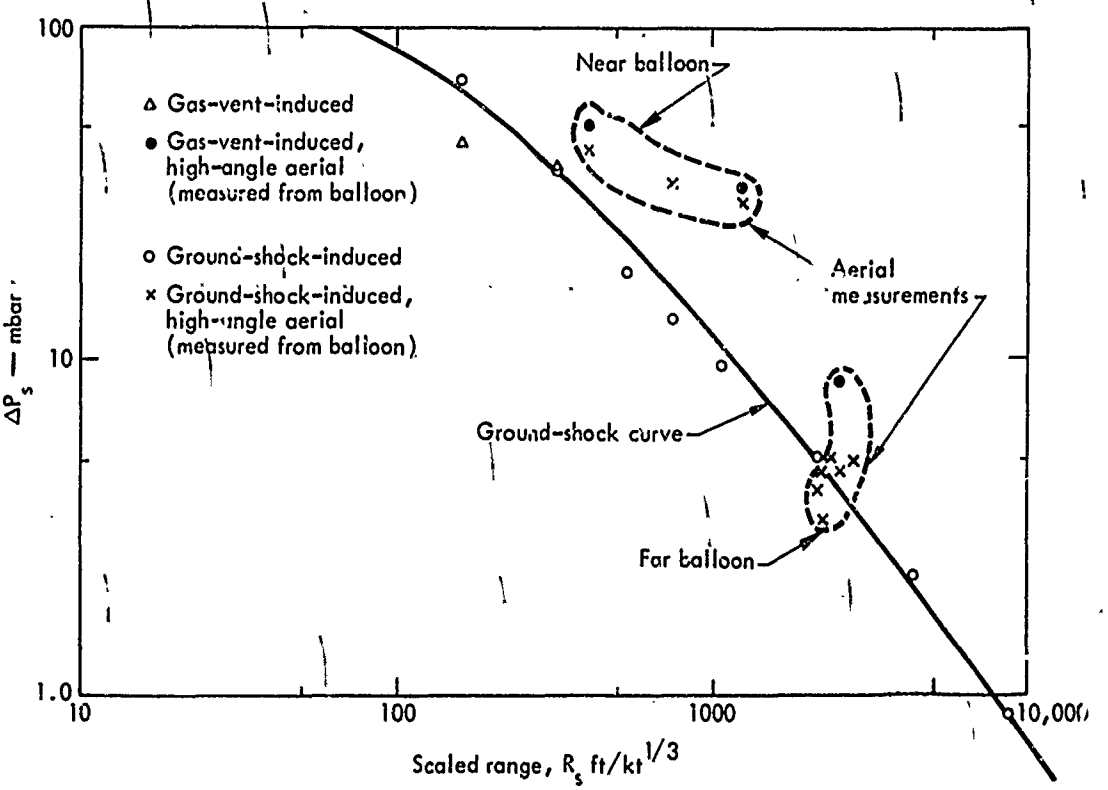

Fig. 5. Pre-Schooner II overpressures (scaled to 1.0 kt at 1000 mbar).

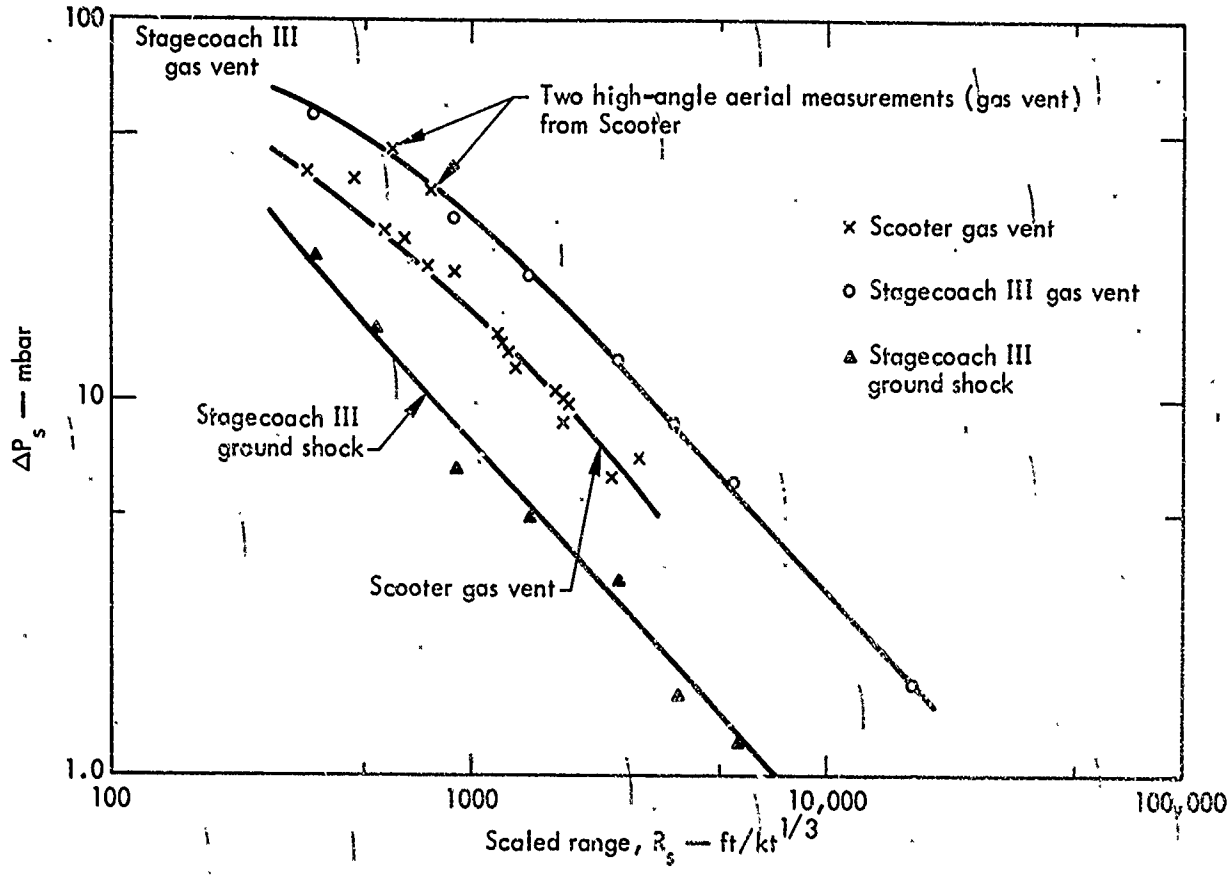

Fig. 6. Stagecoach and Scooter experimental overpressures (scaled to 1.0 kt at 1000 mbar).

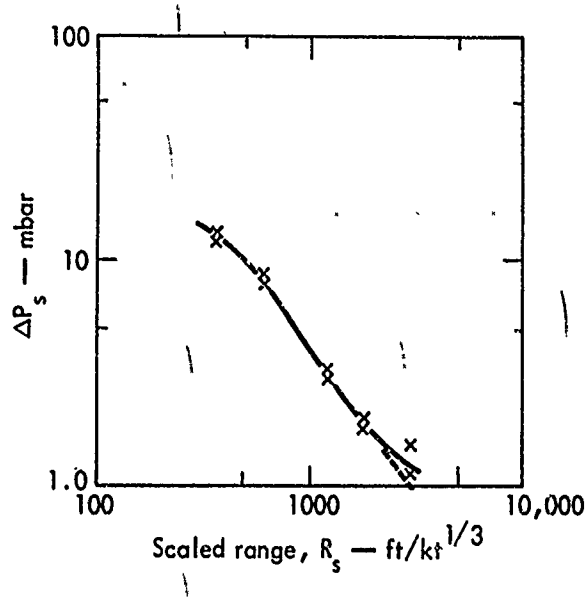

Fig. 7. Scooter ground-shock-induced overpressures (scaled to 1.0 kt at 1000 mbar).

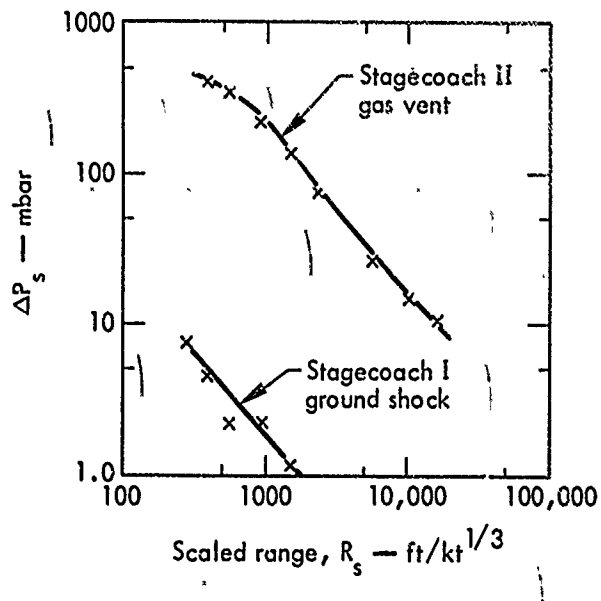

Fig. 8. Stagecoach experimental overpressures (scaled to 1.0 kt at 1000 mbar).

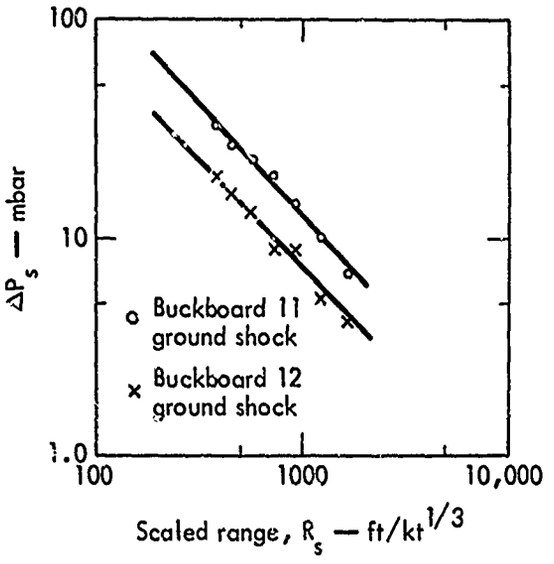

Fig. 9. Buckboard observed ground-shock overpressures (scaled to 1.0 kt at 1000 mbar).

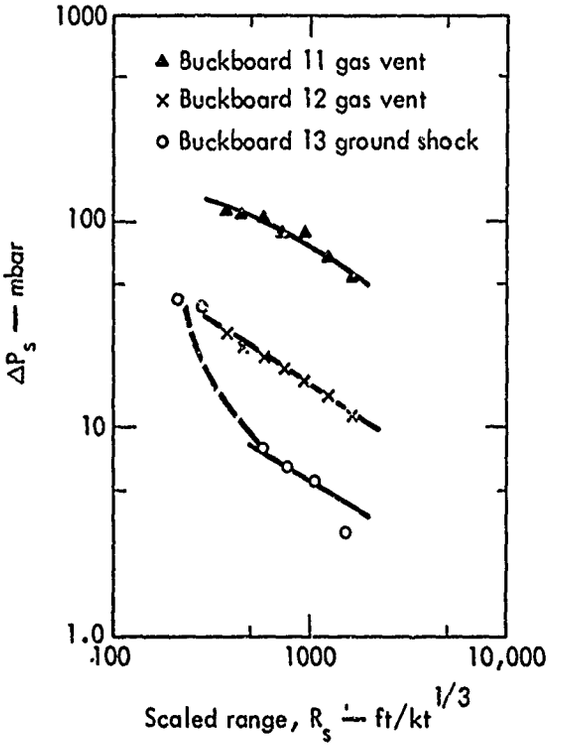

Fig. 10. Buckboard observed overpressures (scaled to 1.0 kt at 1000 mbar).

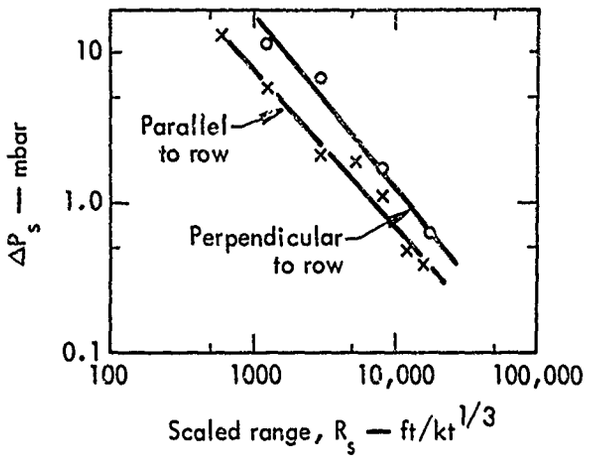

Fig. 11. Dugout ground-shock overpressures (scaled to 1.0 kt at 1000 mbar).

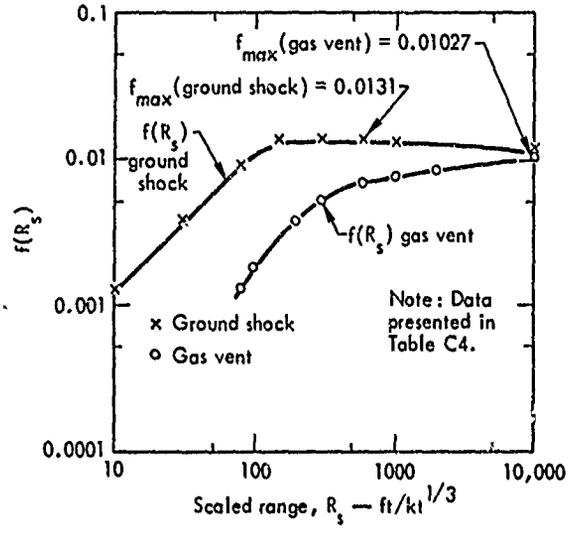

Fig. 12. Cabriolet ground-shock and gas-vent f-values as a function of R_s.

Section 4
Maximum Transmission Factor Results

In this section, the experimental events noted in the previous section and the data tabulated for each event and presented in Tables C1 through C25 will be used to develop maximum transmission factor values, f_{max}, for future event

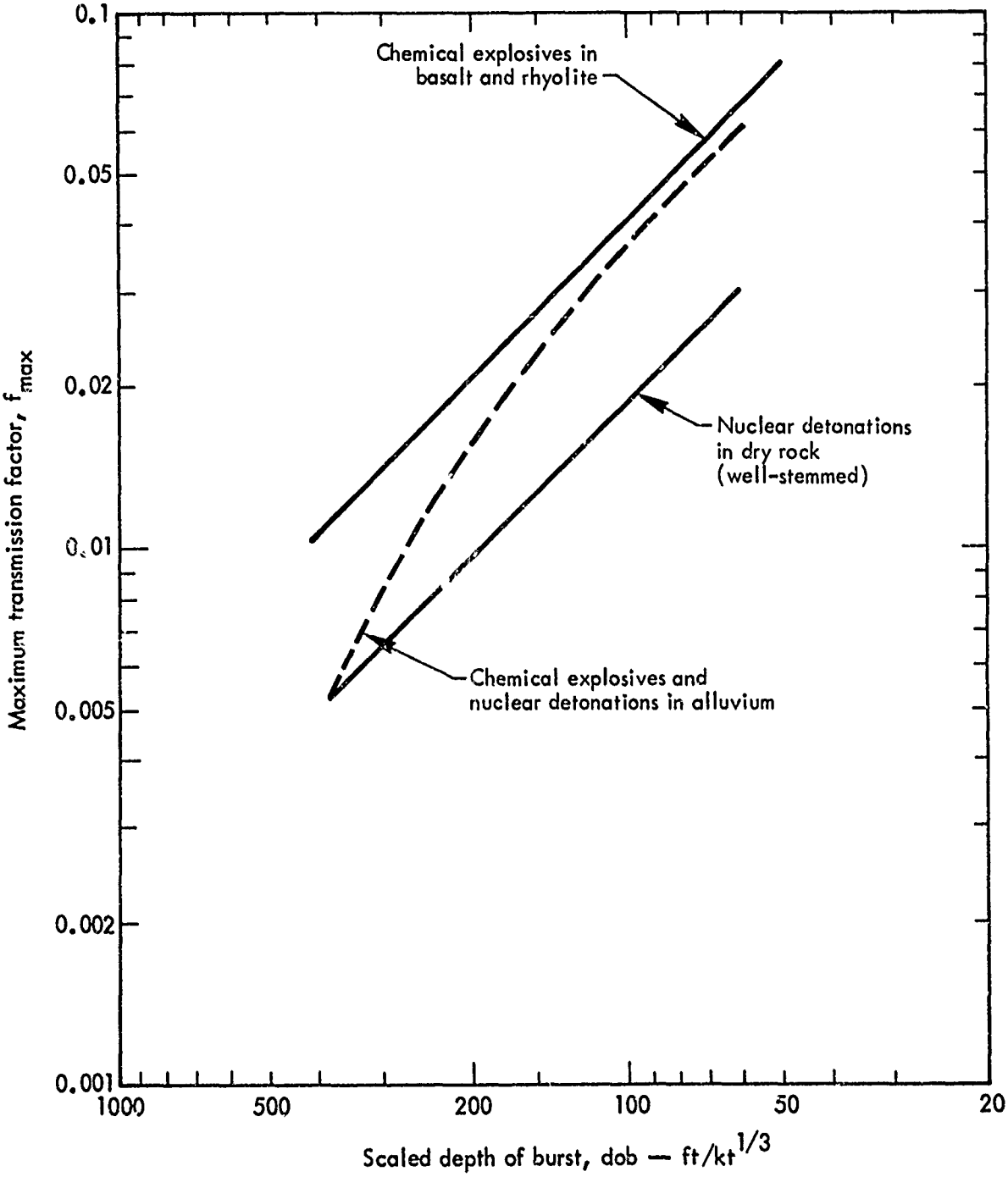

Fig. 13a. Maximum transmission factor f_{max} vs dob for ground-shock overpressures.

prediction purposes. The f_{max} will permit safe-sided prediction of airblast overpressures to be made for all ranges of interest if the type of explosive, medium, and dob are known. Both the ground-shock-induced and gas-vent overpressures may be predicted.

The maximum transmission factors for all large-yield experiments are plotted against dob in Figs. 13a and 14a. Figure 13a shows f_{max} for ground-shock-induced overpressures and Figure 14a depicts the gas-vent values. Figures 13b, 13c, and 13d and Fig. 14b show the individual data points used to construct the lines given in Figs. 13a and 14a. Project names in parentheses indicate a poorly established or uncertain value.

GROUND-SHOCK-INDUCED AIRBLAST FOR NUCLEAR AND CHEMICAL EXPLOSIVES

The nuclear f_{max} values in Fig. 13d lie close to the line labeled "Nuclear Detonations." The Neptune point (only one questionable measurement) falls appreciably above the line. Note that the points for Danny Boy are marked as

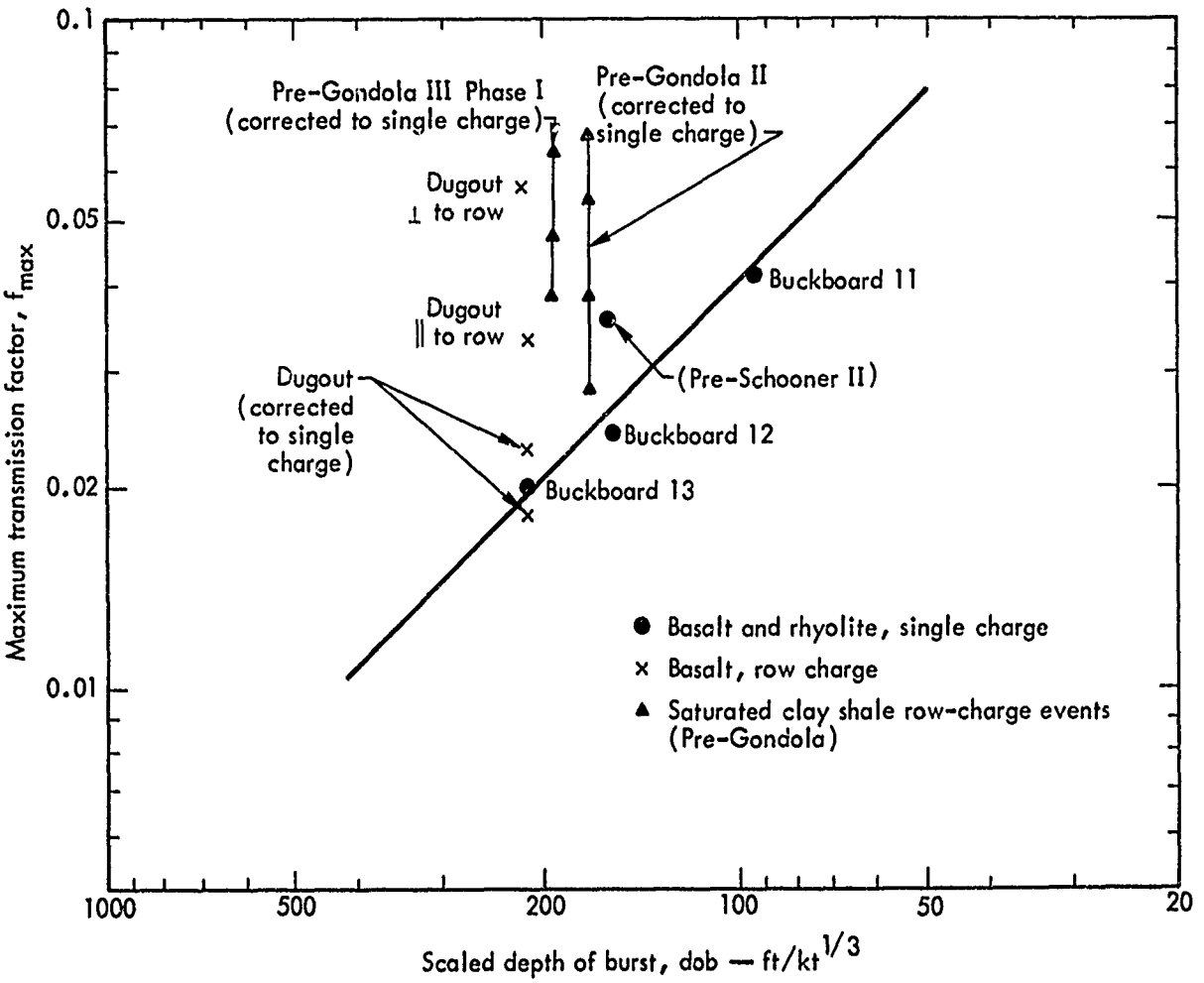

Fig. 13b. Maximum transmission factor f_{max} vs dob for ground-shock-induced overpressures, chemical explosive events in basalt and rhyolite, and chemical explosive events in saturated clay shale (Pre-Gondola experiments with nitromethane).

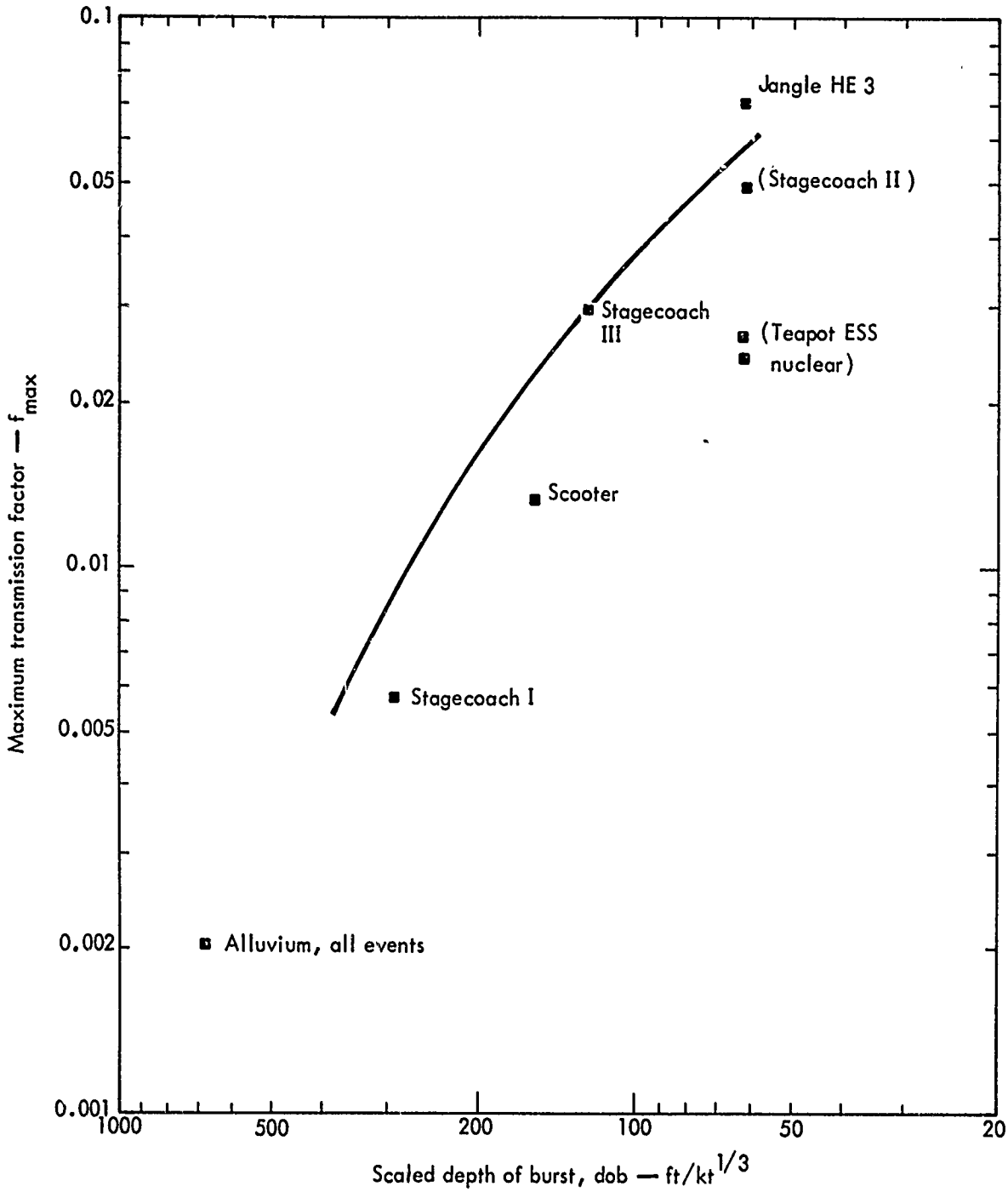

Fig. 13c. Maximum transmission factor f_{max} vs dob for ground-shock-induced overpressures (all events in alluvium).

ranges of uncertainty in f rather than as simple f_{max} points. The Nuclear Detonations line appears to be well-established for predicting nuclear experiments in strong dry rock (90 ft/kt$^{1/3}$ < dob < 300 ft/kt$^{1/3}$, 0.05 kt < W < 50 kt). The Nuclear Detonations line may well be valid for nuclear detonations in alluvium

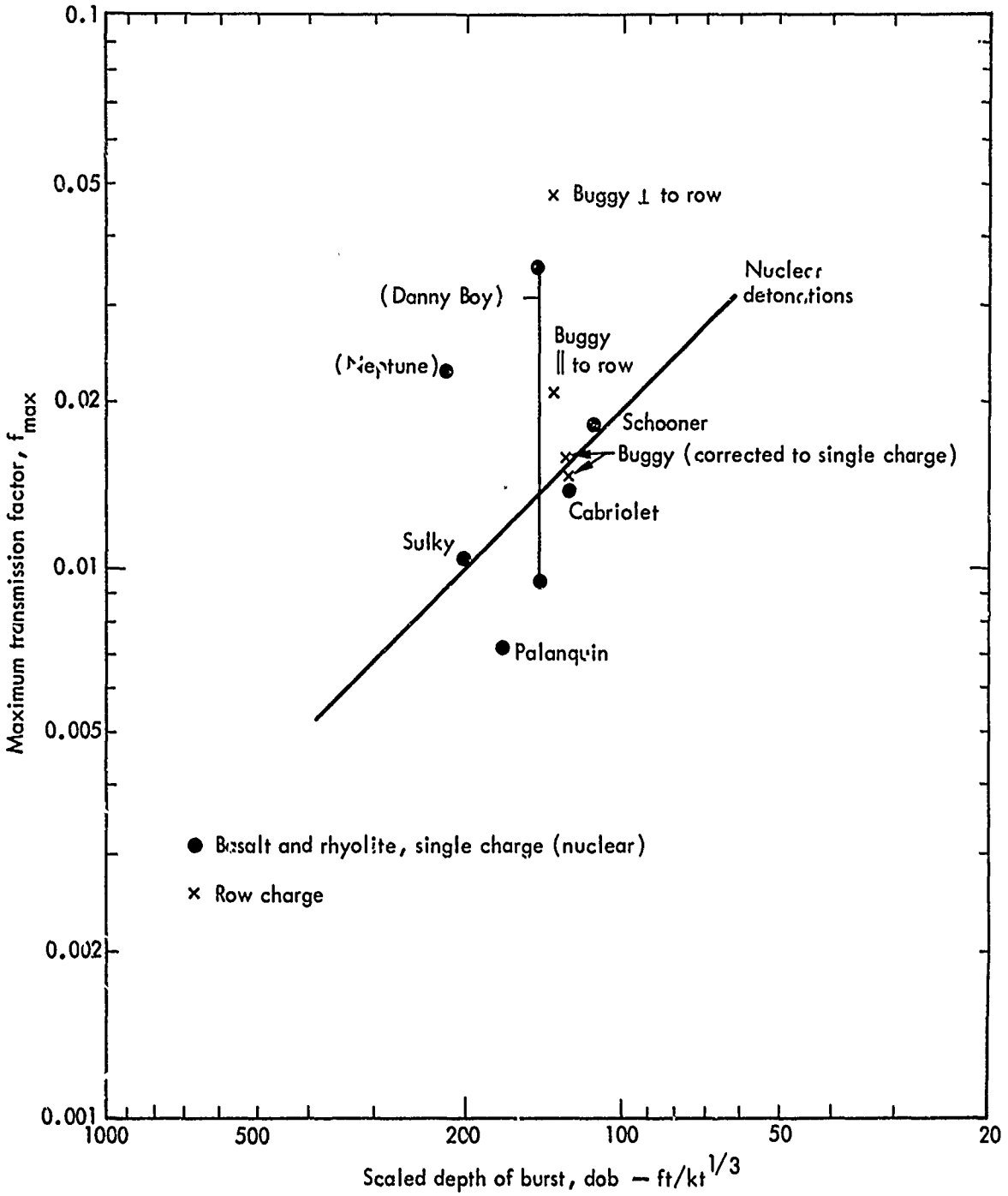

Fig. 13d. Maximum transmission factor f_{max} vs dob for ground-shock-induced overpressures (nuclear events in dry high-strength rock).

as well (60 ft/kt$^{1/3}$ < dob < 300 ft/kt$^{1/3}$), but safer predictions for alluvium events may be obtained by using the alluvium chemical explosive curve described below.

In Fig. 13c, it can be seen that the alluvium chemical explosive experiments form a consistent picture. Figure 13a shows that the f_{max} curve for alluvium falls well above the line for nuclear

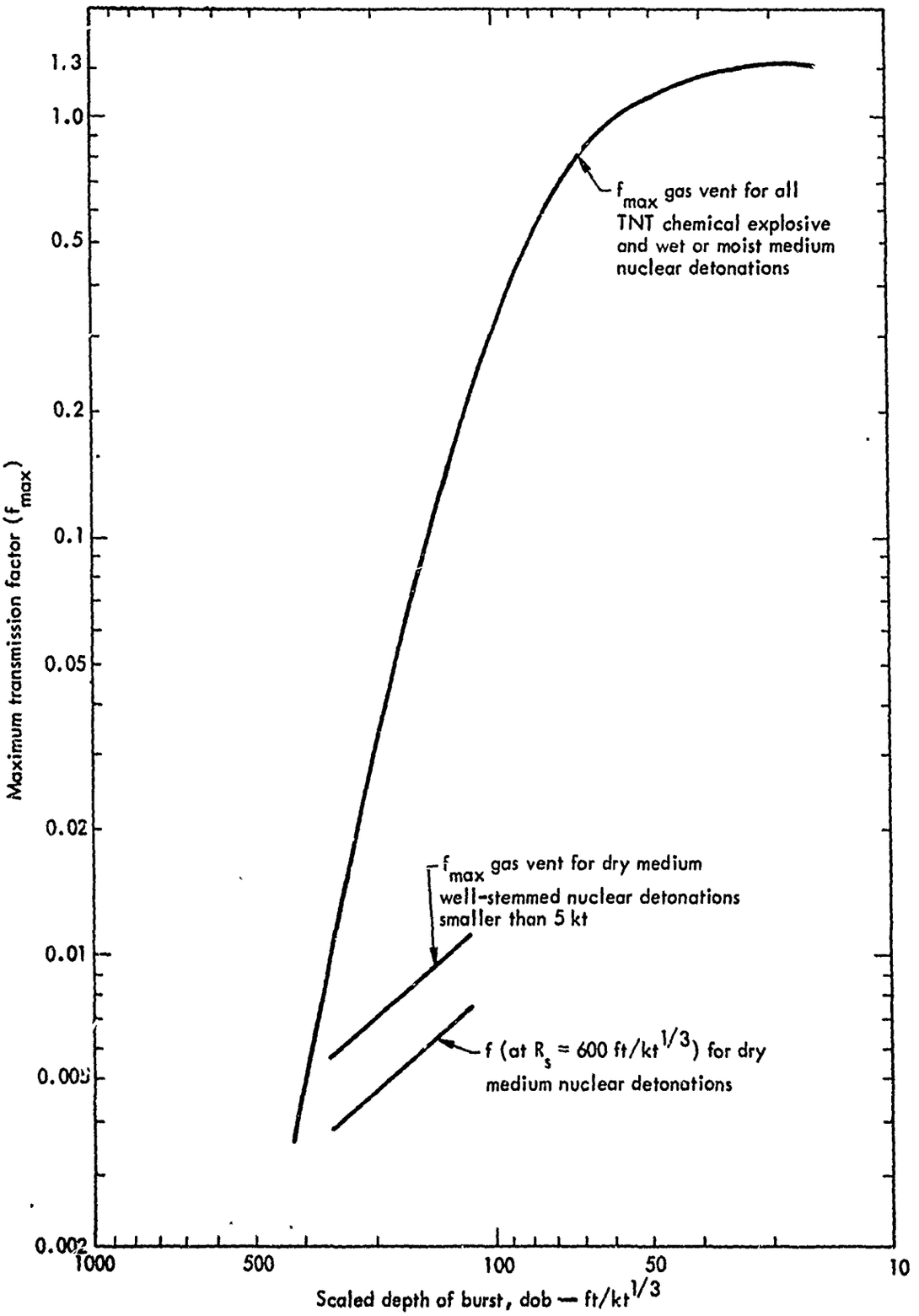

Fig. 14a. Maximum transmission factor f_{max} vs dob for gas-vent-induced overpressures.

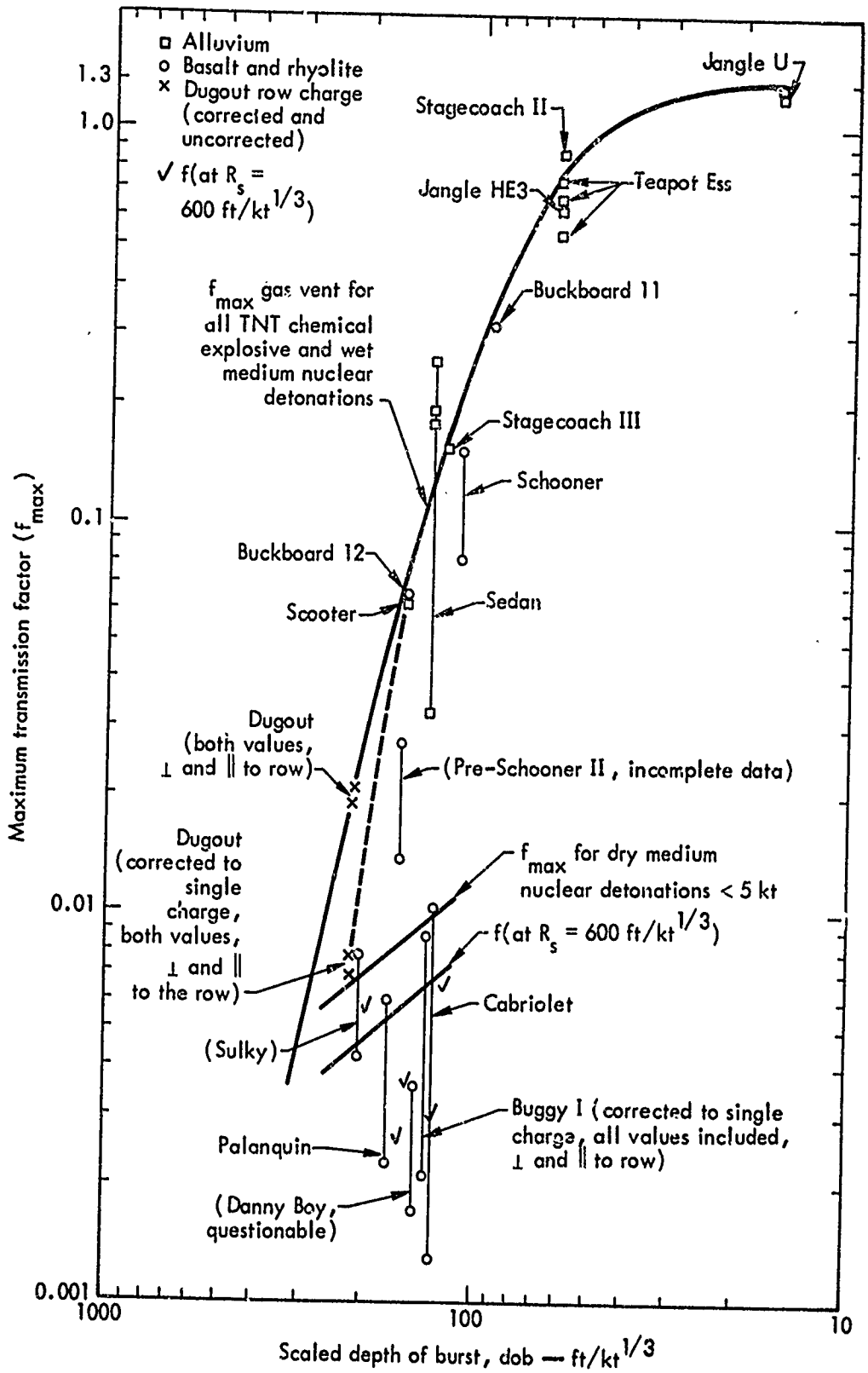

Fig. 14b. Maximum transmission factor f_{max} vs dob for gas-vent-induced overpressures, with observed points.

events in high-strength rock, but the curve may dip rapidly at dob greater than 190 ft/kt$^{1/3}$. Below ≈190 ft/kt$^{1/3}$, the alluvium chemical explosive curve may well coincide with the nuclear line. A suggested prediction curve for chemical explosive detonations in alluvium is shown by the dashed line. It is probably a fraction high at deeper dob. As shown in Fig. 13c, only the Jangle HE-3 experiment falls slightly above this curve. The alluvium chemical explosives prediction curve appears to be valid for all alluvium chemical explosive events with 60 ft/kt$^{1/3}$ < dob < 300 ft/kt$^{1/3}$, 10 tons < W < 1000 tons.

The basalt and rhyolite chemical explosives points in Fig. 13b define a third line which lies almost a factor of two above the nuclear line for strong dry rock. These higher ground-shock-induced overpressures are a very distinct difference between nuclear and chemical explosives; the increased overpressures correlate well with ground surface velocity measurements, which have been found to be systematically higher for chemical explosive detonations in rock than for nuclear detonations.[2] The higher velocities doubtless cause higher ground-shock overpressures. The strong rock chemical explosive line fits all the f_{max} points except Pre-Schooner II, which is slightly high. Pre-Schooner II was a nitromethane experiment in rhyolite. The strong rock chemical explosives curve should prove reliable for situations where 60 ft/kt$^{1/3}$ < dob < 300 ft/kt$^{1/3}$, 10 tons < W < 100 tons, and probably for greater yields as well.

Figures 13b and 13d also show the data points for four row-charge events, Dugout (5-charge chemical explosive row), Buggy (5-charge nuclear row), and Pre-Gondola II and III (which will be discussed in this section). The first two events are represented by labeled points (x's) in Figs. 13b and 13d. The higher point in each case is the f_{max} perpendicular to the row (⊥ to row). The lower point is f_{max} off the end of the row (∥ to row). These f_{max} values have also been corrected back to single-charge values using Vortman's empirical correction; number of charges, n, raised to a power, B (see Section 7). To correct back to single-charge values, the f_{max} values perpendicular to the row have been divided by 3.085 (or $5^{0.7}$); the f_{max} values off the end of the row have been divided by 1.495 ($5^{0.25}$). These corrected "single charge" f_{max} values are plotted in Figs. 13b and 13d as x's (directly below the uncorrected Dugout and Buggy row-charge values). The Dugout points corrected to single-charge values fall very close to the strong rock chemical explosive line, as would be expected (Dugout was nitromethane in basalt). The Buggy points corrected to single-charge values lie on the nuclear strong rock line. Thus, the row-charge experiments provide further verification for the proposed lines.

Figure 13a has been compared with Vortman's recent airblast data. Using Vortman's published diagrams,[1] transmission factors similar to Fig. 13a were computed. These factors are based partly on small-charge data, and apply only at a scaled range of R_s = 630 ft/kt$^{1/3}$. The results are shown in Fig. 15, with ground shock f-lines represented by dashed lines. Again, the basalt f values are higher than alluvium, and the lines

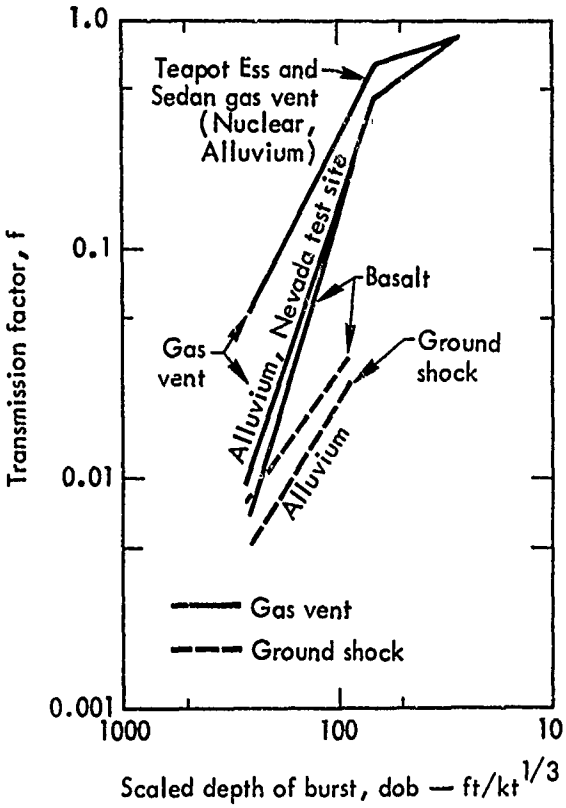

Fig. 15. Transmission factor f at a scaled range R_s = 630 ft/kt$^{1/3}$, following Vortman.[1]

resemble Fig. 13a in form. However, Vortman's lines are somewhat lower, as would be expected—his data were referred to a range of 630 ft/kt$^{1/3}$, quite close to SGZ. They are not intended to be true f_{max} values.

GAS-VENT-INDUCED AIRBLAST FOR CHEMICAL EXPLOSIVES

The situation for gas-vent f_{max} values is, unfortunately, much less clear. Gas-vent prediction curves are plotted in Fig. 14a, with actual data points shown in Fig. 14b. Again, uncertain experiments are enclosed in parentheses. Note that Jangle U, Teapot ESS, Schooner, Sedan, Pre-Schooner II, Cabriolet, Sulky, Palanquin, and Danny Boy are indicated by ranges of uncertainty in f (points connected by a vertical line) rather than as single f_{max} points. The highest point in the range is a probable f_{max} value. All these data show a great deal of scatter, but one fact is clear: the gas-vent f_{max} values fall into two different classes. All chemical explosive experiments and nuclear moist-to-wet medium detonations have very high f_{max} values. All the well-stemmed dry rock nuclear tests have very low f_{max} values. The clearest distinction between these two types of events is gas production. Evidently, nuclear tests in rock produce a rather small amount of vapor, resulting in low vent overpressures. Chemical explosives make their own super-heated gas, giving rise to strong vents. Apparently, boosting by steam vaporization in the adjacent medium is sufficient to bring large moist medium nuclear detonations up near the chemical explosives curve. It is obvious that several potentially complex effects are at work here, and overpressures from future nuclear detonations may be very sensitive to medium moisture content and other factors. Therefore, any prediction curves will apply only to identical explosives under similar conditions. It is also possible that a different type of chemical explosive could produce more vapor, giving rise to a still stronger vent. A case of this sort is discussed below.

A single f_{max} curve is drawn for all the chemical explosive and moist or wet medium nuclear detonations. It is important to remember that this curve represents a near fit to points influenced by a number of different factors. It is an approximation at best. Among the chemical explosive experiments, only Jangle

HE-2 falls appreciably above the curve. This 20-ton detonation, at dob = 21 ft/$kt^{1/3}$, gives $f_{max} \approx 1.5$ to 1.61. The Jangle U nuclear event, at dob = 16 ft/$kt^{1/3}$, indicates an $f_{max} \approx 1.26$ to 1.28. The latter value is considered by the authors to be more realistic. The Pre-Schooner II experiment appears to lie well below the curve. However, Pre-Schooner II (Table C12) peak gas-vent overpressures came from only two gages, both very close to SGZ; even these two values are questionable. The two f points in Fig. 14b derive from these two close-in gages. The true f_{max} at long range is believed to be much higher, probably in agreement with the curve—see, for example, Buckboard 12 and Scooter, both near the same dob. Their close-in f-values are 0.0226 and 0.0338, comparable to Pre-Schooner II. At long ranges, their f_{max} values are 0.0665 and 0.0619, in agreement with the curve. A true long-range f_{max} for Pre-Schooner II should likewise lie close to the curve.

Thus, all chemical explosive experiments in alluvium and strong rock define a single f_{max} curve. The curve is fairly well established for TNT, nitromethane, and similar explosives between 16 ft/$kt^{1/3}$ < dob < 170 ft/$kt^{1/3}$, 10 tons < W < 1000 tons. It is not established for dob's between 170 ft/$kt^{1/3}$ and 215 ft/$kt^{1/3}$. Either the solid curve or the lower dashed curve in Fig. 14b may apply for this region. The solid curve is recommended for safe predictions until further data become available. It is very probable that gas-vent overpressures rapidly decrease below dob = 190 ft/$kt^{1/3}$, at least for TNT and nitromethane in alluvium and basalt. Unfortunately, there is insufficient information to determine the exact depth at which gas vent becomes negligible. Only two statements can be made on the basis of current information: First, for chemical explosives in strong rock, f_{max} becomes small (gas-vent $f_{max} \lesssim 0.014$, or well below the Fig. 14b solid curve) at dob $\approx$ 217 ft/$kt^{1/3}$. Ground shock is definitely dominant at dob $\geq$ 217 ft/$kt^{1/3}$ (ground shock $f_{max} \approx 0.02$). These conclusions are based on Buckboard 13 and Dugout results (comparing gas-vent and ground-shock overpressures). Second, for TNT in alluvium, the gas vent is negligible and ground shock is dominant (ground-shock $f_{max} \approx 0.0056$) by dob = 295 ft/$kt^{1/3}$ (see Stagecoach I). These preliminary results are incorporated in Fig. 14b only in an approximate way. In spite of the fact that the curve in Fig. 14b is probably a little high for strong rock gas-vent overpressures at dob = 217 ft/$kt^{1/3}$, it will be retained for purposes of prediction. Comparing the fitted curve in Fig. 14b to the ground-shock curves (Fig. 13a), it is found that the ground-shock f_{max} curves cross the gas-vent curve at dob = 217 ft/$kt^{1/3}$ (strong rock, chemical explosive) and at dob = 240 ft/$kt^{1/3}$ (alluvium, chemical explosive). This indicates that ground-shock overpressures will be dominant (and will therefore control airblast safety predictions) at dob's greater than 217 ft/$kt^{1/3}$ (strong rock) or 240 ft/$kt^{1/3}$ (alluvium). It is worth repeating that these dob's are most likely a little deeper than the true crossover points, because the gas-vent f_{max} values in Figs. 14a and 14b are probably pessimistic (too high). Figure 14a can doubtless be improved when more data become available.

Vortman's gas-vent f-values at R_s = 630 ft/kt$^{1/3}$ are shown in Fig. 15 (solid lines). They may be compared to the fitted curve in Fig. 14a.

EXPLOSIVE OR MEDIUM DEPENDENCE EFFECTS

After it has been established that the curve in Fig. 14a fits reasonably well all chemical explosive data, it may be asked whether there are any differences between explosive types or media. Detailed examination of f-values does reveal certain differences between alluvium and basalt. At a given dob, alluvium $f(R_s)$ is slightly greater than basalt $f(R_s)$ at close-in ranges $R_s \approx 600$ ft/kt$^{1/3}$. Vortman observed this same effect for gas-vent overpressures at R_s = 630 ft/kt$^{1/3}$ (Fig. 15, gas-vent, solid lines). Recall that Vortman's results also included small-yield experiments. The f-values for Nevada Test Site alluvium were significantly higher than those for basalt. However, if the f-values are examined at greater ranges, there are indications of the opposite effect: basalt values appear larger than the alluvium. This trend is best seen for $f(R_s)$ with $R_s > 1000$ ft/kt$^{1/3}$, and for the f_{max} values. In other words, the basalt f values increase more rapidly with range, finally becoming greater than the alluvium f values. This effect is a direct result of the low overpressure attenuation rate observed for the Buckboard chemical explosive experiments. Gas-vent overpressure curves for these events indicate an attenuation rate of R^{-1} even at rather long ranges, and do not converge rapidly on $R^{-1.2}$. These shallow curves cause the relatively high f_{max} values. In addition, the Buckboard results extend only to scaled ranges shorter than 2000 ft/kt$^{1/3}$. Therefore, it is not possible to say with certainty whether the curves have converged on $R^{-1.2}$. It is somewhat dangerous to compare basalt f_{max} values determined for these short ranges with the better established alluvium f_{max} values at longer ranges. It does appear probable that the "true" long-range f_{max} values are at least as high or higher for basalt than for alluvium.

Data were also examined to determine whether any differences existed in the overpressures observed from TNT and nitromethane explosives. No clear trend emerges from the limited gas-vent data (cf., Pre-Schooner II nitromethane and Buckboard 12 or Scooter TNT at $R_s \approx 300$ ft/kt$^{1/3}$). However, the ground-shock f values at a given range are a little high for Pre-Schooner II when compared to Buckboard 12 basalt at any scaled range. It can be tentatively concluded that nitromethane gives slightly higher ground-shock overpressures (and ground-shock f_{max} values) than TNT at the same dob. This is the expected effect, since nitromethane has a somewhat higher energy yield per unit weight than TNT. However, this effect remains unverified for gas-vent overpressures. More data are needed.

One chemical explosive row-charge experiment is also plotted in Fig. 14b. This is Dugout, a five-charge (nitromethane) row in basalt. Both the perpendicular to the row ($\perp$) and off the end of the row ($\parallel$) gas-vent f_{max} values (uncorrected) fall near f = 0.02. When these are corrected to single-charge f-values (see Table C5), the results are as

follows: f_{max} ⊥ to row, corrected = 0.0068, and f_{max} ∥ to row, corrected = 0.0076. These corrected f-values are plotted as x's in Fig. 14b. Both values lie well below the gas-vent f_{max} curve (and well below the ground-shock f_{max} values for Dugout). This experiment provides part of the evidence that gas vent is small by dob = 217 ft/kt$^{1/3}$, at least in strong rock. An estimated gas-vent curve can be drawn through the Dugout points (dashed curve in Fig. 14b). This curve must be considered very approximate, and is not recommended for predictions at this time.

PRE-GONDOLA IN CLAY SHALE

The remaining row-charge data are quite unusual. They constitute the only overpressure data for nitromethane detonations in saturated clay shale. All the peak overpressures are ground-shock-induced, but they fall above the ground-shock curve, even as high as the gas-vent curve. The corrected single-charge f-values for Pre-Gondola are plotted in Fig. 13b as individual points (calculated f for each measured overpressure) rather than as f_{max} values. All points are symbolized by triangles. The Pre-Gondola II experiment was a five-charge row with a mean yield per charge of 28 tons, and an equivalent dob = 173 ft/kt$^{1/3}$. All of its observed f-values were corrected to single-charge f values using n = 5 charges. The Pre-Gondola III Phase I experiment consisted of two rows, each with seven 1-ton charges; dob was 195 ft/kt$^{1/3}$. The f-values were corrected to single charge using n = 7 charges. The corrected f-values, as plotted in Fig. 13b, lie almost as high as the gas-vent curves (Fig. 14a). Those for Pre-Gondola III Phase I are actually a little higher. The variation of f with dob, on the other hand, is roughly consistent with the ground-shock f-value lines. It is important to remember that Pre-Gondola III, Phase I was an experiment with seven 1-ton charges in each row, and that there may have been slight airblast reinforcement between the two adjacent seven-charge rows. In addition, the Pre-Gondola II row used charges of varying yield. For these reasons, the results are far from ideal. Pre-Gondola overpressure measurements were taken at only two or three scaled ranges, and the data are not sufficient to establish a definite trend for attenuation rate (or a well-determined value of f_{max}). Until further data become available, the following clay shale prediction method is recommended: For all events in saturated weak media similar to the Pre-Gondola medium with 200 ft/kt$^{1/3}$ > dob > 170 ft/kt$^{1/3}$, use f_{max} = 0.06 (for single-charge predictions). Modify for multiple-charge predictions as in Section 8. This procedure should produce pessimistic predictions at least to scaled ranges of several thousand ft/kt$^{1/3}$.

GAS-VENT-INDUCED AIRBLAST FOR NUCLEAR EXPLOSIVES

Nuclear gas-vent overpressures fall into two classes: moist or wet* or soil media, and dry rock media. The moist and soil media data derive from only four

*"Moist or wet media" is defined as media with moisture content appreciably exceeding 1% by weight.

experiments: Jangle U (1.2-kt, alluvium), Teapot ESS (1.2-kt, alluvium), Schooner (31-kt, rock containing a moist region), and Sedan (100-kt, wet alluvium). Figure 14b shows the range of measured points (rather than f_{max}) for all these experiments. They all agree roughly with the chemical explosive curve. Sedan points (large yield) scatter about 40% above the curve, and Schooner points (strong rock with a large moist seam in the vaporization region) lie about 32% below it. This agreement is remarkably good, but may be coincidental (see Appendix A). Nonetheless, the chemical explosive curve is the best available means of predicting wet medium detonations, as long as they are reasonably similar to Sedan or Teapot alluvium or Schooner moist rock. Even for similar events, it would be prudent to allow an added safety factor. Explosions in very weak wet media may produce substantially higher overpressures. With these cautionary notes in mind, the chemical explosive curve (Fig. 14a) can be used to predict nuclear detonations in moist media, 16 ft/kt$^{1/3}$ < dob < 160 ft/kt$^{1/3}$, 0.1 kt < W < 100 kt. This curve is not considered reliable for detonations larger than 100 kt (see Appendix A).

The dry medium nuclear detonations in rock form a more coherent picture. There are only five experiments, but venting behavior is quite consistent. In all cases, the gas-vent pulse is superimposed on a negative phase following the ground-shock pulse. The ground-shock peak overpressures are always dominant and must be considered in safety predictions. The gas-vent peaks are still of interest, since they are only slightly smaller than the ground-shock pulses (see tables for Cabriolet, Palanquin, Buggy and Sulky). The range of the gas-vent f-values and the f_{max} values are plotted in Fig. 14b. The straight line "f_{max} dry medium nuclear detonations" (labeled in Figs. 14a and 14b), represents a rough fit to these points. Note that the individual points scatter about this line by a factor of 2.5. The Danny Boy point is low because gas-vent overpressures were small and could only be observed to a range of 587 ft/kt$^{1/3}$. Beyond this range, they were overwhelmed by the stronger ground-shock pulse. Thus, the Danny Boy point represents a close-in f-value, not a true f_{max} value. Its disagreement with the line is not significant. To compare trends between f-values and f_{max}, one can plot f-values at some chosen range, since these values should be more consistent than f_{max}. All experiments have measured overpressures near R_s = 600 ft/kt$^{1/3}$. Therefore, f (at R_s = 600 ft/kt$^{1/3}$) is plotted as indicated by the checkmarks in Fig. 14b. A mean line drawn to represent f (at R_s = 600 ft/kt$^{1/3}$) is seen to fall below the f_{max} line. The same general trend of the line is evident, but the points still scatter about the line by a factor of 1.7.

One of the experiments plotted in Fig. 14b, Buggy I, was a five-charge nuclear row in basalt. The observed f-values for Buggy were corrected to single-charge f values using the formulae given in Table C6. Figure 14b shows the complete range of corrected f-values, both perpendicular to and off the end of the row (uncorrected f-values for Buggy are not shown). The checkmark indicates the corrected f (at R_s = 600 ft/kt$^{1/3}$)

perpendicular to the row. The largest corrected values of "f" are approximately f = 0.0085, both perpendicular to and off the end of the row. These values are in good agreement with the single-charge f_{max} values for the other nuclear dry rock experiments.

The nuclear dry rock lines in Fig. 14 are intended for use in predicting the approximate amplitude of the gas-vent pulse, and other information they contain should not be taken too literally. In particular, the slope of these lines probably does not give a good indication of the manner in which the gas-vent pulse is suppressed with dob. The measured f-values represent the amplitude of a small overpressure peak superimposed on the aftereffects of a dominant ground-shock pulse. This amplitude is not accurately determined and may be grossly affected by the behavior of the preceding stronger pulse. The apparent slope of these lines may be more closely related to the behavior of the ground-shock pulse than to any true gas-vent effect. The true gas-vent amplitude doubtless decreases more rapidly with dob than Fig. 14 would indicate.

The nuclear dry rock f lines in Fig. 14a may be used to predict gas-vent overpressures for well-stemmed nuclear detonations in dry rock. The upper line "f_{max}" predicts overpressure at all ranges. The lower line should give a slightly better estimate of overpressure at R_s = 600 ft/kt$^{1/3}$. For reasons stated in the previous paragraph, neither of these lines should be used outside the range for which they were established: strong dry rock nuclear detonations with 125 ft/kt$^{1/3}$ < dob < 250 ft/kt$^{1/3}$, and 0.05 kt < W < 5 to 10 kt.

GROUND-SHOCK AND GAS-VENT-INDUCED AIRBLAST FOR ALUMINIZED AMMONIUM NITRATE SLURRY (STEMMED AND UNSTEMMED DETONATIONS)

There is one additional set of airblast data which has not yet been discussed. As mentioned in the chemical explosives discussion, the near-coincidence of the chemical explosive f-curves is a result of the consistent gas production and burning characteristics of the various explosive materials. Ammonium nitrate blasting agents currently being used do not resemble TNT and the others in these respects. Only one set of airblast data is available for ammonium nitrate cratering detonations. These data derive from a series of experiments conducted in weak interbedded sandstone and shale, near Trinidad, Colorado.[11] Airblast was measured at ranges of a few hundred feet to several miles from ammonium nitrate fuel oil (ANFO) and aluminized ammonium nitrate slurry (AN slurry) detonations. Both single-charge experiments and simultaneous and delayed row-charge detonations were included. Several 1-ton AN slurry near-surface bursts were also observed.

Most of the buried ANFO experiments in this series gave startling results. Gas-vent overpressures varied widely in a manner not directly related to dob; in one case, airblast approached that expected for a surface detonation of the same yield! Evidently, if ANFO vents while still burning and high cavity pressure exists, huge amounts of energy may be coupled into the blast wave. One ANFO experiment produced very low overpressures, similar to the observed airblast for TNT and nitromethane at the

same depth. In this case, the vent apparently occurred somewhat late, and burning was complete at vent time. The "slow" reaction behavior, which renders ANFO quite suitable for surface burst airblast experiments, causes very erratic results when it is used in buried detonations. Anomalous venting characteristics appear, and the airblast cannot be reliably predicted for buried applications. Use of the ANFO explosive may be questionable where surface burst airblast overpressures are unacceptable. This subject needs more work. Data and detailed discussion for the ANFO detonations may be found in Ref. 11.

Fortunately, the venting behavior of AN slurry is more consistent. All the close and intermediate-range airblast data for each Trinidad slurry experiment are listed in Tables C22 through C24. Results from the buried single-charge AN slurry events (B-4 through B-8, B-14) are used to examine f_{max} as a function of dob. In this case, the airblast measurements are too sparse to permit accurate fitted overpressure curves. Therefore, an f-value is calculated for each observed overpressure (Table C22). These f-values are plotted as a function of dob in Fig. 16. The highest observed f-values for the individual experiments were found between 4000 and 21,000 ft/kt$^{1/3}$ scaled range, a reasonable location for f_{max} (and inside the range of appreciable meteorological effects). The f_{max} curves are drawn through the highest observed f-points in Fig. 16. One line shows the fitted ground-shock-induced f_{max}. Two curves give estimates of gas-vent-induced f_{max}; the higher solid curve provides a high or pessimistic estimate, while the lower dashed curve is a best fit. As expected, the gas-vent airblast is more rapidly suppressed with increasing dob than the ground-shock-induced component. Ground-shock-induced airblast becomes dominant at a dob $\approx$ 210 to 220 ft/kt$^{1/3}$ for this explosive-medium combination. Figure 16 also shows that both the gas-vent and ground-shock airblast exceed that observed for TNT in all media (Figs. 13a through 14b). The gas vent is strong because of the exceptionally early (but erratic) vent times observed for this explosive-medium combination.[11] Cavity pressure at the early vent times is correspondingly higher than for other explosives. No immediate explanation is available for the high ground-shock-induced airblast. Note that the different experiments plotted in Fig. 16 show a certain amount of scatter and inconsistency in behavior. Shot B-7, at dob = 226 ft/kt$^{1/3}$, produced an exceptionally strong gas vent, stronger than shot B-6 at a shallower depth. This case indicates erratic venting behavior for AN slurry, similar to but less pronounced than that of ANFO. Such variability may be partly due to the explosive itself and partly a function of inhomogeneities and local changes in the medium characteristics; it may also be caused by the use of drill cuttings as stemming material at Trinidad (as opposed to more restrictive stemming criteria for past chemical explosive detonations). Behavior of this sort reduces the confidence level of airblast predictions based on Fig. 16.

The Trinidad data do not provide a definitive picture of the attenuation rate. Most single-charge experiments are

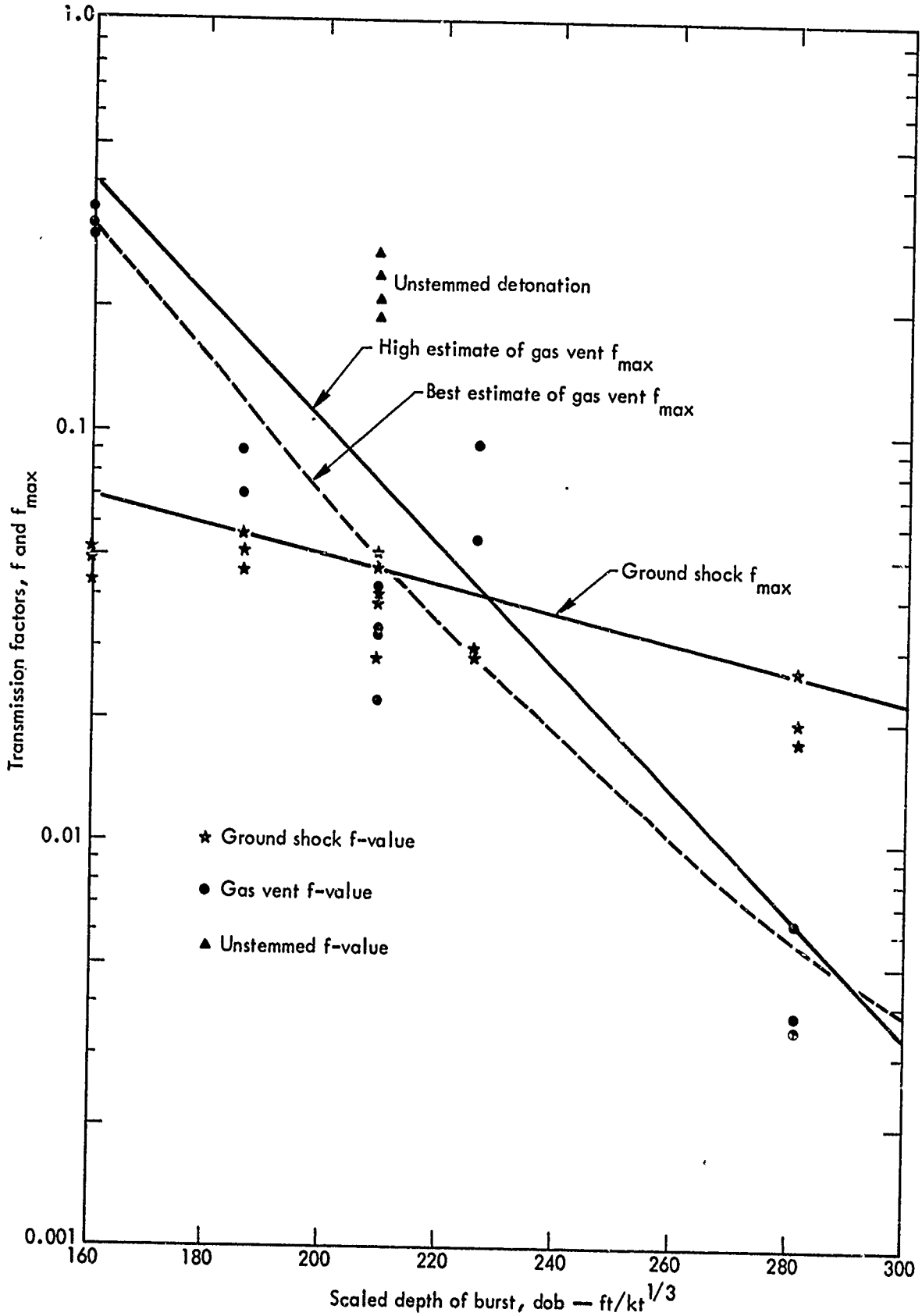

Fig. 16. Observed single-charge transmission factors f and fitted transmission factor curves f_{max} as a function of dob for aluminized ammonium nitrate slurry detonations in sandstone and weak rock.

consistent with a rate of $R^{-1.2}$, and the f-values appear to have leveled off by scaled ranges on the order of several thousand ft/kt$^{1/3}$. Thus, the fitted curves in Fig. 16 should give valid f_{max} values for AN slurry.

No close-in gages were used in these experiments. Therefore, no data are available in the turnover region of the single-charge overpressure curves. There is some indication that the closest measured overpressures and f-values are slightly low for the deepest experiments (airblast pulses most strongly directed upward).

At very long ranges, local propagation effects and meteorology come into play. These effects were observable for some Trinidad experiments as a decrease in f at very long ranges. Only the close and intermediate range data are used in this investigation. Transmission factors almost always decrease at longer ranges, indicating a negative temperature gradient or sound velocity gradient (sound refracted upward, away from ground level). However, one Trinidad experiment gave a relatively close tropospheric sound focus, the first time that such an event has been clearly recorded. The focus occurred at a range of 32,300 ft (scaled range 301,000 ft/kt$^{1/3}$) from near-surface shot B-11. The observed 0.55-mbar (unscaled) peak overpressure at this location was a factor of 1.8 greater than the expected $R^{-1.2}$ value.* Since no vertical meteorology is available, there is no possibility of calculating a path for the refracted signal. Refraction due to strong winds or an inversion condition nearly 3000 ft above ground level is suspected (Ref. 11).

Shot B-15 was an unstemmed event at dob = 209 ft/kt$^{1/3}$. A shaft approximately 1.17 ft in diameter (or 12 ft/kt$^{1/3}$) was left open to the surface. A strong initial airblast pulse was recorded at all gage stations. This pulse completely dominated the airblast and was due to combined effects of ground shock and "cannon muzzle blast" from the unstemmed shaft. The calculated f-values are plotted as triangles in Fig. 16. They are obviously larger than the corresponding stemmed experiments, and $f_{max} = 0.27$. On the average, the unstemmed f-values lie a factor of 5.5 to 6.5 above the comparable gas-vent stemmed values. For prediction purposes, multiply the stemmed gas-vent f_{max} by 6.0. Technically, this number applies only to aluminized AN slurry detonations near optimum depth in sandstone, with an open shaft to the surface 12 ft/kt$^{1/3}$ in diameter and a charge configuration exactly identical to the test experiment (1-ton AN slurry charge at dob = 209 ft/kt$^{1/3}$). However, the very early time venting behavior through an open hole is not expected to be strongly affected by the surrounding medium. Thus, the 6.0 multiplication factor should be approximately correct for most chemical explosive detonations near or somewhat below optimum depth of burst. The shaft diameter should be close to 12 ft/kt$^{1/3}$; shaft size variations or extreme differences in charge configuration or yield may modify the observed airblast.

Additional results of the Trinidad series are described in Section 9 (near-surface bursts) and Appendix B

*Also, this overpressure fell about a factor of 2.0 above extrapolated close-in overpressures for the experiment.

(row-charge experiments). AN slurry near-surface bursts are predicted using the standard TNT surface burst curve (Section 9). The Trinidad row-charge tests revealed wide and inexplicable variations in airblast reminiscent of the ANFO single-charge results. A preliminary method of predicting airblast from AN row charges is given in Appendix B.

Section 5
Buried Single-Charge Prediction Procedures

This section presents single-charge prediction procedures using the f_{max} method and compares the predicted lines with actual observations of large-yield events. Aerial gage measurements of airblast from cratering experiments are also discussed and compared to ground level values.

SINGLE-CHARGE PREDICTION

Given the f_{max} curves of the previous section, overpressures may be predicted in the following manner. First, calculate the dob for the experiment to be predicted:

$$\text{dob} = \frac{\text{DOB (in ft)}}{[\text{Yield W (in kt)}]^{1/3}}$$

Then go to the appropriate curves, Figs. 13a, 14a, or 16, and read off a ground-shock f_{max} and a gas-vent f_{max}. The following is a summary of the correct curves to use:

Ground-Shock f_{max} Values:

(1) Nuclear detonations, 60 ft/kt$^{1/3}$ < dob < 300 ft/kt$^{1/3}$, 0.05 kt < W < 50 kt. Use the Nuclear Detonations line (lower line) in Fig. 13a (strong rock only).

(2) Chemical explosive (TNT and nitromethane) and nuclear in alluvium, 60 ft/kt$^{1/3}$ < dob < 300 ft/kt$^{1/3}$, 10 tons < W < 1000 tons. Use the center (dashed) curve in Fig. 13a.

(3) Chemical explosive (TNT and nitromethane) in all strong rock media, 60 ft/kt$^{1/3}$ < dob < 300 ft/kt$^{1/3}$, 10 tons < W = 100 tons or larger. Use the upper (basalt and rhyolite) chemical explosives line in Fig. 13a.

(4) Chemical explosive (nitromethane) in saturated clay shale, dob > 170 ft/kt$^{1/3}$, all yields. Use ground-shock $f_{max} \cong 0.06$. Gas-vent airblast is negligible for all chemical explosive events in water or saturated media below 170 ft/kt$^{1/3}$ dob.

(5) Aluminized ammonium nitrate slurry detonations (AANS) in sandstone or weak rock, 160 < dob < 300 ft/kt$^{1/3}$, 0.5 < W < 100 tons. Use the AN ground-shock line shown in Fig. 16.

Gas-Vent f_{max} Values:

(1) Chemical explosive (TNT and nitromethane) in alluvium and strong rock, 16 ft/kt$^{1/3}$ < dob < 300 ft/kt$^{1/3}$, 10 tons < W < 1000 tons. Use solid (upper) curve in Fig. 14a.

(2) Nuclear detonations in alluvium, moist media, rock with wet regions,

16 ft/kt$^{1/3}$ < dob < 160 ft/kt$^{1/3}$, 0.1 kt < W < 100 kt. Use solid (upper) curve in Fig. 14a.

(3) Nuclear detonations, well-stemmed in dry rock, with 125 ft/kt$^{1/3}$ < dob < 250 ft/kt$^{1/3}$, 0.05 kt < W < 5 to 10 kt. Use the dry medium nuclear f_{max} line in Fig. 14a. This line gives only approximate predictions of the amplitude of the gas-vent pulse (ground shock is dominant). The line on the bottom, f (at R_s = 600 ft/kt$^{1/3}$), may also be used to predict the overpressure at a scaled range of R_s = 600 ft/kt$^{1/3}$ only.

(4) Aluminized ammonium nitrate slurry detonations (AANS) in sandstone or weak rock, 160 ft/kt$^{1/3}$ < dob < 300 ft/kt$^{1/3}$, 0.5 tons < W < 100 tons. Use either of the two AN gas-vent curves shown in Fig. 16 (solid or dashed; they are quite close together and selection will make little difference in the prediction).

(5) Unstemmed detonations (open shaft 12 ft/kt$^{1/3}$ in diameter), at or near optimum depth of burst; aluminized ammonium nitrate slurry in sandstone or weak rock, W≈1 ton. Multiply the predicted gas-vent f_{max} by 6.0. This technique is also applicable to other types of chemical explosive events and to other yields, although the predictions may prove less accurate.

After obtaining the ground-shock and gas-vent f_{max} values, make the predictions and plot them on a sheet of log-log graph paper. To make the predictions, select at least three or four appropriate standard line points from Table 1, scale them back to the yield and P_0 of the experiment to be predicted, then multiply each overpressure ΔP by f_{max} (gas-vent) and by f_{max} (ground-shock). This procedure yields two sets of prediction points, one for gas-vent and one for ground-shock. When plotted, the sets of points define two lines of slope $R^{-1.2}$. These are the predicted lines. While two points would be sufficient to define each straight line, it is desirable to use several as a check on the accuracy of the calculations.

Summary of Prediction Procedure

To predict the airblast overpressure ΔP as a function of true range R, for an experiment of specified explosive type, yield W (kt), and ambient atmospheric pressure P_0 (mbar):

(1) Determine f_{max} (gas-vent) and f_{max} (ground-shock) from Figs. 13a and 14a or from Fig. 16, as described above.

(2) Select several points (R_s, ΔP_s) from the standard $R_s^{-1.2}$ line (some sample standard line points are tabulated in Table 1).

(3) Since the standard line points are scaled for a yield of 1 kt and an ambient pressure of 1000 mbar, scale them to the yield W and ambient pressure P_0 of the detonation of interest:

$$\Delta P = \Delta P_s \left(\frac{P_0}{1000}\right)$$

$$R = R_s \left(\frac{W}{1.0\ \text{kt}}\ \frac{1000}{P_0}\right)^{1/3}.$$

(4) Scaling the standard points (R_s, ΔP_s) to the experiment in question gives a new set of points: (R, ΔP); (scale at least 3 or 4 points to assure accuracy of scaling and plotting). Multiply each ΔP by f_{max} (gas-vent). This gives the gas-vent predicted points: (R, ΔP (gas-vent)). Predict ground-shock overpressures in the

same way, multiplying ΔP by f_{max} (ground-shock). Then plot the $(R, \Delta P$ (gas-vent)$)$ points and the $(R, \Delta P$ (ground-shock)$)$ points on a sheet of log-log graph paper. The points define two lines of slope $R^{-1.2}$, which are the predicted gas-vent and ground-shock overpressures. Note that, for the close-in region (R_s < 3000 ft/kt$^{1/3}$ for gas-vent overpressures and R_s < 600 ft/kt$^{1/3}$ for ground-shock overpressures), the $R^{-1.2}$ line will overpredict the airblast overpressures. Section 6 presents a procedure for refining the predictions in this range.

(5) All the overpressures listed in Table 1, and thus all the predicted overpressures, are expressed in millibars (mbar). If desired, convert all predicted overpressures from mbars to psi by dividing by 69: ΔP (in psi) = ΔP (in mbar)/69.0.

Sample Problem

Predict gas-vent and ground-shock overpressures for a 20-ton (0.02-kt) TNT experiment in alluvium. The ambient pressure P_0 at the time of detonation will be about 868 mbar. The depth of burst is 34 ft. First, find the dob:

$$\text{dob} = \frac{\text{DOB}}{W^{1/3}} = \frac{34 \text{ ft}}{(0.02)^{1/3}} = 125 \text{ ft/kt}^{1/3}.$$

The experiment is in alluvium. Using the dashed (alluvium) curve in Fig. 13a, find f_{max} (ground-shock) = 0.03. From the chemical explosive curve in Fig. 14a, f_{max} (gas-vent) = 0.17.

Go to Table 1 and select a few appropriate points at ranges of interest:

R_s	ΔP_s (mbar)
500	816
1000	357
3000	95.4

Scale these points back to a 20-ton experiment at P_0 = 868 mbar:

$$\Delta P = \Delta P_s \left(\frac{868}{1000}\right) = 0.868 \, \Delta P_s$$

$$R = R_s \left(\frac{0.02}{1.0} \frac{1000}{868}\right)^{1/3} = 0.285 \, R_s.$$

Tabulate the values of R and ΔP:

R (ft)	ΔP
142	709 mbar = 10.28 psi*
285	310 mbar = 4.49 psi
855	82.8 mbar = 1.20 psi

For gas-vent overpressure predictions, multiply all the overpressures (either in psi or mbar, as desired) by f_{max} (gas-vent) = 0.17 and tabulate:

R (ft)	ΔP gas-vent (psi)
142	1.75
285	0.764
855	0.204

For ground-shock overpressure predictions, multiply the overpressures by f_{max} (ground-shock) = 0.03 and tabulate:

R (ft)	ΔP ground-shock (psi)
142	0.308
285	0.135
855	0.036

*Convert to psi by dividing by 69.

These gas-vent and ground-shock points are plotted in Fig. 17. They define two straight lines, which are the predicted gas-vent and ground-shock overpressures. The conditions specified for this sample problem are the same as for the Stagecoach III chemical explosive experiment. The actual observed Stagecoach III overpressures are plotted in Fig. 17 for comparison.

To demonstrate further the prediction method, predictions have been performed for several other single-charge nuclear and chemical explosive experiments in various media. The resultant prediction lines, together with the observed points, are shown in Figs. 17 through 24. The f_{max} used is listed in the figure in each case. Please note that Figs. 17 through 24 are plotted in terms of true ranges and overpressures for each experiment (not scaled to 1.0 kt, etc.). Some of these figures have ΔP in psi instead of mbar to maintain comparability with the originally published data.

OVERPRESSURES ABOVE GROUND LEVEL

All the data on which the above prediction technique is based refer to ground level or near ground level overpressures. There has recently been some interest in aerial airblast, at high elevations above the point of detonation. Reed believes that elevated overpressures may have considerable effect on the airblast energy propagated to very long ranges[9,12-14]. There is a limited amount of experimental information on elevated airblast, deriving mostly from the Scooter and Pre-Schooner II detonations (Tables C11 and C12, respectively). These experiments used either balloon-borne or pole-supported gages, relatively close-in to SGZ.

The Scooter experiment had several elevated gages, but only the two (very close-in to SGZ) measured gas-vent overpressures higher than the ground level values at the same range. These two gages were at scaled ranges of R_S

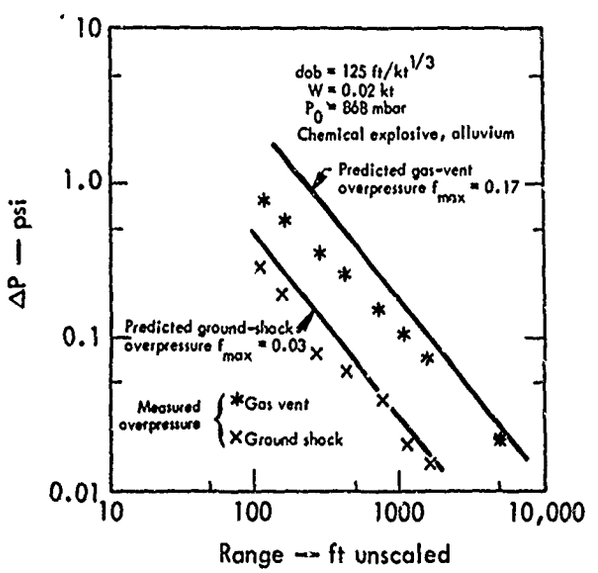

Fig. 17. Observed and predicted airblast overpressures for Stagecoach III.

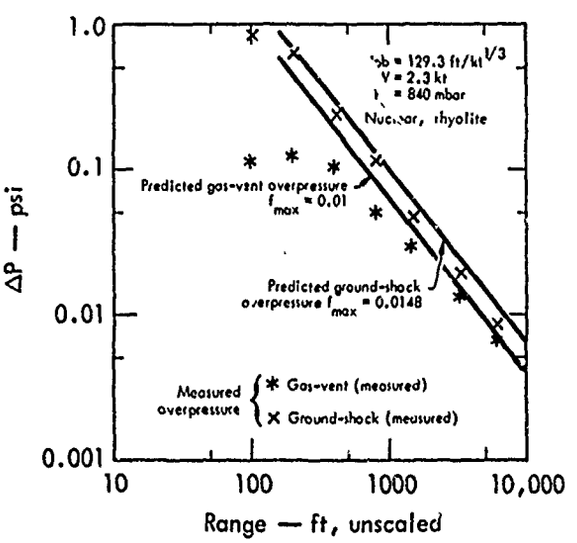

Fig. 18. Observed and predicted airblast overpressures for Cabriolet.

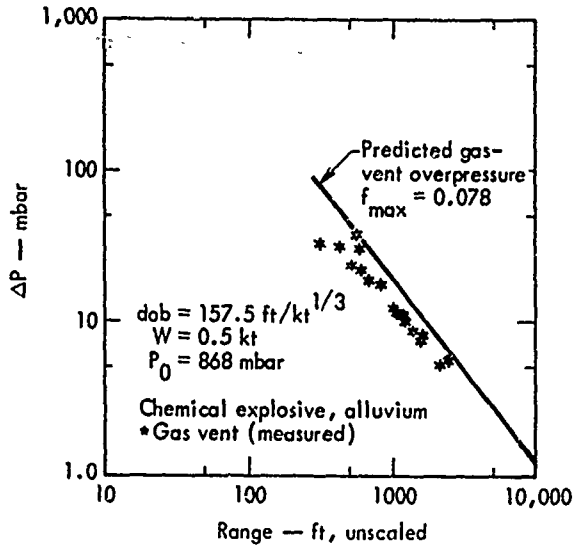

Fig. 19. Observed and predicted airblast overpressures for Scooter.

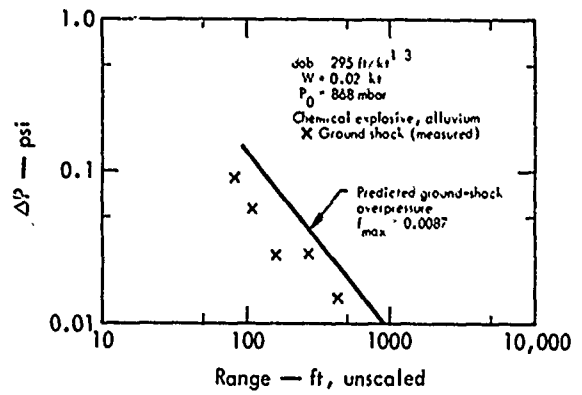

Fig. 20. Observed and predicted airblast overpressures for Stagecoach I.

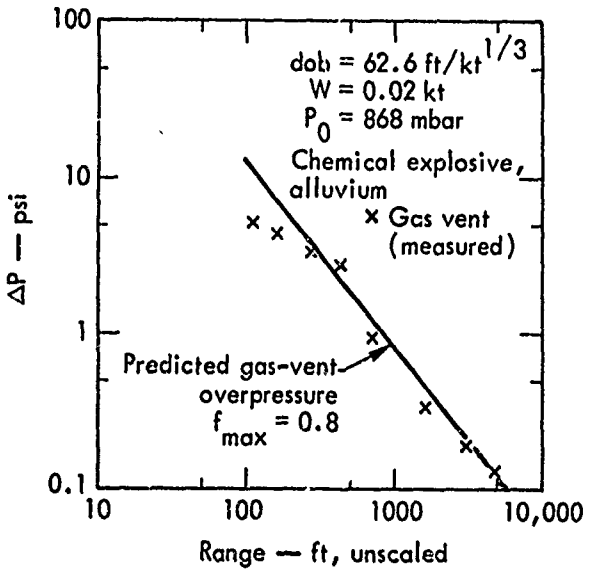

Fig. 21. Observed and predicted airblast overpressures for Stagecoach II.

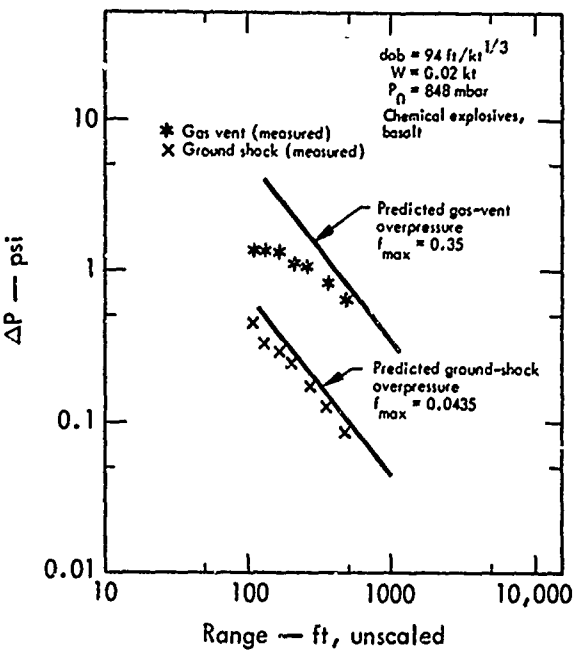

Fig. 22. Observed and predicted airblast overpressures for Buckboard 11.

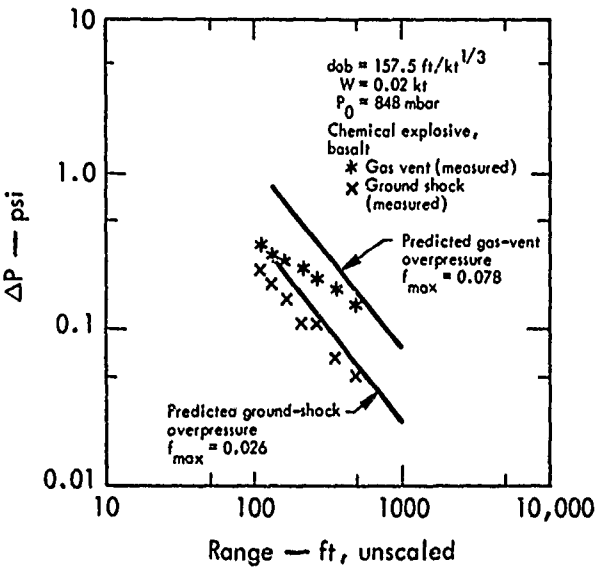

Fig. 23. Observed and predicted airblast overpressures for Buckboard 12.

= 644 ft/kt$^{1/3}$ and R_s = 810 ft/kt$^{1/3}$. Their overpressures are plotted in Fig. 6. These overpressures are high relative to the ground level fitted line by factors of 1.77 and 1.63, respectively. All other elevated gages, at longer ranges, gave

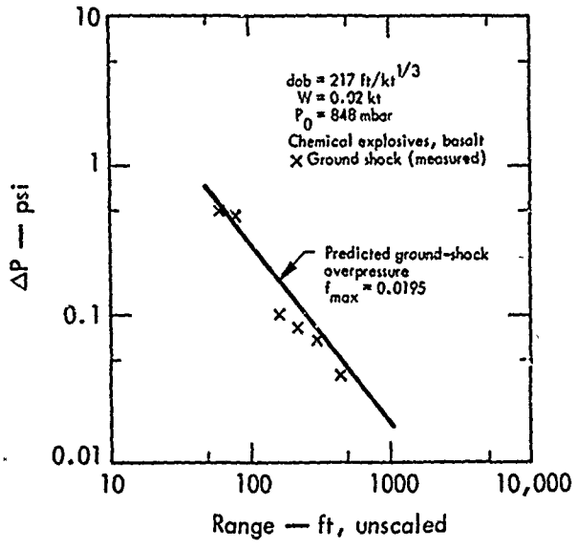

Fig. 24. Observed and predicted airblast overpressures for Buckboard 13.

peak overpressures which fell very close to the ground level peak overpressures.

Pre-Schooner II also had a number of elevated gage measurements. These data included both gas-vent and ground-shock overpressures. The results are shown in Fig. 5. Again, the close-in elevated overpressures are high, but those at longer ranges appear consistent with ground level measurements. The close-in ground shock overpressures are definitely high: the first (R_s = 410 ft/kt$^{1/3}$, angle from the vertical θ = 59 deg) is high by a factor of 1.45. The next (R_s = 756 ft/kt$^{1/3}$, θ = 34 deg) is a factor of 2.04 high. The third (R_s = 1260 ft/kt$^{1/3}$, θ = 23 deg) lies a factor of 3.21 above the ground level overpressures. All the more distant elevated gages (R_s = 2180 to 2780 ft/kt$^{1/3}$, θ = 40 to 81 deg) gave overpressures very close to tne ground level curve. The gas-vent overpressures reveal much the same picture. The twc close-in measurements are high by roughly 1.66 (R_s = 410 ft/kt$^{1/3}$, θ = 59 deg) and 3.46 (R_s = 1260 ft/kt$^{1/3}$, θ = 23 deg). Note that the gas-vent overpressures are high by about the same factor as the corresponding ground-shock overpressures. There is only one accurate long-range gas-vent elevated overpressure (at R_s = 2520 ft/kt$^{1/3}$, θ = 49 deg). This value may be slightly high, but it is difficult to be certain. There are no reliable ground level long-range gas-vent overpressures with which to compare it. All the ground level gages were overranged. It seems most probable that this elevated value is not high.

On the basis of this limited information, it can be tentatively concluded that the shock front is definitely inhomogeneous close-in to SGZ for both gas-vent and ground-shock overpressures. The overpressures are highest for angles close to the vertical (directly above SGZ), and drop to a minimum at ground level. However, the pressure front tends to "even out" (become more nearly hemispherical) at long ranges. Roughly speaking, close-in aerial overpressures are high by a factor of 2 (relative to ground level overpressures at the same range) at θ = 34 deg from the vertical. They are high by a factor of 3.2 at θ = 23 deg from the vertical. These effects have largely disappeared by a range of R_s = 2700 ft/kt$^{1/3}$. For $\theta > 40$ deg and $R_s > 2700$ ft/kt$^{1/3}$, aerial overpressures have decreased to essentially ground level values. The overpressures at angles closer to the vertical than 40 deg may still be somewhat high; there are no data to decide this point.

It should be noted that aerial data for both Scooter and Pre-Schooner II underwent considerable smoothing during the

course of data reduction. The above conclusions are based on the smoothed data.

There is one additional elevated ΔP value, for the Palanquin nuclear experiment. This came from a gage mounted 35 ft above the ground, at a range of 3280 ft. Unfortunately, calibration for the gage was lost. In comparing this gage tracing with the ground level gage at the same range (3280 ft), there is some indication that the aerial ground-shock-induced overpressure may be 15% higher. The difference, if real, is probably a result of slight constructive shock reinforcement (reflected shock) at the elevated gage.

Section 6
Prediction in Turnover Region (Very Close-In Airblast)

EMPIRICAL RANGE-DEPENDENT f RATIOS

The f_{max} prediction procedure of Section 5 predicts an overpressure line of slope $R_s^{-1.2}$ which fits the observed overpressure observations located highest relative to (closest to) a standard $R_s^{-1.2}$ reference line. It produces slightly pessimistic predictions at intermediate-to-long ranges from subsurface explosive events. However, it predicts overpressures which are excessive at close-in ranges, near the turnover region of the curve. Overpressures in the close-in region, generally of interest only for scientific work and close-in gage sensitivity settings, may be predicted using the procedures presented in this section.

The turnover region is a result of two effects mentioned earlier: gages inside the rising mound radius "see" a local or ground-transmitted ground-shock overpressure, rather than the combined effect of the entire mound piston. There is naturally a transition region between the large "combined" overpressures at longer ranges and the relatively small local overpressures inside the piston area. Likewise, the nearby gages are partially shielded from the gas-vent pulse by the height and general configuration of the rising mound. Again, there is a transition region between the near and distant gages. These effects will be discussed from an empirical viewpoint, and a rough method will be developed for predicting them.

The approach used is to compare the observed overpressures as functions of range with a standard $R_s^{-1.2}$ line, and to analyze f-values as functions of scaled range. If overpressures followed a precise $R^{-1.2}$ attenuation with range, f would be constant at all ranges and always equal to f_{max}. Since the experimental data show that overpressure curves turn over close to SGZ, the close-in f values will decrease below f_{max}. The behavior of the turnover can be examined by taking a ratio $f(R_s)/f_{max}$ and plotting it as a function of range. This ratio has been calculated for the best of the available experiments, particularly those which have good close-in overpressure measurements. The results are plotted in Figs. 25 through 28.

It will be noted that all curves show the characteristically decreasing ratio

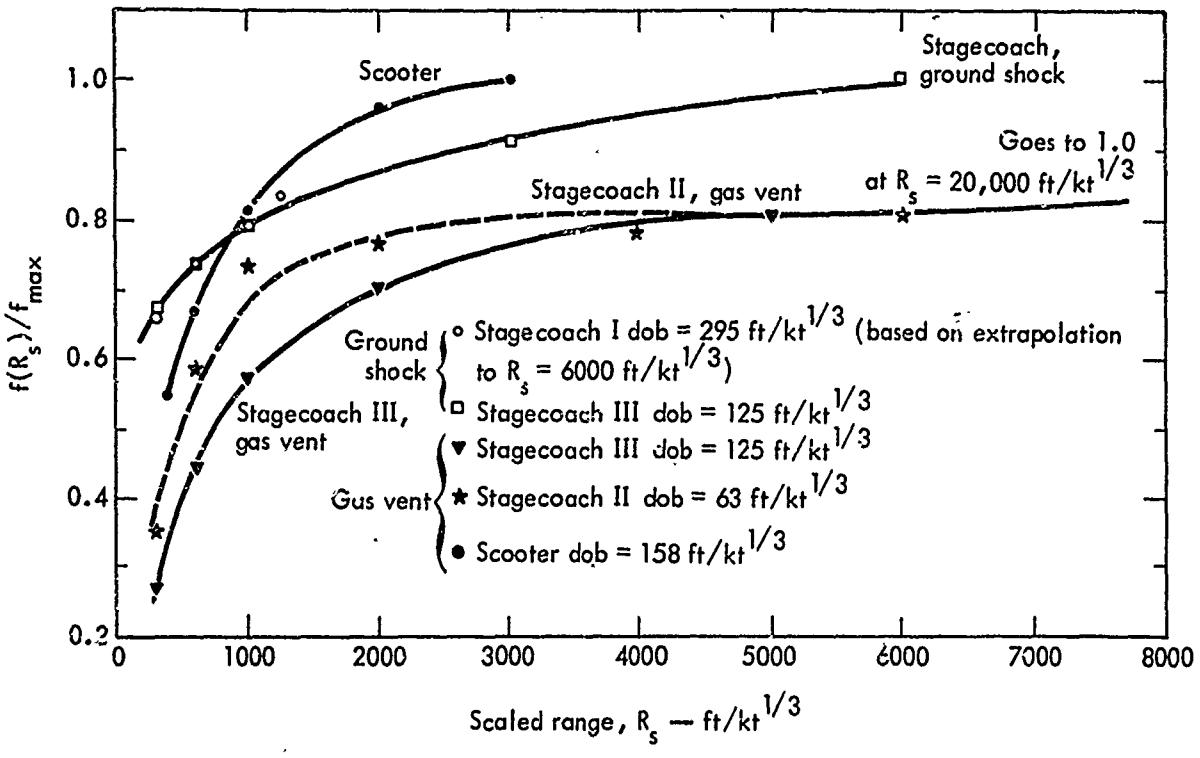

Fig. 25. Ratio $f(R_S)/f_{max}$ as a function of scaled range for Stagecoach and Scooter ground-shock and gas-vent overpressures (chemical explosive in alluvium).

moving in toward SGZ. There are two distinct sorts of decrease. Far from SGZ, the curves are smooth, almost straight lines, with gradually steeper slopes close to SGZ. Very close in, they suddenly undergo a sharp turnover. The shallow part of each curve represents a gradual deviation from $R^{-1.2}$ slope, perhaps approaching R^{-1} before the turnover occurs. The very steep close-in portion is the true turnover.

CHEMICAL EXPLOSIVES TURNOVER CURVES

Figure 25 shows the curves for chemical explosives in alluvium. Mean curves have been fitted through some of the better established points. Gas-vent curves are shown for Scooter and Stagecoach II and III. A ground-shock curve is fitted through Stagecoach I and III data. One fact is immediately evident. The gas-vent curves all begin to turn over sharply at long ranges from SGZ. The well-defined gas-vent turnover region extends at least from R_s = 300 ft/kt$^{1/3}$ to R_s = 1500 or 2000 ft/kt$^{1/3}$. The ground-shock curve (based only on Stagecoach III and extrapolated Stagecoach I data) is very shallow—obviously the slope does not deviate much from $R^{-1.2}$, even as close as $R_s \approx$ 1000 ft/kt$^{1/3}$. The hint of a sharp turnover begins only at R_s = 300 to 600 ft/kt$^{1/3}$. The very close-in behavior of this turnover cannot be defined because Stagecoach overpressure measurements were not taken closer than $R_s \approx$ 300 ft/kt$^{1/3}$.

Figure 26, chemical explosives in strong rock, gives further information

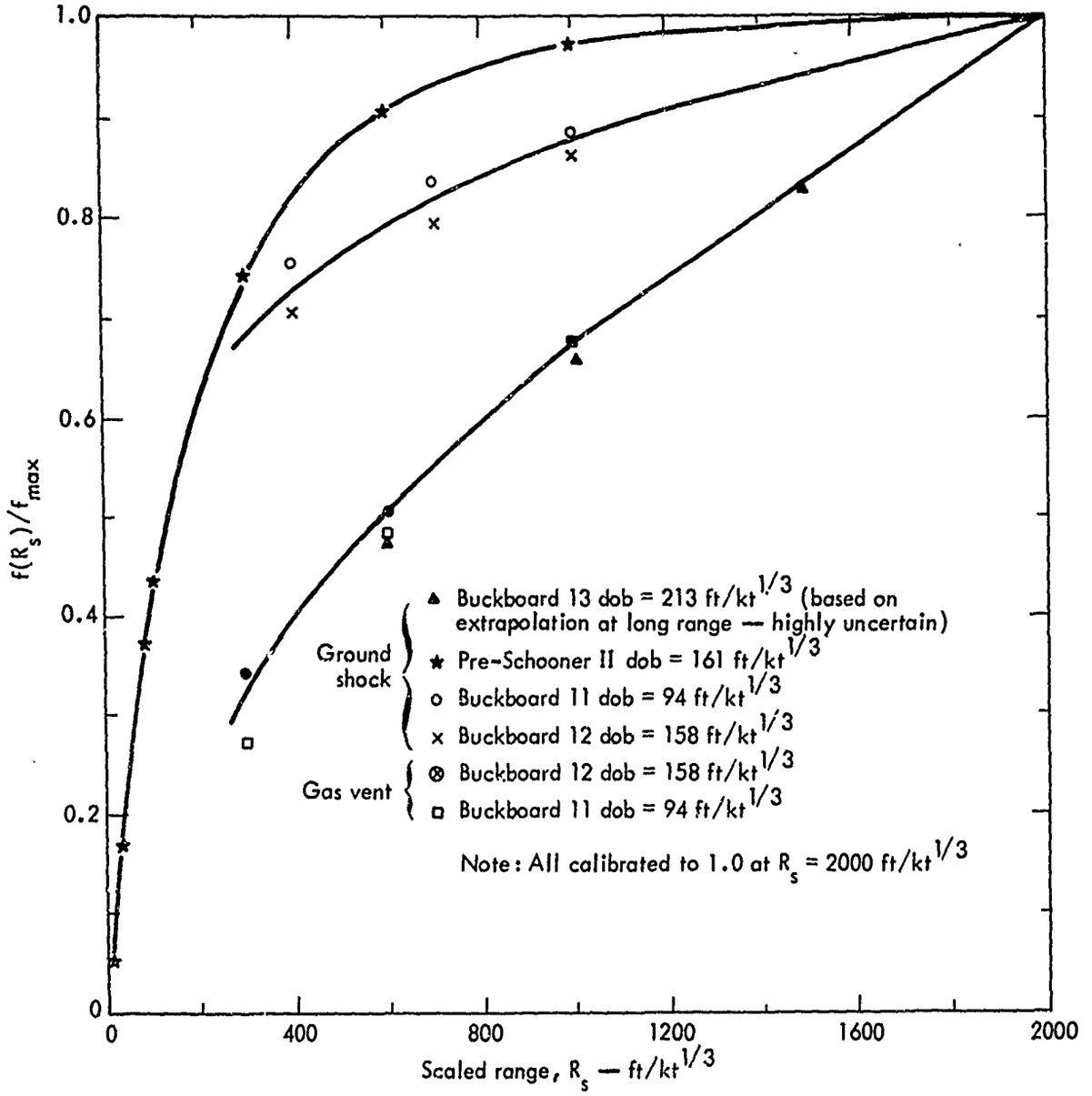

Fig. 26. Ratio $f(R_S)/f_{max}$ as a function of scaled range for Buckboard and Pre-Schooner ground-shock and gas-vent overpressures (chemical explosive in basalt and rhyolite, respectively).

about the close-in turnover. Pre-Schooner II had accurate close-in ground-shock overpressures, which define the shape of the curve in the turnover region. The $f(R_s)/f_{max}$ ratio is close to one at long ranges (little deviation from $R^{-1.2}$ slope). A sharp turnover occurs inside R_s = 300 to 600 ft/kt$^{1/3}$. This sharp turnover region definitely extends inside the ground-piston area, $R_s \approx 200$ ft/kt$^{1/3}$. Ground-shock overpressures from Buckboard 11 and 12 (Fig. 26, middle line) show the same trend, although they do not go close enough to define the turnover. There is a gradual deviation from $R^{-1.2}$ at long ranges, but the slope begins to

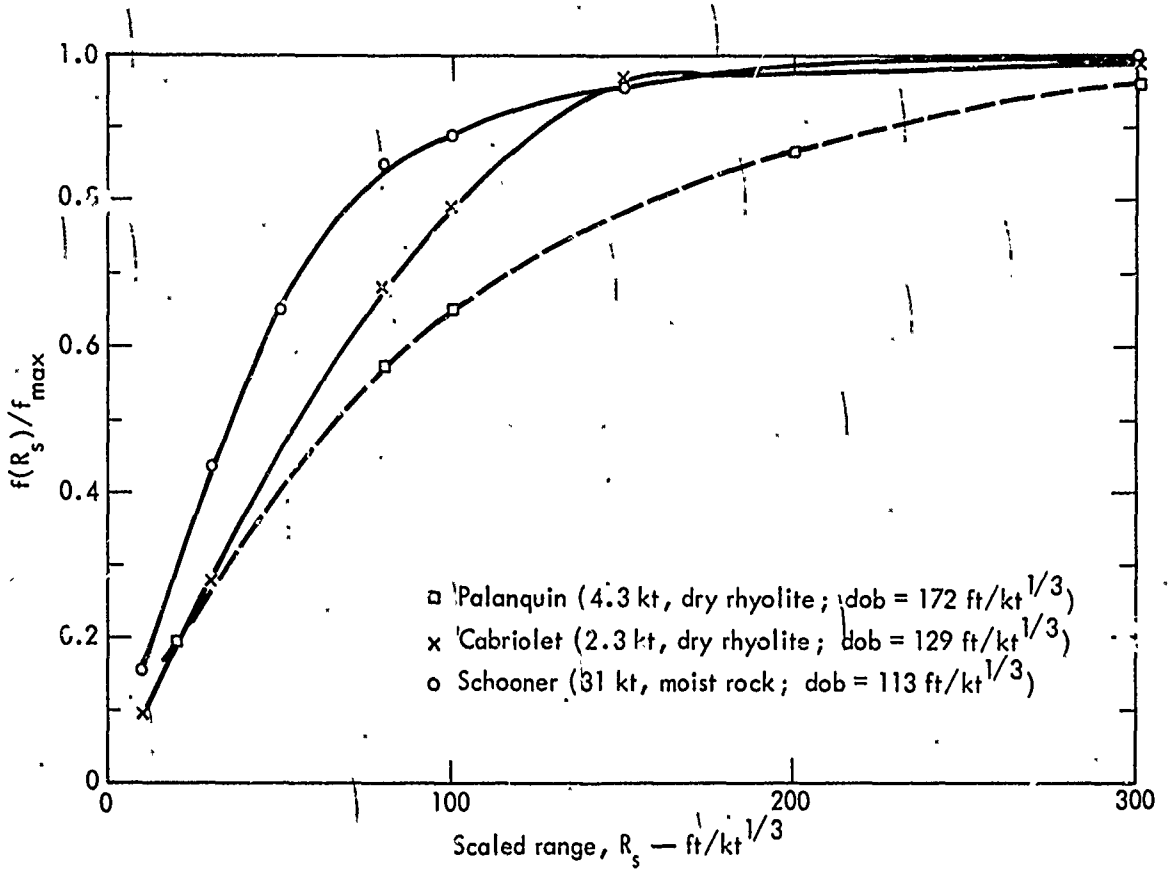

Fig. 27. Ratio $f(R_S)/f_{max}$ as a function of scaled range for Cabriolet, Schooner, and Palanquin ground-shock overpressures (nuclear detonations).

increase by $R_s = 400$ $ft/kt^{1/3}$. Gas-vent overpressures from Buckboard 11 and 12 (Fig. 26, lower line) reveal quite a different picture. The gas-vent f-values show a steep decrease, indicative of sharp deviation from $R^{-1.2}$ behavior. The deviation is quite appreciable at R_s = 1000 $ft/kt^{1/3}$. Evidently, this distance is already within the turnover region. The most distant overpressure measurements from these two experiments lie near $R_s \approx 1700$ $ft/kt^{1/3}$, and are probably still in the outer boundaries of the turnover region. This fact accounts for the curiously low attenuation rate of the fitted lines ($\lesssim R^{-1}$). Ground-shock measurements from Buckboard 13 appear to behave like the gas-vent curves. This indication is very dubious, because Buckboard 13 overpressures were low (deeply buried experiment) and showed enormous scatter. The indicated small attenuation rate (and thus the steep $f(R_s)/f_{max}$ curve) is based on an extrapolated straight line fitted through only three points. A fourth point slightly farther out indicates higher attenuation, on the order of $R^{-1.2}$. Thus, a reasonable change of the unreliable fit of Buckboard 13 could cause it to behave like the other ground-shock curves (Buckboard 11 and 12).

NUCLEAR TURNOVER CURVES

Three well-observed nuclear experiments* give still better information on

*Palanquin, Schooner, and Cabriolet, all in strong rock.

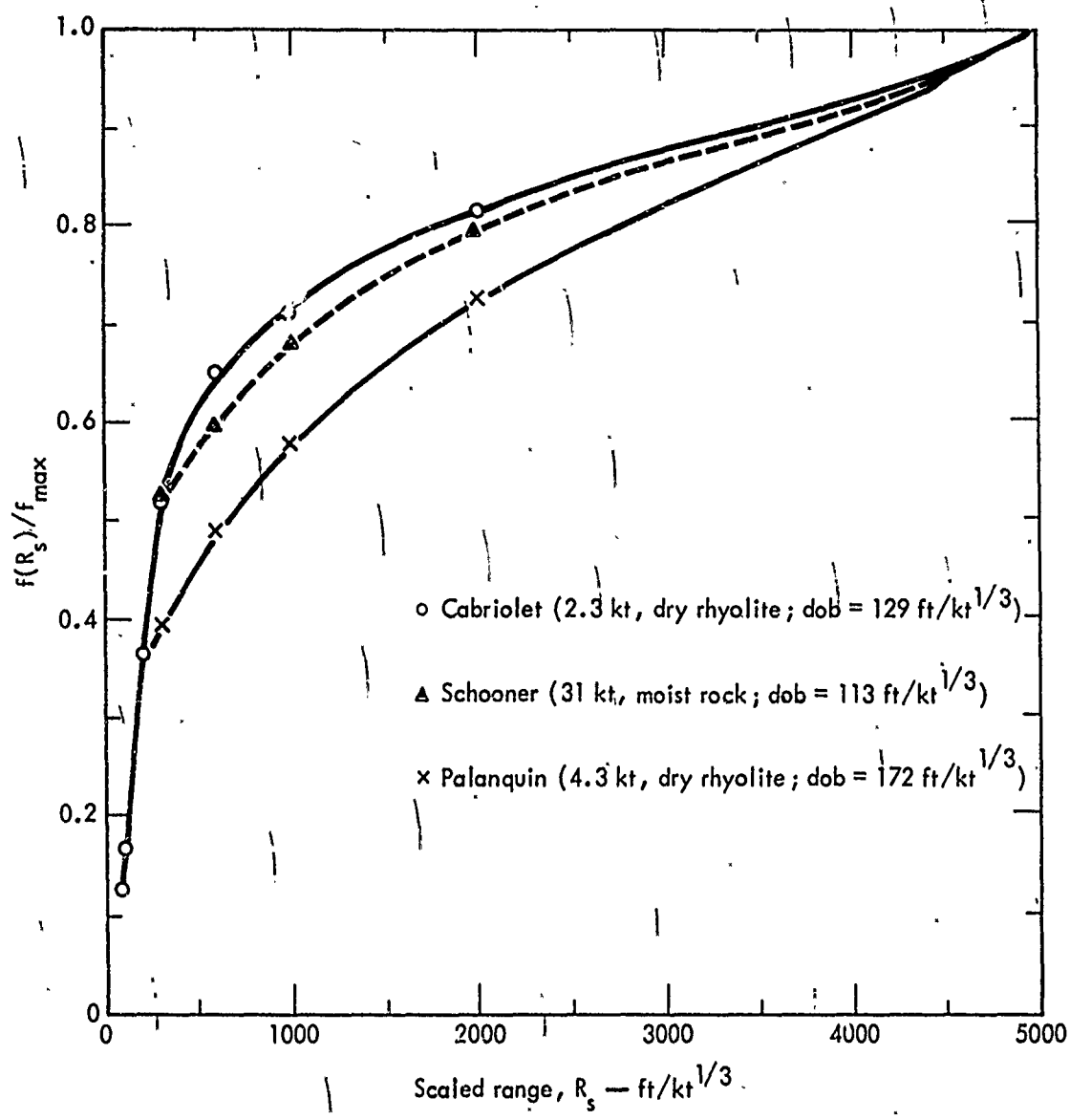

Fig. 28. Ratio $f(R_s)/f_{max}$ as a function of scaled range for Cabriolet, Schooner, and Palanquin gas-vent overpressures (nuclear detonations).

very close-in airblast. These events are particularly useful in establishing the ground-shock turnover very close to SGZ. Figure 27 shows the ground-shock $f(R_s)/f_{max}$ ratios only (note that the values plotted in the figure extend no farther than R_s = 300 ft/kt$^{1/3}$). Curves for the three experiments are quite similar. The sharpest turnover occurs inside R_s = 150 to 200 ft/kt$^{1/3}$. This is the transition region where smaller ground-transmitted local overpressures become dominant, and it is quite well-defined in Fig. 27. The Palanquin curve appears shallower than the other two and remains low at slightly greater scaled ranges. Palanquin was at a somewhat deeper dob. The effective ground piston is larger and less well-defined for a deep experiment and the local overpressures are lower; thus, the transition from ground-transmitted to air-transmitted pulse is

less sharp; the fitted overpressure curve tends to be a smoothed curve of gradually changing slope. The Palanquin curve appears shallow because the edge of the ground-piston effect is not "seen" as sharply in the limited number of overpressure data points.

The nuclear experiments also demonstrate gas-vent turnover quite nicely. In Fig. 28, the overpressures begin to drop below $R^{-1.2}$ behavior far from SGZ. Appreciable deviations occur around R_s = 2500 ft/kt$^{1/3}$. The sharpest part of the turnover falls in the range R_s = 200 to 2000 ft/kt$^{1/3}$. Cabriolet defines the extreme inner region of the turnover. Sharp dropoff continues near SGZ. Inside $R_s \approx$ 200 ft/kt$^{1/3}$, $f(R_s)$ decreases to about 0.3 to 0.4 times f_{max}. Evidently, the close-in ground level gages are very well shielded from the gas-vent pulse. This is the expected effect, since venting occurs near the crown (separated from near gages) and shielding by the body of the mound is greatest close-in. Again, the Palanquin curve lies significantly below and is shallower than its two companions. In this case, the effect is very probably real. Gas venting for deep experiments (Palanquin) occurs later in the mound history, near the top of the mound. Basic geometry for deep bursts also indicates that the gas-vent pulse energy should be concentrated in a smaller vertical angle (i.e., the vent should be more strongly directed toward the vertical). Therefore, close-in gages are well-shielded, with most of the pulse energy escaping in a near-vertical direction (not seen by the gages). Since the shock is strongly concentrated in one direction, more time is required for the shock front to "even out" into a nearly hemispherical configuration. The shock energy feeds back more slowly to ground level. The overpressures are relatively lower (and $f(R_s)/f_{max}$ is relatively smaller) at close to intermediate ranges before the shock front approaches a hemisphere.

PREDICTION PROCEDURES

Close-in overpressures can be predicted using the above results. Corrections are applied only for $R_s < 3000$ ft/kt$^{1/3}$ for gas-vent overpressures, or for $R_s < 300$ to 600 ft/kt$^{1/3}$ for ground-shock overpressures. To predict, simply make a single-charge prediction, as in Section 5. Then select an appropriate curve from the turnover region figures using the following guidelines:

(1) For all chemical explosives in alluvium: Use Fig. 25. Use the Scooter curve for gas-vent predictions. Use the Stagecoach I and III ground-shock curve for ground-shock predictions.

(2) For chemical explosives in basalt or rhyolite: Use Fig. 26. Use the bottom Buckboard 11 and 12 curve for gas-vent predictions. Use the Pre-Schooner II curve (upper curve) for ground-shock predictions.

(3) For nuclear experiments in strong rock: Use Fig. 27 for ground-shock predictions. Use Fig. 28 for gas-vent predictions. Select the curve which is closest to the proposed experiment in dob.

Caution:

The above gas-vent curves are valid only for experiments near optimum depth of burst. Shallow experiments may be

underpredicted close-in, since airblast is less concentrated toward the vertical at shallow depths for reasons discussed under "Nuclear Turnover Curves" (Palanquin), above. In addition, the nuclear curves apply only to well-stemmed events in dry high-strength rock.

Next, use the selected curve to correct the Section 5 ($R_s^{-1.2}$) predicted overpressures. The procedure is as follows: at any scaled range $R_s < 3000$ ft/kt$^{1/3}$ for gas-vent overpressures, or $R_s < 300$ to 600 ft/kt$^{1/3}$ for ground-shock overpressures, read the value of $f(R_s)/f_{max}$ from the curve. Then multiply the predicted ΔP at R_s by $[f(R_s)/f_{max}]$. This gives the correct predicted overpressure. If desired, predict overpressures for several close-in ranges, plot, and draw a smooth curve through the points.

Section 7
Row- and other Multiple-Charge Configurations

This section discusses row- and multiple-charge experiments, data, and factors which influence airblast overpressures from multi-charge configurations. Section 8 presents a procedure for predicting airblast overpressures from multi-charge detonations.

FACTORS INFLUENCING ROW-CHARGE AIRBLAST

Multiple-charge events may occur in simple or complex configurations, with varied delay times between successive detonations. Thus far, most airblast data refer to simultaneously detonated row and square array events. The simplest cases will be examined for purposes of empirical prediction.

Three new factors appear in the functional dependence of row-charge overpressures: (1) the number of charges in the row, "n"; (2) the scaled spacing between the charges S (ft/kt$^{1/3}$)— S = (charge separation, in ft)/(W in kt)$^{1/3}$; and (3) the azimuth from the row axis at which overpressure is measured. The overpressures are larger perpendicular to the axis of the row ($\perp$ to the row) than off the ends of the row ($\parallel$ to the row).

It must be determined how these factors control row-charge overpressures. One approach is to compare single-charge experiments with row charges. The ideal situation would be to compare two events with all factors identical except the number of charges. Unfortunately, many of the available comparison experiments are also influenced by differences in medium, burial depth, explosive type, yield, etc.

PREVIOUS EMPIRICAL PREDICTION STUDIES

In an early attempt to study row-charge effects, Vortman[15,16] compared overpressures from Dugout (5-charge row, 20-ton nitromethane charges in basalt) to those from a small experiment (11-charge row, 8-lb charges in alluvium). On the basis of these two row detonations, Vortman found that peak overpressure at a given scaled range

depended mainly on "n." He established an empirical dependence of the form:

$$\Delta P \ (\perp \text{ to row}) = n^{0.7} \Delta P \ (\text{single charge})$$

$$\Delta P \ (\parallel \text{ to row}) = n^{0.25} \Delta P \ (\text{single charge})$$

where "ΔP (single charge)" is the expected overpressure at a given range for one of the charges in the row (or for one charge of average yield at the average dob for a row of differing charges); "ΔP (⊥ to row)" and "ΔP (∥ to row)" are the respective overpressures at the same range perpendicular to and off the end of the row.

Unfortunately, the excellent fit obtained for the above two experiments proved partly fortuitous. Vortman later showed that the Dugout peak overpressures were ground-shock-induced, while those from the small-charge row were due to gas vent. Thus, inconsistent experimental conditions invalidated the comparison.

Better estimates of row-charge airblast reinforcement may be made by comparing similar large-yield detonations. There are only two such events for which complete airblast data exist. They are Dugout (above) and Buggy (5-charge row, 1.1-kt nuclear charges, also in basalt). Dugout overpressures can be compared to the very similar Buckboard 13 single-charge experiment (TNT, basalt).[4,15,16] Buggy can be compared to several single-charge nuclear detonations in strong rock. In both cases, perpendicular and off-the-end overpressures exceed the corresponding single-charge overpressures by about the same amounts. Both experiments are consistent with a relation of the form:

$$\left.\begin{array}{l} \Delta P \ (\perp \text{ to row}) \\ \quad = n^{0.7} \Delta P \ (\text{single charge}) \\ \Delta P \ (\parallel \text{ to row}) \\ \quad = n^{0.25} \Delta P \ (\text{single charge}) \end{array}\right\} \begin{array}{l} \text{for} \\ \text{ground} \\ \text{shock} \\ \text{peaks} \\ \text{only} \end{array}$$

This coincides with Vortman's relation determined using Dugout and a small-charge row. However, the data are still based on just two experiments, both of which are 5-charge rows in basalt.

In other work, Vortman[6] attempted to eliminate the experimental inconsistencies of the above tests by observing carefully controlled row shots in a single medium (dry lake playa). All detonations used identical 64-lb charges at fixed depths of burst. The tests encompassed rows of 2 to 25 charges, at two different spacings. Thus, it was hoped, the effects of n and of charge spacing could be isolated.

Some difficulties arose during the course of these experiments. Measured overpressures were not reproducible, airblast attenuation with range was not reproducible and deviated from that expected for large-yield shots, the airblast waves changed form with range, etc. Some of the problems were related to the use of small-yield charges. Small-charge experiments often show nonrepeatable effects, and results may not extrapolate perfectly to larger yields. Other problems may be common to all row-charge experiments. First, measurements were taken over a rather restricted range of distances. As mentioned previously, the overpressure peaks for a row charge are separated in time. They achieve partial combination and converge on a reasonable attenuation rate only at large scaled distances. The

change in waveform with range is explained by shielding effects: the closest gages are partially protected from the gas-vent pulse by mound shielding and the upward direction of the vent. Thus, close-in gas-vent overpressures are low relative to the ground-shock values. They grow relatively larger at long ranges, until the gas-vent too converges on $R^{-1.2}$ attenuation. Close-in mound shielding may be further increased off the ends of the row by the presence of several successive intervening mounds at the time of gas vent. Obviously, the various influences combine to decrease the gas-vent amplitude seen by nearer gages. The shock wave will be far more distorted. It will require a greater distance to even out into a more hemispherical configuration and approach $R^{-1.2\cdots}$ attenuation. These effects were well-observed during Vortman's experiments. In some cases, the gas-vent peak was actually smaller than the ground-shock pulse close-in, but became slightly larger at great ranges. It is now evident that no reasonable attenuation rates or transmission factors can be based on close-in gas-vent data, particularly for row charges.

In spite of these difficulties, it is believed that Vortman's derived ratios (ratio of row charge to single charge airblast) are roughly correct for charges of small yield. His results may be briefly summarized as follows: The ratios of row charge to single charge for "mean" overpressures (smoothed to an approximate fit over all ranges) were determined for all experiments. It was found that the ratio of row charge to single charge airblast did indeed follow a power law relationship to the number of charges in the row. Vortman's empirically derived relations are:

Scaled intercharge spacing, S, of 165 ft/kt$^{1/3}$:

$$\Delta P\ (\perp \text{ to row}) = n^{0.9}\ \Delta P\ (\text{single-charge})\ \text{for ground-shock}$$
$$= n^{0.9}\ \Delta P\ (\text{single-charge})\ \text{for gas-vent}$$
$$\Delta P\ (\parallel \text{ to row}) = n^{0.4}\ \Delta P\ (\text{single-charge})\ \text{for ground-shock}$$
$$= n^{0.7}\ \Delta P\ (\text{single-charge})\ \text{for gas-vent}$$

Scaled intercharge spacing, S, of 252 ft/kt$^{1/3}$:

$$\Delta P\ (\perp \text{ to row}) = n^{0.8}\ \Delta P\ (\text{single-charge})\ \text{for ground-shock}$$
$$= n^{0.4}\ \Delta P\ (\text{single-charge})\ \text{for gas-vent}$$
$$\Delta P\ (\parallel \text{ to row}) \cong \Delta P\ (\text{single-charge})\ \text{for ground-shock}$$
$$\cong \Delta P\ (\text{single-charge})\ \text{for gas-vent}$$

Note that, for the wider spacing, $\Delta P\ (\parallel \text{ to row}) \approx \Delta P\ (\text{single-charge})$. Wide spacing increased the time interval between overpressure peak arrivals. The increased interval was sufficient so that overlap of the peaks was negligible, and the peaks were not able to combine. The overpressure was effectively decreased to single-charge values. Sometimes it is not feasible to use wide charge spacing. However, the increased time interval can be duplicated by using delayed detonations. It is necessary to retard the successive peak arrivals by an amount equivalent to the delay due to wider charge spacing, above. In Vortman's experiment, the

spacing was increased by 53% over optimum spacing. Successive peak arrivals can be retarded by the same amount if successive detonations are delayed by

Delay time (sec)

$$= 0.53 \frac{\text{Optimum spacing (in ft)}}{\text{Sonic velocity in air (ft/sec)}}.$$

Delay times of this order are probably tolerable without greatly decreasing the volume of the crater excavated. Note that this delay time will apply only off the starting end of the row (end where the detonation series is initiated). The peaks will arrive closer together off the other end, possibly increasing the overpressure. However, in many instances, damage is likely to be of concern in one particular direction. This technique provides a means of decreasing row-charge overpressures to nearly single-charge values in that direction.

ROW-CHARGE f_{max} PREDICTION METHOD

Returning to the problem of simultaneous detonations, there remains one very important question: Which of the empirical relations is correct for predicting large-yield airblast? One disadvantage of the above studies is that they tend to weight or to emphasize close-in overpressures. As has been seen, the row-charge pulses are still in the process of combining at these ranges, and have not converged on a reasonable attenuation rate. Therefore, predictions based on close-in overpressures are in danger of underpredicting at longer ranges. The f_{max} approach will be used, based on overpressures at the farthest available ranges from SGZ. The f-values at these ranges should be truly comparable to the f_{max} values shown in Figs. 13a and 14a.

This approach is particularly applicable to the large experiments Buggy and Dugout, since measured overpressures extend to about R_s = 10,000 and 15,000 ft/$kt^{1/3}$, respectively. At these long ranges, even gas-vent overpressures have essentially converged on $R^{-1.2}$ attenuation. Therefore, row-charge f-values can be safely compared to their single-charge counterparts. A "difference factor" can be found which tells how many times larger row charge ΔP's are than those for a comparable single charge. The difference factor is given by:

Difference Factor

$$= \frac{f_{\text{long range}}\ \text{(row charge)}}{f_{max}\ \text{(single charge)}}$$

$$= \frac{\Delta P\ \text{(long range, row charge)}}{\Delta P\ \text{(same range, single charge)}},$$

where the charges in the row and the single charge are emplaced at the same dob, and in the same medium. The f_{max} (single-charge) may be taken from Figs. 13a and 14a, or from a similar single-charge experiment of the same "per charge" yield at the same dob.

The number of charges in the row, n, is known. Therefore, assuming an empirical fit of the form ΔP (row charge) = n^B ΔP (single charge), the exponent B can be found:

$$n^B = \frac{\Delta P\ \text{(row charge)}}{\Delta P\ \text{(single charge)}}$$

$$= \frac{f_{max}\ \text{(row)}}{f_{max}\ \text{(single charge)}}$$

= difference factor.

Results are listed in Tables 4 and 5. The values of "B" are in the last column of each table. In most cases, single charge f_{max} values from Figs. 13a and 14a were used in the calculations. The B's ⊥ to and ∥ to the row are tabulated for all row-charge experiments. In some instances, more than one exponent is listed. These values are for several different ranges (i.e., for individual overpressure data points) rather than just the maximum range. In one case (Rappleyea array charge, dob = 189 ft/kt$^{1/3}$), a second set of B values is given in parentheses after the first set. These second B values are calculated on the basis of measured

Table 4. Calculated B exponents for observed row and array detonations (ground-shock B values).

Experiment (dob, medium)	$f_{row\ charge}$	f_{max} or ($f_{single\ charge}$)	Difference factor	$B\left(\Delta P_{row} = n^{B} \times \Delta P_{single\ charge}\right)$
Dugout[a]	⊥ 0.0557	0.0194	2.87	⊥ 0.655
(217 ft/kt$^{1/3}$, basalt)	∥ 0.0330	0.0194	1.70	∥ 0.33
Buggy[a]	⊥ 0.0467	0.0147[b]	3.18	⊥ 0.719
(130 ft/kt$^{1/3}$, basalt)	∥ 0.0209	0.0147[b]	1.42	∥ 0.218
Vortman[a]	⊥ 0.0545-0.0744	0.0194	2.81-3.84	⊥ 0.641-0.835
(217 ft/kt$^{1/3}$, playa)	∥ 0.0223-0.0311	0.0194	1.15-1.603	∥ 0.087-0.293
Rappleyea[c,17]	0.0452	0.0221 or (0.0216)[d]	2.045 or (2.1)	0.445 or (0.460)
	0.0764	0.0221 or (0.0281)	3.46 or (2.72)	0.77 or (0.62)
(189 ft/kt$^{1/3}$, playa)	0.0806	0.0221 or (0.0350)	3.65 or (2.30)	0.805 or (0.517)
Rappleyea[c]	0.0447	0.0168	2.66	0.608
(252 ft/kt$^{1/3}$, playa)	0.0475	0.0168	2.83	0.646
	0.0436	0.0168	2.60	0.594
Rappleyea[c]	0.0323	0.0136	2.38	0.539
(315 ft/kt$^{1/3}$, playa)	0.0360	0.0136	2.65	0.605
	0.0485	0.0136	3.57	0.79
Dugout (Vortman's results, derived solely from a comparison with Buckboard 13 as the single charge)		—	⊥ 3.28	⊥ 0.738
		—	∥ 1.39	∥ 0.204

[a]Five charges in a row; assume n = 5.

[b]Nuclear line, Fig. 13d.

[c]Five charges in a square array, using n = 5.

[d]Parentheses indicate alternate estimate based on Rappleyea comparison single-charge detonation.

Table 5. Calculated B exponents for observed row and array detonations (gas-vent B values).

Experiment (dob, medium)	$f_{row\ charge}$	f_{max} or ($f_{single\ charge}$)	Difference factor	B ($\Delta P_{row} = n^B \times \Delta P_{single\ charge}$)
Dugout	⊥ 0.021	0.0066[a,b] or 0.021[a,c]	3.18 or 1.0	⊥ 0.719[a] or 0.0[a]
(217 ft/kt$^{1/3}$, basalt)	∥ 0.0199	0.0066[a,b] or 0.021[a,c]	3.02 or 0.95	∥ 0.686[a] or 0.0[a]
Buggy	⊥ 0.0262	0.0099	2.65	⊥ 0.605
(130 ft/kt$^{1/3}$, basalt)	∥ 0.0222	(nuclear dry rock line)	2.24	∥ 0.501
Vortman	⊥ 0.0249-0.0544	0.020 0.020	1.245-2.72	⊥ 0.136-0.62
(217 ft/kt$^{1/3}$, playa)	∥ 0.0192-0.0472	0.020 0.020	1.0-2.36	∥ 0.0-0.534
Rappleyea[17]	0.082	0.0375 or (0.0579)[d]	2.19 or (1.417)	0.487 or (0.216)
	0.149	0.0375 or (0.0785)	3.97 or (1.90)	0.856 or (0.398)
(189 ft/kt$^{1/3}$, playa)	0.161	0.0375 or (0.1026)	4.3 or (1.57)	0.905 or (0.28)
Rappleyea	0.0238	0.0099	2.40	0.544
(252 ft/kt$^{1/3}$, playa)	0.0245 ?	0.0099	2.48	0.564
	0.0239	0.0099	2.42	0.549
Rappleyea	0.00968	0.0041	2.36	0.533
(315 ft/kt$^{1/3}$, playa)	0.00936	0.0041	2.28	0.512
	0.01320	0.0041	3.22	0.726

[a] B = 0 for Dugout compared to the chemical explosive gas-vent curve (i.e., Dugout row f_{max} coincides with the fitted curve single-charge f_{max}). This fact indicates that the deeply buried Dugout nitromethane row-charges are behaving in a manner rather similar to nuclear explosives in dry high-strength rock (in regard to gas-vent airblast overpressures), or that the chemical explosive gas-vent f_{max} curve in Fig. 14b is too high at dob = 217 ft/kt$^{1/3}$. The dashed line might be more appropriate at this depth. In order to resolve the difficulty, Dugout results are provisionally compared to the gas-vent f_{max} line for nuclear detonations in dry high-strength rock (Fig. 14b), giving the higher values of B listed above.

[b] Nuclear line, dry medium nuclear detonations, Fig. 14b.

[c] Chemical explosive curve, Fig. 14b.

[d] Parentheses indicate alternate estimate based on Rappleyea's comparison single-charge detonation.

overpressures from an identical single-charge experiment at the same ranges and under the same conditions.

Results of the row-charge experiments (Dugout, Buggy, and one of Vortman's small-charge rows) are consistent with earlier studies:

ΔP (⊥ to row) $\approx n^{0.7}$ ΔP (single charge) for ground-shock

$\approx n^{0.7}$ ΔP (single charge) for gas-vent

$$\Delta P \ (\| \text{ to row}) \approx n^{0.25} \ \Delta P \ (\text{single charge}) \text{ for ground-shock}$$
$$\approx n^{0.50} \text{ to } n^{0.70} \ \Delta P \ (\text{single charge}) \text{ for gas-vent}$$

The exponents for the Rappleyea five-charge square arrays are also of interest:

$$\Delta P \ (\text{square array}) \approx n^{0.6} \text{ to } n^{0.8} \ \Delta P \ (\text{single charge}) \text{ for gas-vent and ground-shock}$$

There is some indication that the exponents may be slightly smaller for the gas-vent pulse.

The contradiction between large-yield experiments and the aforementioned small-charge study is still present. Any analysis of the large-yield strong rock data gives roughly the same result for ground-shock-induced overpressures:

$$\Delta P \ (\perp \text{ to row}) \approx n^{0.7} \ \Delta P \ (\text{single charge}) \text{ for ground-shock}$$
$$\Delta P \ (\| \text{ to row}) \approx n^{0.25} \ \Delta P \ (\text{single charge}) \text{ for ground-shock}$$

Vortman, from the small charge row comparisons, found:

$$\Delta P \ (\perp \text{ to row}) \approx n^{0.9} \ \Delta P \ (\text{single charge}) \text{ for both ground-shock and gas-vent}^*$$
$$\Delta P \ (\| \text{ to row}) \approx n^{0.4} \ \Delta P \ (\text{single charge}) \text{ for ground-shock}^*$$
$$\Delta P \ (\| \text{ to row}) \approx n^{0.7} \ \Delta P \ (\text{single charge}) \text{ for gas-vent}^*$$

Part of the difference may be due to effects which are nonscaling with yield. Overpressures off the end of small-charge rows tend to be low at close distances. However, they quickly approach the perpendicular overpressures at greater ranges where the shock front is beginning to "even out" into a hemisphere, and the row appears almost as a point source. This fact explains the relatively large exponent found by Vortman[6] off the end of the small-charge rows:

$$\Delta P \ (\| \text{ to row}) \approx n^{0.4} \text{ to } n^{0.7} \ \Delta P \ (\text{single charge}).$$

For large-yield experiments, on the contrary, overpressures remain low off the ends of the row. Azimuthal variations in the shock front are permanently established, and propagate to great ranges. Apparently, these variations are "frozen in," either by local meteorological conditions or by the sheer linear dimensions of the shock front (a given scaled distance corresponds to much greater linear distance for these large experiments). Overpressure peaks still tend to combine off the ends of the row, but not completely. Redistribution of energy over the shock front is only partial, and pressure never approaches a true hemisphere. Airblast converges on $R^{-1.2}$, but it converges on a lower $R^{-1.2}$ line off the ends of the row than perpendicular to it. Thus arises the small exponent for ground-shock overpressures, $\Delta P \ (\| \text{ to row}) = n^{0.25} \ \Delta P$ (single-charge).

This entire question of nonscaling effects cannot be satisfactorily resolved until better data exist. A most useful experiment would be a large yield 10- to 20-charge row, similar to Dugout (chemical) or Buggy (nuclear) in strong rock. The results of such an experiment could be combined with those of Buggy or Dugout to establish the exponent B at all ranges, $\perp$ and $\|$ to the row. Until such information becomes available, the

*Applies to all closely spaced small charge experiments.

empirical formulae in the following section are recommended for predicting row-charge airblast.

Delayed row-charge detonations, double row detonations, and row-charge airblast for AN slurry and ANFO detonations in sandstone and weak rock are discussed in Appendix B. Use the results of that discussion to predict for ammonium nitrate and other chemical explosive detonations of intermediate yield, and for delayed and double row events.

Section 8
Buried Row- and other Multiple-Charge Prediction Procedures

To predict row-charge overpressures, perform a single-charge overpressure prediction for one charge in the row. Use its single-charge yield and dob just as if airblast were being predicted for a single charge. In those cases where successive charges in the row have different yields or dob, use the mean yield and mean dob to make the single-charge prediction.

Next, multiply the predicted overpressures at all ranges by a correction factor n^B, where n = the number of charges in the row. The correction factors are given below.

For large-yield cratering events (W $\gtrsim$ 10 tons) in strong rock, well stemmed, nuclear explosives, TNT, and nitromethane, use:

ΔP ($\perp$ to row) = $n^{0.7}$ ΔP (single charge at the same range) for ground-shock and gas-vent overpressures

ΔP ($\parallel$ to row) = $n^{0.2}$ ΔP (single charge at the same range) for ground-shock overpressures

ΔP ($\parallel$ to row) = $n^{0.6}$ ΔP (single charge at the same range) for gas-vent overpressures

Note that these relations will predict correctly using the f_{max} method for Dugout and Buggy (as in Figs. 13b, 13d, and 14b).

For moderate yield (W$\approx$ 1 to 40 tons) nitromethane and chemical explosives detonations near optimum depth (170 ft/$kt^{1/3}$) in saturated weak media, use ground-shock f_{max} (single charge) $\approx$ 0.05 to 0.06, and:

ΔP ($\perp$ to row) = $n^{0.7}$ ΔP (single charge) for ground-shock overpressures

ΔP ($\parallel$ to row) = $n^{0.41}$ ΔP (single charge) for ground-shock overpressures

(Ground-shock-induced airblast is dominant for row- and single-charge detonations near optimum depth in saturated weak media.) These relations are based on an analysis of data from the Pre-Gondola row-charge events in saturated clay shale (Tables C19 and C20 and Ref. 18).

For other row-charge detonations of smaller yield per charge (a few pounds to one ton):

ΔP ($\perp$ to row) = $n^{0.9}$ ΔP (single charge at the same range) for ground-shock and gas-vent

ΔP ($\parallel$ to row) $\approx n^{0.4}$ ΔP (single charge at the same range) for ground-shock

ΔP ($\parallel$ to row) $\approx n^{0.7}$ ΔP (single charge at the same range) for gas-vent

For all square array detonations, where n is the total number of charges in the array (n = 4 or 5):

ΔP (array) = $n^{0.65}$ to $n^{0.8}$ ΔP (single charge at same range) for ground-shock

ΔP (array) = $n^{0.6}$ to $n^{0.7}$ ΔP (single charge at same range) for gas-vent

For all aluminized ammonium nitrate slurry detonations, see Appendix B. For delayed row-charge and double-row detonations, see Appendix B.

The above procedure requires a complete single-charge airblast prediction before the row-charge prediction can be made. The preliminary single-charge prediction is often useful for comparison with the row-charge results. If a single-charge prediction is not desired, the row-charge procedure can be shortened slightly. First, calculate the dob for a single charge in the row, just as in the single-charge technique. Read off the appropriate single-charge f_{max} value (s) from Figs. 13a, 14a, or 16. Do not proceed with the remainder of the single-charge prediction. Instead, multiply f_{max} (single charge) by n^B ($\perp$ to the row). Use this new value to predict perpendicular overpressures. Next, multiply f_{max} (single charge) by n^B ($\parallel$ to the row). Use this value to predict overpressures off the end of the row. This procedure automatically multiplies all overpressures by the appropriate n^B, without the need to go through an entire single-charge prediction.

Section 9
Surface Burst Predictions

Surface bursts are frequently used for airblast calibration prior to a buried detonation, and are also useful in estimating the greatest possible airblast in case of an accident or in predicting airblast for events at very shallow depths. Therefore, a surface burst overpressure curve is included. This curve is based on the most recent data from the Canadian Distant Plain and Prairie Flat operations, and from the Sailor Hat events. These experiments cover the yield range from 50 to 500 tons, and most were near-surface TNT hemispheres or similar configurations. Overpressures derive from several different types of gages, from photogrammetric shock wave radius-time data, and from Airblast Time-of-Arrival Detector data (ABTOAD, used in the Canadian experiments). The results are thus firmly founded on several independent sources, and should be reliable to $\Delta P_s \approx 3000$ mbar. The experimental results have been tabulated, then scaled to a yield of W = 1.0 kt at an ambient pressure P_0 = 1000 mbar. The experimental and scaled results are listed in Tables C26 through C30.*

*Tables C26 through C30 are presented in Appendix C.

Individual scaled points for all experiments are plotted in Fig. 29.

A pessimistic mean curve has been fitted through the individual points in Fig. 29. This curve, shown in Fig. 30, will be used for predictions. Several points from the Distant Plain experiments have also been included in the figure. These points are included because they come from a "good" series of 20-ton experiments, and fall well below the fitted curve. The theoretical 1-kt nuclear free-airburst overpressure curve (IBM Problem M) is also plotted for comparison. It falls below the surface burst curve, as expected. Sample ΔP_m values along the IBM curve are listed in Table 6.* The IBM curve refers to free-air explosions, and cannot be used in predicting surface bursts.

TNT PREDICTIONS

To predict overpressures from any TNT surface detonation, use the upper

*More complete data for the IBM curve are given in Table C31 (Appendix C).

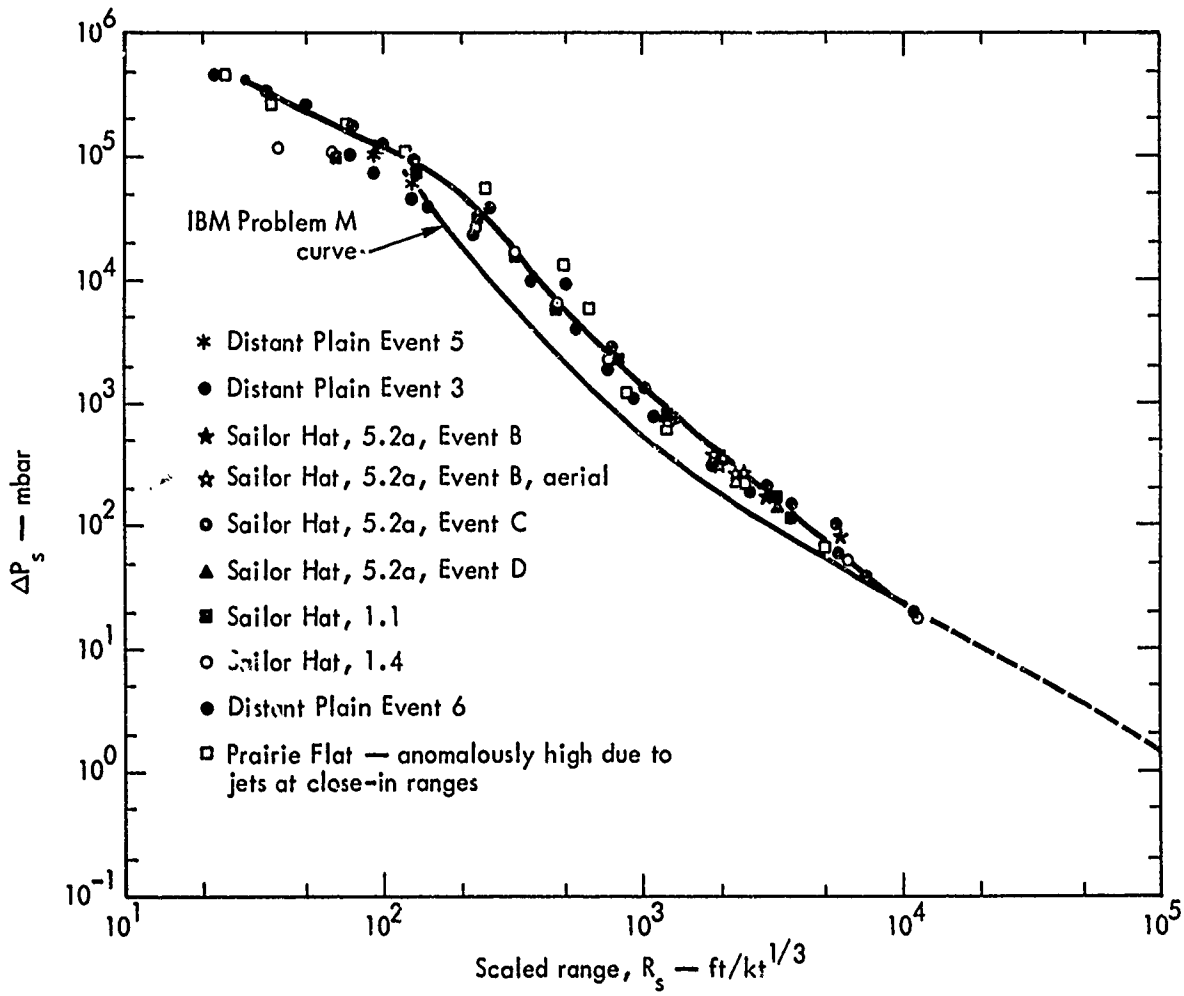

Fig. 29. Chemical explosive surface-burst overpressures (scaled to 1.0 kt at 1000 mbar).

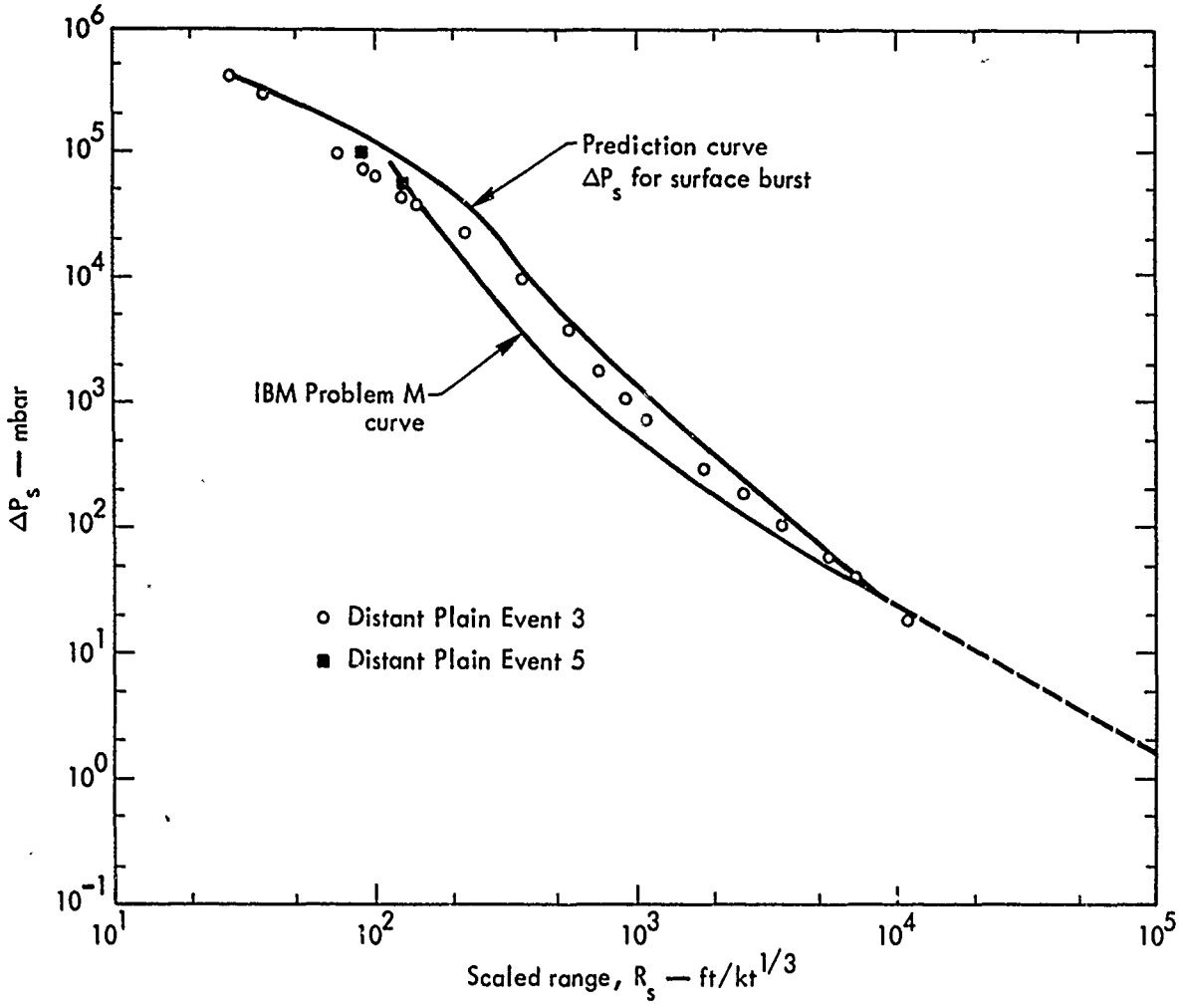

Fig. 30. General prediction curve for chemical explosive surface-burst overpressures.

Table 6. Sample points selected from IBM Problem M curve, for free-air bursts only.

P_0 = 1000 mbar ambient pressure
C_0 = 1139 ft/sec sonic velocity
Yield = 1.0 kt nuclear
R_m = scaled range, in ft/kt$^{1/3}$
ΔP_m = IBM curve overpressure, in mbar

R_m (ft/kt$^{1/3}$)	ΔP_m (mbar)
9000	25.5
5000	54.0
2000	176
1000	491
500	1930
200	17800

curve in Fig. 30. This curve gives $\Delta P_{surface\ burst}$ as a function of scaled range R_s(ft/kt$^{1/3}$), scaled to 1.0 kt at P_0 = 1000 mbar. It may be scaled back to any desired yield and ambient pressure using the scaling relations in Section 5. Prediction should be accurate for all TNT surface bursts, where W = 1 to 1000 tons.

ANFO PREDICTIONS

The above prediction method using Fig. 30 applies only to TNT and similar explosives. Overpressure data are now available from three ANFO surface

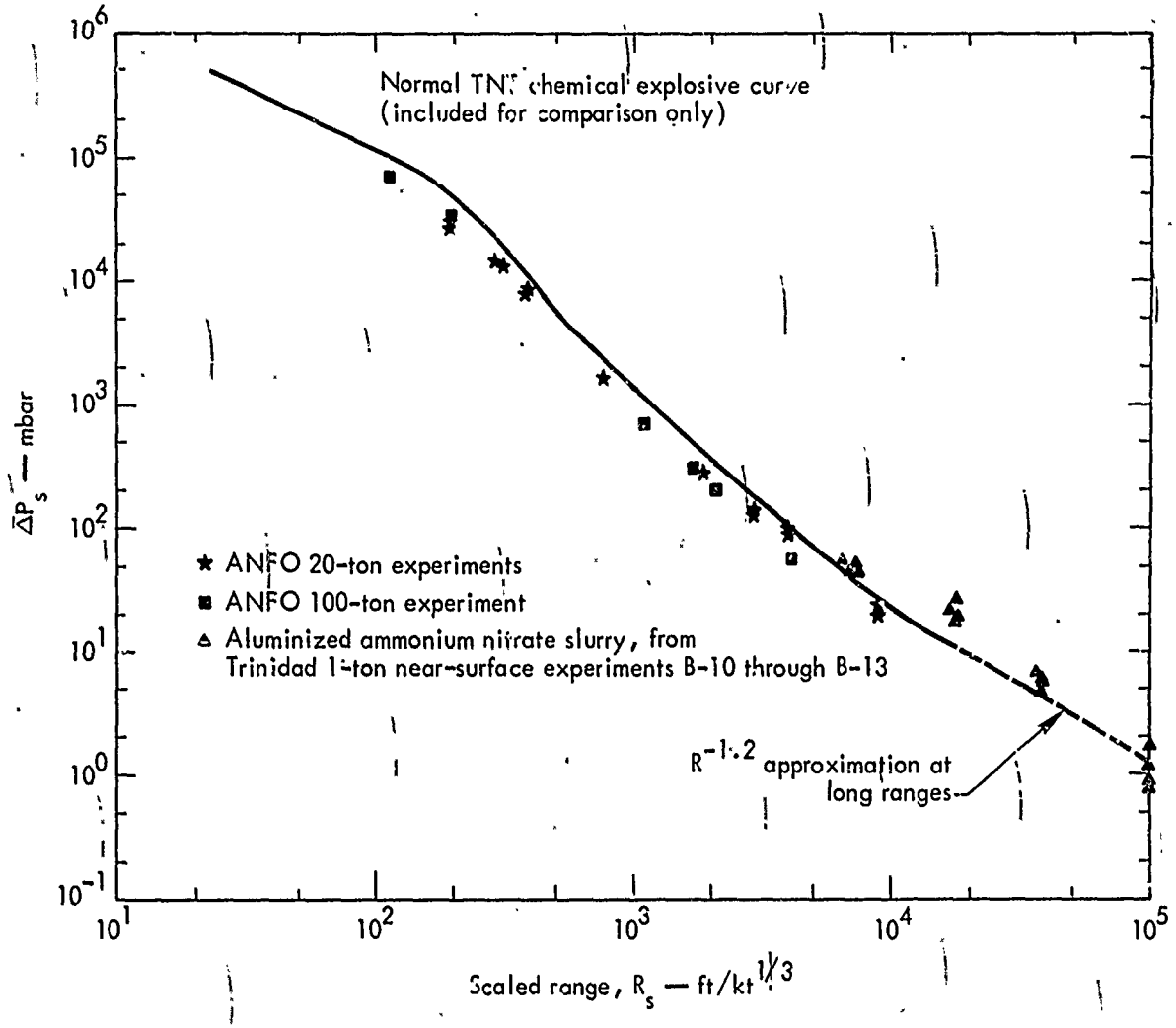

Fig. 31. Surface-burst overpressures for ANFO and aluminized AN slurry explosives (scaled to 1.0 kt at 1000 mbar).

bursts. These data have been scaled to 1.0 kt at 1000 mbar. They are tabulated in Table C30 and plotted in Fig. 31. The normal TNT chemical explosive curve is also plotted for comparison. ANFO overpressures lie below the TNT curve at close ranges, and approach it near $R_s \approx 4500$ ft/kt$^{1/3}$. The individual ANFO points in Fig. 31 may be scaled to predict future ANFO surface bursts.

ALUMINIZED AN SLURRY PREDICTIONS

Recent results from four Project Trinidad 1-ton near-surface detonations indicate that aluminized ammonium nitrate slurry explosive produces greater airblast than does ANFO. Overpressure data from these experiments (B-10 through B-13) are compiled in Table C22, and the scaled data points are plotted in Fig. 31. These points are at relatively long scaled ranges and refer to very small yield (1-ton) events. A great deal of scatter is evident, but the individual measurements fall around or slightly above the TNT surface burst curve. The points for the surface and shallowly buried detonations are higher than those

for the slightly elevated events, indicating that the reflected blast energy is more efficiently coupled into the peak overpressure pulse if the detonation is at or somewhat below the surface. Theoretically, one would expect doubling of the free-air burst energy* at a given scaled range from a surface event (hemispherical shock wave propagation as compared to a spherical free-air shock wave). This ideal condition is evidently not fulfilled for the elevated events. However, the difference between surface and slightly elevated events is small compared to the scatter of the data points. It is recommended that the TNT surface burst curve (Fig. 30) be scaled to predict all aluminized ammonium nitrate slurry surface and near-surface events.

*That is, doubling of the effective yield W, not of the overpressures.

Summary

Two procedures have been developed for predicting the ground-shock-induced and gas-vent airblast overpressures from single- and multiple-charge subsurface detonations of chemical and nuclear explosives. Both procedures are empirical, and are based on field-measured data for large-yield chemical and nuclear detonations.

One procedure, valid for ranges generally of interest in making airblast safety predictions, employs transmission factors which are dependent on the depth of burst, the geologic medium, and the type of explosive. The transmission factors correctly predict airblast overpressures from ground-shock at ranges greater than 200 to 600 ft/kt$^{1/3}$ and from gas vent at ranges greater than 1000 to 3000 ft/kt$^{1/3}$. At locations closer to SGZ, overpressures will be overpredicted (safesided).

The second procedure permits prediction of the airblast overpressures in the close-in region for detonations near optimum depth by use of range-dependent transmission factors. The range-dependent transmission factors are determined as a function of depth of burst, medium, and explosive.

Both transmission factors are determined relative to a standard line, the $R_s^{-1.2}$ line, which has an attenuation rate of $R^{-1.2}$ and passes through a point at a scaled range of 9000 ft/kt$^{1/3}$ where the overpressure is 25.5 mbar for an ambient atmosphere of 1000 mbar. Use of the standard line simplifies the prediction calculations, because the slope of the line is constant rather than varying as is the case with procedures that employ an air- or surface-burst line as the reference.

The empirical prediction methods presented are well-founded for the types of events which have been extensively investigated. Their chief weaknesses lie in the prediction of detonations employing new types of explosives or of detonations in media for which data are not available or are insufficient to provide a suitable empirical base.

Appendix A
Anomalous Results for Large-Yield Nuclear Experiments in Moist Media

As noted in the text, there are serious problems with moist or wet medium nuclear gas-vent overpressures. The relevant data come from only three experiments, Sedan and Teapot ESS (both in alluvium), and Schooner (moist rock). These data are difficult to interpret, but indicate very large gas-vent overpressures, particularly for Sedan.

The Sedan Event gave a very sharp gas-vent pulse of short scaled duration, a waveform more similar to surface bursts than normal buried detonations. The peak overpressure at a given scaled range was significantly higher than that expected for similar chemical explosive experiments (cf. Scooter, Stagecoach III, and others near the same dob). However, the integrated impulse under Sedan's sharp, brief overpressure peak was about equal to the corresponding scaled impulse under Scooter's broader peak. These facts suggest that Sedan's vent transferred almost the same fraction of total energy into its airblast wave. The transfer occurred over a shorter scaled time period, producing a higher peak pressure. Vortman[19] has suggested that the Sedan cavity vented when its scaled size was small and pressure relatively high—perhaps through a large vent. Such circumstances could explain the short duration and high peak pressure. The main requirement is that scaled energy stored in cavity gas at venting be about equal for Sedan and Scooter. According to this view, total gas production and energy transfer into airblast should be roughly similar for Sedan and chemical explosive experiments.

Vortman's interpretation of the Sedan vent is quite interesting, but seems incomplete on certain points. Sedan vented at a scaled time $[t/(W)^{1/3}]$ consistent with or slightly earlier than the venting times observed for chemical explosive experiments in alluvium. There is no immediate explanation of why the cavity volume should be relatively smaller and pressure higher at this time. In reality, it is probably difficult to compare the cavity histories of nuclear and chemical explosive detonations in this manner. They have very different early-time behavior. The chemical event quickly produces its own volume of reaction gases and behaves in a fairly consistent way. Nuclear detonations like Sedan must shock the surrounding medium, producing steam. The cavity gas equation-of-state history will depend on how much gas gets into the cavity, and how quickly. There may be strong medium-dependent effects involved. Steam boosting is apparently quite important to the nuclear explosive vent, and it is not completely analogous to chemical explosive gas production. There is no accurate way to compare the two types of events short of obtaining actual medium-dependent cavity pressure histories from one of the computer cratering codes. Even the codes would provide reliable answers only for those

events in which they are known to work—in other words, for those previously observed events with established cratering parameters that have been related back to the code's working procedure.

This point brings up the third and most important difficulty with the Sedan-type events. It has been suggested that high Sedan overpressures may be evidence of a nonscaling effect. In other words, the mechanisms producing airblast do not follow simple cube root scaling, but give rise to relatively stronger peak venting pressures for large yield detonations. Perhaps these nonscaling effects are also responsible for the peculiar waveform of the Sedan vent. The nonscaling question is not academic; effects of this sort could vastly increase damaging overpressures from megaton-size detonations of the type proposed for large civil works projects such as the Atlantic-Pacific Interoceanic Canal. Unfortunately, the data currently available are not sufficient to support a definitive empirical study of yield effects. Another large detonation (≈1 megaton), preferably in a medium similar to Sedan, is very badly needed. Allowance should be made for possible large overpressures in planning and calibrating the airblast experiments.

The airblast information currently available from large-yield buried nuclear experiments unfortunately furnishes very poor material for comparison, because it derives from four dissimilar experiments: Cabriolet (2.3 kt at dob = 130 ft/$kt^{1/3}$, in dry rhyolite), Palanquin (4.3 kt at dob = 172 ft/$kt^{1/3}$, in dry rhyolite), Schooner (31 kt at dob = 113 ft/$kt^{1/3}$, in partly wet basalt), Sedan (100 kt at dob = 137 ft/$kt^{1/3}$, in wet alluvium). The gas-vent airblast data from these events may be crudely compared by using the transmission factor f-values at certain scaled ranges (f_{max} values cannot be compared because the Sedan overpressure data do not extend to intermediate ranges, and some of the limited close-range data are of dubious quality; see the Sedan report[19]). The depth of burst dependence must first be removed from the f-values by approximately normalizing them to some convenient dob (e.g., dob = 150 ft/$kt^{1/3}$). The dob dependence of f for nuclear bursts in various media is not precisely known, so even this preliminary step cannot be reliably accomplished. However, a rough comparison of f-values for the above four experiments, at scaled ranges $R_s \approx 600$ and $R_s \approx 1000$ ft/$kt^{1/3}$, does show a strong apparent yield dependence effect. Sedan has the highest f-values by a large margin. This apparent yield effect may be clearly demonstrated by plotting normalized f-values as a function of yield in a log-log graph. Straight line fits through typical points plotted for the above four events give f-values which increase dramatically with increasing yield. In fact, the fitted lines would indicate that $f \approx 1.0$ for yields of 625* to 780† kt (normolized to dob ≈ 150 ft/$kt^{1/3}$).

Estimates of f based on the above procedure are almost certainly too pessimistic (give excessively high f-values for large-yield events). Most of the apparent yield-dependence is attributable to

*Derived from a fit to the normalized f-values at a range R_s = 600 ft/$kt^{1/3}$.

†Derived from a fit to the normalized f-values at a range R_s = 1000 ft/$kt^{1/3}$.

medium effects—Cabriolet and Palanquin (small yields) were in dry high-strength rock, Schooner (intermediate yield) was in partly wet rock, and Sedan (large yield) was in wet alluvium. Thus, the indicated high f's for large-yield experiments are probably too conservative and not meaningful. More airblast data are needed to settle the remaining questions in this area.

Appendix B
Airblast from Aluminized AN Slurry Row-Charge Detonations in Weak Rock (Project Trinidad) and from Delayed and Double Row-Charge Detonations

Airblast from a row of charges at a given average scaled depth is greater than the airblast from a comparable single charge at the same scaled depth of burst (dob). The increase is normally measured by the "difference factor" between row-charge and single-charge peak overpressures at a given scaled range. The difference factor is directly related to the number of charges in the row n by some exponential relationship n^B (Section 7). The difference factors and B's may depend on such parameters as the scaled intercharge spacing, the overall size of the row (linear dimensions, not scaled dimensions), and the direction (azimuth) from the row. The value of B is usually largest for closely spaced charges, for small-size rows (small-yield experiments), and for the direction perpendicular to the axis of the row. Other parameters which may affect the derived value of B include the explosive and medium, the dob, the peak overpressure ΔP (absolute strength), the range at which overpressure is measured, and the number n itself (indicating that a simple n^B dependence is inadequate to describe the difference factor). It was hoped that some simple n^B law could be discovered to fit the Trinidad, Colorado experiments,[11] just as for previous tests (Section 7). Trinidad experiments fell between the large-charge detonations (Buggy, Dugout) and the small-charge tests in yield and actual row size. Therefore, the B's might be expected to lie between the large B values observed for small-charge rows (efficient airblast reinforcement) and the smaller B values observed for large-charge rows ($B \approx 0.7$ perpendicular to the row, $B \approx 0.25$ off the end of the row; inefficient reinforcement).

Unfortunately, the experimental results (Tables C23 and C24) show great scatter, indicating extremely erratic behavior, particularly for the gas-vent-induced airblast. Part of this scatter is due to considerable variations in the attenuation rates and waveforms, even for similar experiments.[11] All close and intermediate range peak overpressures, as well as the calculated f-values, are listed in Tables C23 and C24. Again, due to incompleteness of the data, it was necessary to calculate an f for each observed overpressure rather than use a fitted curve. A maximum observed f-value was selected for each gage line on each row. The maximum values were found at scaled ranges between 3700 and 37,000 $ft/kt^{1/3}$. Maximum f-values off the ends of the rows tended to fall at fairly long scaled ranges, once more showing the relatively slower combination of widely separated overpressure peaks off the ends of the rows. The closest overpressures were relatively low and close-in attenuation rates were less than $R^{-1.2}$ for most off-the-end measurements. The perpendicular measurements, on the other hand, showed slightly more efficient combination of the overpressure peaks at all ranges, producing somewhat greater reinforcement

(higher f-values), and the maximum f-values were reached at closer scaled ranges. Detailed discussion of the individual experiments may be found in Ref. 11.

The maximum f-value for each gage line was compared to the corresponding single-charge f_{max} at the same average dob (from Fig. 16). Difference factors (n^B = row-charge f_{max}/single-charge f_{max}) were calculated for each row-charge f_{max}. The "best fit" single-charge curves were used in these calculations.* Finally, the values of B were determined. Results are listed in Tables B1 (ground-shock-induced airblast) and B2 (gas-vent-induced airblast). The calculated B values obviously show an enormous amount of scatter, with the gas-vent results being less consistent than ground-shock values. In fact, both sets of values vary from near zero (near single-charge airblast) to almost 1.0 (perfect acoustic reinforcement between the expected peak single-charge signals from all charges in the row). Variability of this order indicates true differences between the behavior of individual experiments rather than a flaw in the single-charge fitted f_{max} values.

Calculated B values are plotted as a function of dob in Figs. B1a and B1b. Ground-shock-induced values, perpendicular to and off the end of the rows, and gas-vent-induced values, perpendicular to and off the end of the rows, are plotted separately for clarity. This plot should reveal any dob dependence of the calculated B values, thus showing any inadequacies of the fitted single-charge

*The lower (or "best fit") gas-vent f_{max} curve in Fig. 16 was used to obtain the gas-vent f_{max} values as a function of dob.

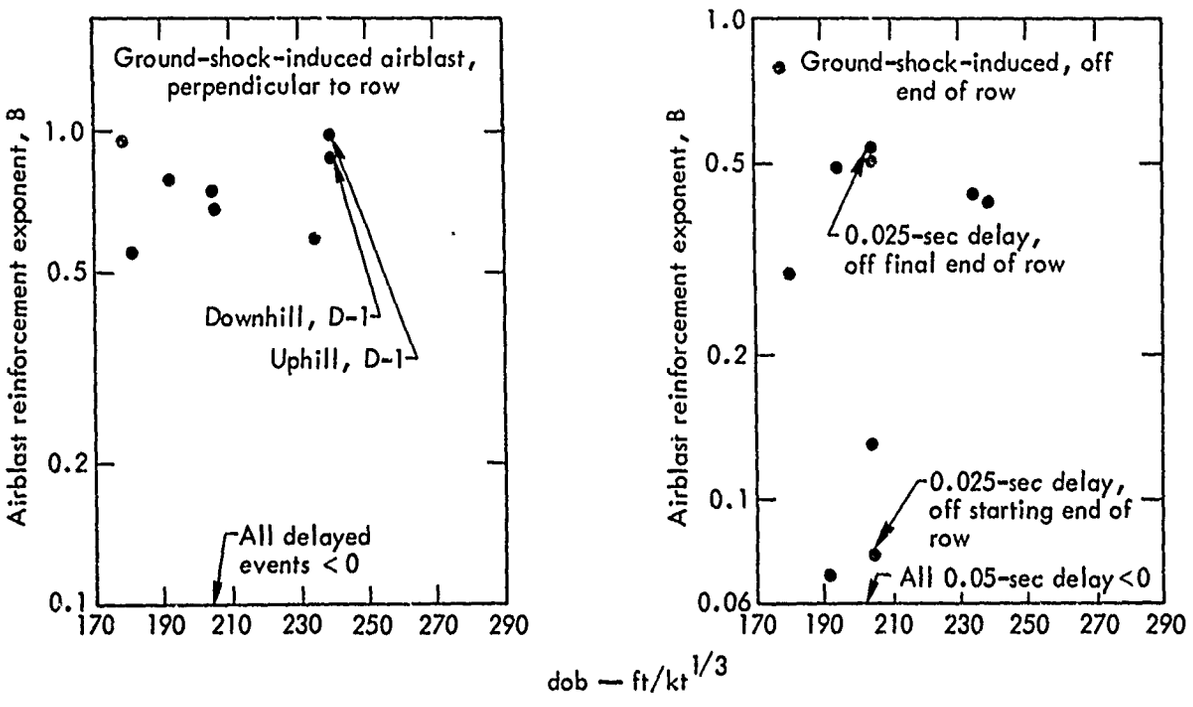

Fig. B1a. Row-charge ground-shock-induced airblast reinforcement exponent B as a function of dob for Trinidad experiments.

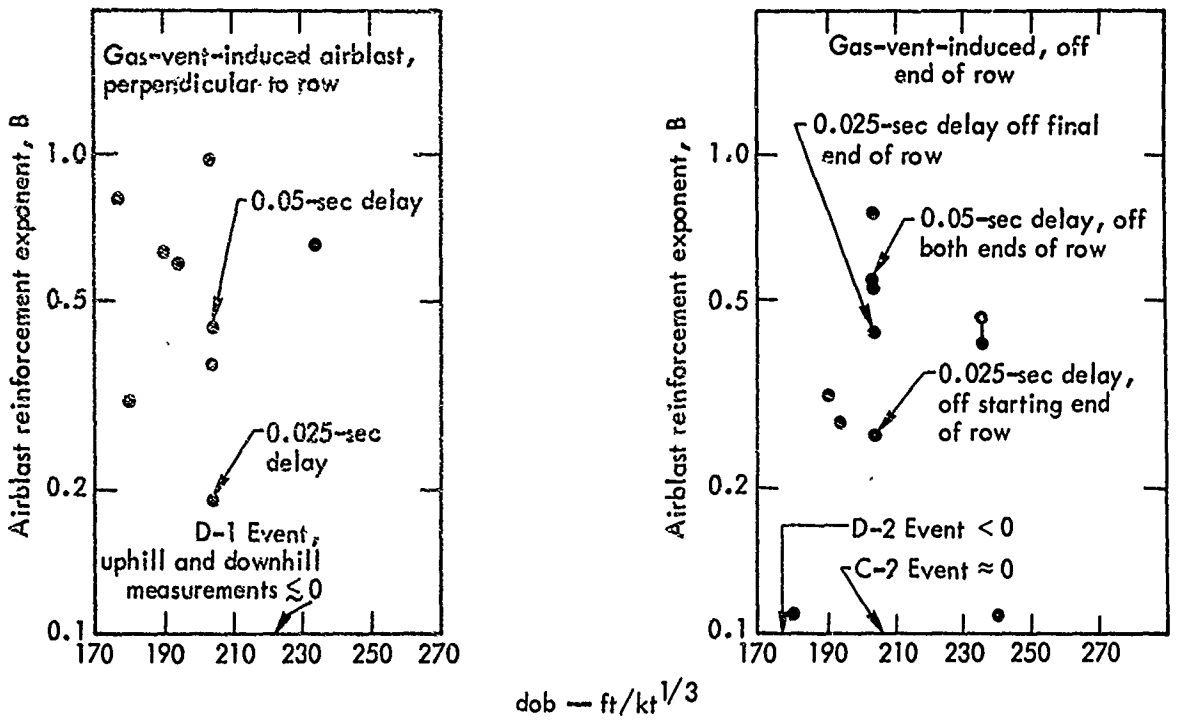

Fig. B1b. Row-charge gas-vent-induced airblast reinforcement exponent B as a function of dob for Trinidad experiments.

f_{max} curves (Fig. 16) used to calculate the row-charge difference factors. It should also uncover any shock-strength dependence of the row-charge signal reinforcement efficiency (shallower bursts give stronger airblast). No correlations are apparent in any of the scaled depth graphs. Next, the B-values are plotted as a function of the number of charges in the row, n (see Figs. B2a and B2b). This figure should show any n dependence of the reinforcement, revealing systematic inadequacies of the assumed exponential n^B law. No significant correlation is found. Finally, B is plotted as a function of average scaled spacing between the charges in each row (Figs. B3a and B3b). This is the quantity expected to correlate most strongly with row-charge airblast reinforcement. The gas-vent B values appear to decrease slightly with increased intercharge spacing, as expected, but again no strong or consistent correlation is found.

A few experiments were atypical in configuration and deserve separate comment. The Trinidad, Colorado D-1 experiment (9-charge row) was conducted on a sidehill slope. Perpendicular gage lines were used both uphill and downhill from the row. Results show no really significant difference in the peak overpressures between the two directions, although the uphill results are fractionally higher in most cases.

Two of the experiments were double rows. The C-6 consisted of two simultaneous 5-charge rows separated by 39 ft. In spite of the wide separation, very strong reinforcement occurred between the respective ground-shock-induced signals from the two rows and between the

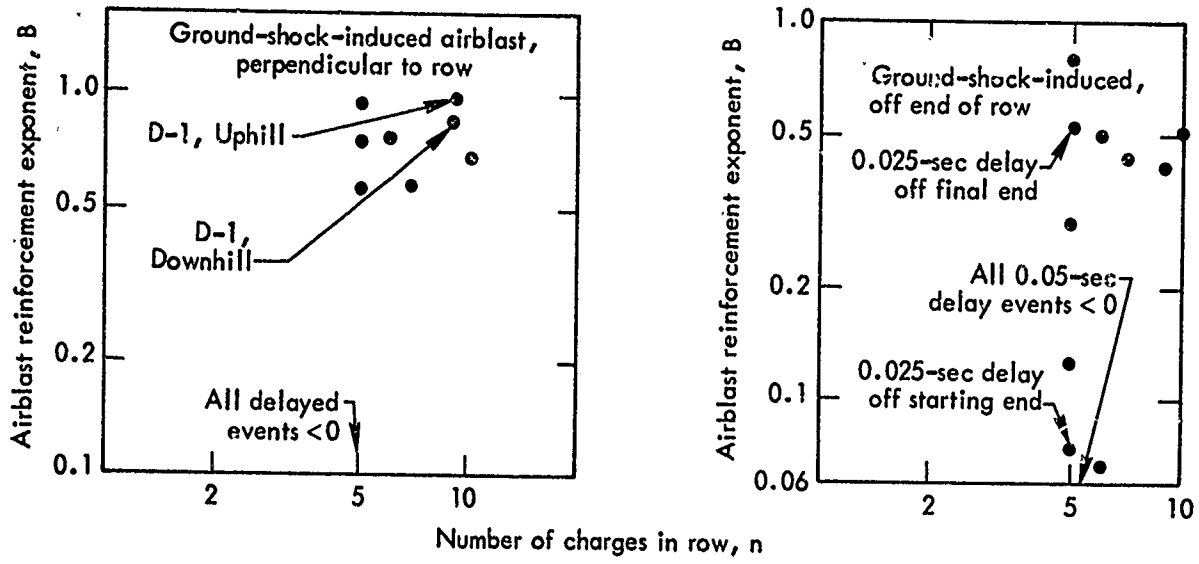

Fig. B2a. Row-charge ground-shock-induced airblast reinforcement exponent B as a function of number of charges in row, n, for Trinidad experiments.

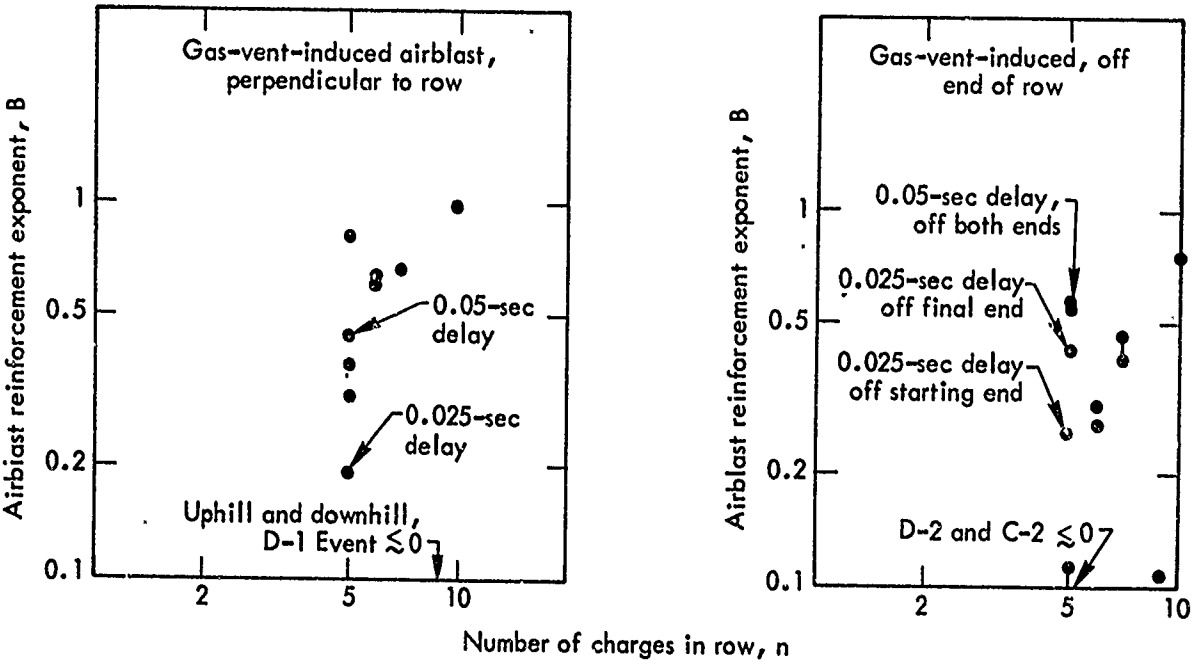

Fig. B2b. Row-charge gas-vent-induced airblast reinforcement exponent B as a function of number of charges in row, n, for Trinidad experiments.

gas-vent signals from the two rows. Therefore, the B-values were calculated on the basis of n = 10. Both airblast signals from this experiment were extremely strong, and the calculated B values were high in spite of the allowance for ten charges. The reason for the very strong reinforcement is not known. The Pre-Gondola III, Phase I nitromethane detonation in saturated clay shale gave

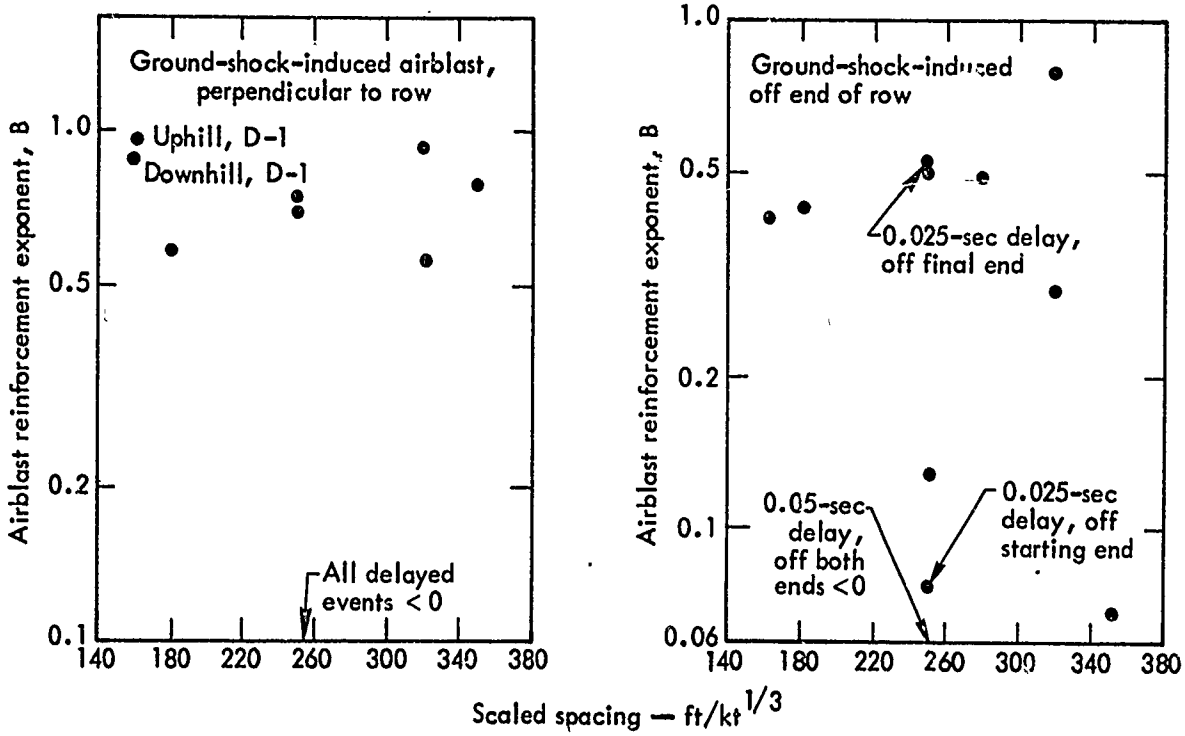

Fig. B3a. Row-charge ground-shock-induced airblast reinforcement exponent B as a function of average scaled intercharge spacing for Trinidad experiments.

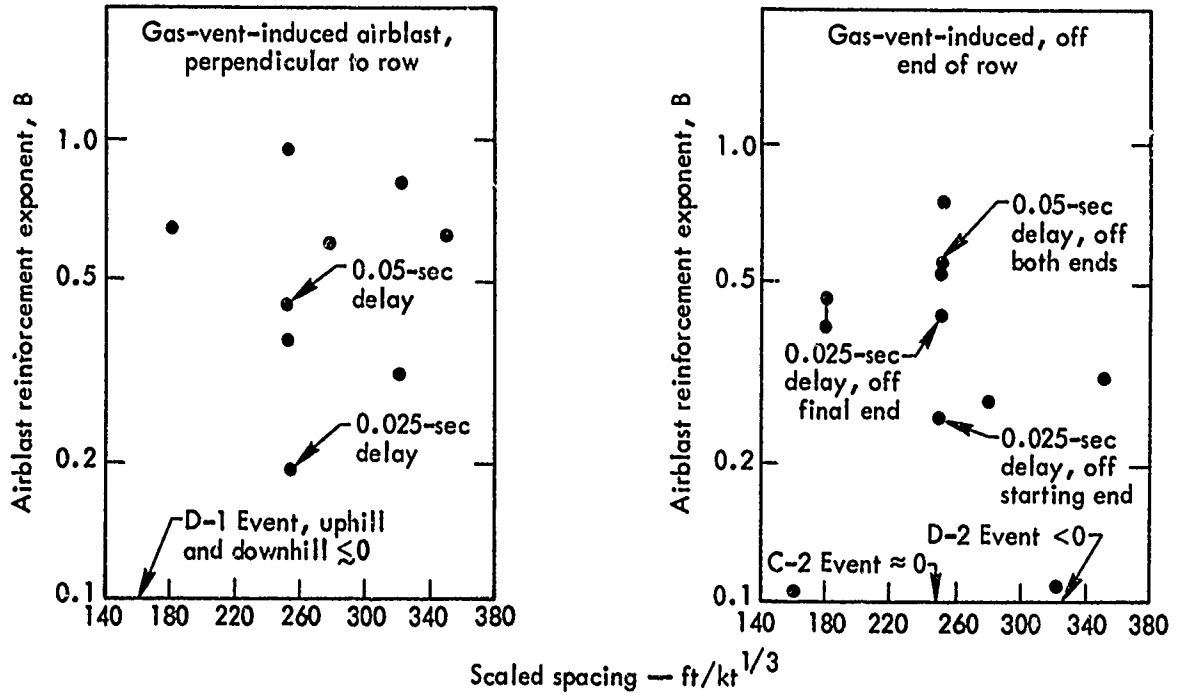

Fig. B3b. Row-charge gas-vent-induced airblast reinforcement exponent B as a function of average scaled intercharge spacing for Trinidad experiments.

virtually no reinforcement between ground-shock-induced signals from two rows (seven 1-ton charges in each row, at dob = 195 ft/kt$^{1/3}$). However, the Pre-Gondola rows were 1200 ft/kt$^{1/3}$ apart, as compared to 390 ft/kt$^{1/3}$ for the C-6 rows. It seems probable that closely spaced double rows (much closer than Pre-Gondola III, Phase I) will always give strong airblast reinforcement; therefore, in predicting airblast, it is necessary to use the total number of charges in both rows for n.

The other Trinidad double row, D-3, contained six charges in each row. The rows were 40 ft apart (or about 337 ft/kt$^{1/3}$ scaled separation). However, there was a 0.25-sec delay between the rows. Sound travels over 250 ft in 0.25 sec, equivalent to a scaled distance of about 2100 ft/kt$^{1/3}$ for this case. This delay proved sufficient to prevent strong reinforcement between the signals, and all data were reduced on the assumption that n = 6 (number of charges in one row). The ground-shock signal perpendicular to the 2-ton row was superimposed on a negative phase from the 1-ton row,* and was the only signal which could not be separately identified. These results support the conclusion that double rows at wide separation do not cause reinforced airblast (row separation must be $\gtrsim$1100 ft/kt$^{1/3}$; or there must be an inter-row delay time equivalent to the time required for sound to travel this far). The conclusion: for wide separation or long delay times, use n = number of charges in each row, and predict the airblast due to each row separately; for close double rows, use n = number of charges in both rows. This procedure should give safe-sided airblast predictions.

The Trinidad experiments also provided the first accurate information concerning airblast suppression by delayed detonation of the charges in a single row. The 5-charge C-4 row (0.05-sec intercharge delay) and the 5-charge C-5 row (0.025-sec intercharge delay) gave usable airblast measurements which can be compared to similar single-charge and multiple-charge events. The f_{max} and B values for rows C-4 and C-5 give the following indications:

Ground-Shock-Induced Airblast, Intercharge delays:

Perpendicular to the row, delays $\geq$ 0.25 sec/kt$^{1/3}$: ΔP (row charge) = ΔP (single charge).

Off the starting end of the row (end at which the detonation sequence is begun), delays $\geq$ 0.25 sec/kt$^{1/3}$: ΔP (row charge) = ΔP (single charge).

Off final end of the row (end at which the detonation sequence is concluded):

Delay = 0.25 sec/kt$^{1/3}$: ΔP (row charge) = predicted ΔP (row charge for no delay).

Delay > 0.5 sec/kt$^{1/3}$: ΔP (row charge) = ΔP (single charge).

Gas-Vent-Induced Airblast, Intercharge delays:

Perpendicular to the row, delays $\geq$ 0.25 sec/kt$^{1/3}$: ΔP (row charge) $\approx n^{0.45}$ to $n^{0.55}$ ΔP (single charge). (This is an estimate.)

Off both ends of the row, all delays:

ΔP (row charge) = predicted ΔP (row charge for no delay).

*The 1-ton row was closer to the perpendicular gage line, and its signal arrived first.

These results should apply most accurately to events similar to C-4 and C-5 (dob ≈ 204 ft/kt$^{1/3}$ in sandstone; charge spacing ≈ 250 ft/kt$^{1/3}$). However, they provide guidelines for predicting airblast from all delayed row-charge detonations.

Ground-Shock-Induced and Gas-Vent-Induced Airblast, Simultaneous Row Charges:

Accepted mean data from Tables B1 and B2 are summarized in the following prediction scheme. This scheme applies to all simultaneous aluminized AN slurry row-charge events near optimum spacing (160 to 350 ft/kt$^{1/3}$) in sandstone or weak rock. The results must be considered approximate at best. First, make a normal single-charge airblast prediction using Fig. 16.* Then:

Ground-Shock-Induced Overpressures:

Perpendicular to the row:

$$\Delta P \text{ (row charge)} = n^{0.75}\, \Delta P \text{ (single charge)}.$$

Off the end of the row:

$$\Delta P \text{ (row charge)} = n^{0.5}\, \Delta P \text{ (single charge)}.$$

Gas-Vent-Induced Overpressures:

Perpendicular to the row:

$$\Delta P \text{ (row charge)} = n^{0.6}\, \Delta P \text{ (single charge)}.$$

Off the end of the row:

$$\Delta P \text{ (row charge)} = n^{0.45}\, \Delta P \text{ (single charge)}.$$

Prediction for Double Rows:

At close interrow spectrum (≈350 ft/kt$^{1/3}$), use the above prediction scheme with n = number of charges in both rows. At wide row separations (≳1100 ft/kt$^{1/3}$) or long interrow delays (≳1.1 sec/kt$^{1/3}$), use n = number of charges in each row to predict the peak overpressures from each row separately. The pulses from the two rows will not combine, and no reinforcement is expected either perpendicular to or off the end of the rows. However, partial reinforcement may occur in certain situations if the total row length exceeds the product of the delay time (in seconds, unscaled)* and the local sonic velocity. There is currently no good experimental evidence for rows this long. Reinforcement may also be expected for delayed double rows in directions such that the delay is not sufficient to prevent overlapping of the pulses (for example: in the perpendicular direction closest to the last of the two rows detonated, the pulses arrive somewhat closer together and may tend to overlap).

Prediction for Delayed Charges in a Single Row:

See the discussion above concerning airblast for intercharge delays.

*The single-charge predictions are performed using the mean yield and the mean dob for the individual charges in the row.

*Delay time between the two rows.

Table B1. Ground-shock-induced overpressure reinforcement correction factors for Trinidad row-charge detonations.

ΔP (row charge) = $n^B \Delta P$ (single charge at same scaled range).
Parentheses indicate alternate or uncertain value.

Event	n	Direction	Difference factor, n^B	B
C-1	5	Perpendicular to row	2.44	0.554
		Parallel to row	1.60	0.292
C-2	5	Perpendicular to row	3.31	0.744
		Parallel to row	1.23	0.128
C-3	7	Perpendicular to row	3.08	0.578
		Parallel to row	2.30 (1.51)	0.428 (0.212)
C-4[a]	5	Perpendicular to row	(0.622)	<0
		Parallel to starting end	(0.727)	<0
		Parallel to final end	(0.781)	<0
C-5[b]	5	Perpendicular to row	(0.850)	<0
		Parallel to starting end	1.13	0.076
		Parallel to final end	2.29	0.515
C-6	10[c]	Perpendicular to row	4.90	0.690
		Parallel to row	3.21	0.506
D-1	9	Perpendicular to row, uphill	8.42	0.97
		Perpendicular to row, downhill	6.83	0.874
		Parallel to row	2.46	0.41
D-2	5	Perpendicular to row	4.55	0.940
		Parallel to row	3.56	0.789
D-3	6[d]	Perpendicular to 1-ton row	4.07	0.784
		Parallel to 1-ton row	1.13	0.068
	6[e]	Perpendicular to 2-ton row	—	—
		Parallel to 2-ton row	2.42	0.493

[a] Delay = 0.05 sec.

[b] Delay = 0.025 sec.

[c] Double row, treated as one row of ten charges.

[d] One-ton charges.

[e] Two-ton charges.

Table B2. Gas-vent-induced overpressure reinforcement correction factors for Trinidad row-charge detonations.

ΔP (row charge) = n^B ΔP (single charge at same scaled range).
Parentheses indicate alternate or uncertain value.

Event	n	Direction	Difference Factor, n^B	B
C-1	5	Perpendicular to row	1.63	0.304
		Parallel to row	1.19	0.108
C-2	5	Perpendicular to row	1.80	0.365
		Parallel to row	(1.0)	(0)
C-3	7	Perpendicular to row	3.50	0.644
		Parallel to row	2.16-2.44	0.396-0.459
C-4[a]	5	Perpendicular to row	2.03	0.44[b]
		Parallel to starting end	2.37	0.536
		Parallel to final end	2.33	0.526
C-5[c]	5	Perpendicular to row	1.36	0.191
		Parallel to starting end	1.50 (1.21)	0.252 (0.118)
		Parallel to final end	1.95	0.415
C-6	10[d]	Perpendicular to row	9.26 (5.42)	0.966 (0.734)
		Parallel to row	5.66 (4.42)	0.753 (0.645)
D-1	9	Perpendicular to row, uphill	(1.0)	(0)
		Perpendicular to row, downhill	(0.505)	<0
		Parallel to row	1.26	0.105
D-2	5	Perpendicular to row	3.67	0.808
		Parallel to row	(0.88)	<0
D-3	6[e]	Perpendicular to 1-ton row	3.05	0.622
		Parallel to 1-ton row	1.73	0.306
	6[f]	Perpendicular to 2-ton row	2.92	0.538
		Parallel to 2-ton row	1.62	0.269

[a] Delay = 0.05 sec.

[b] Highly questionable because of very rapid attenuation of the gas-vent overpressures with distance perpendicular to C-4 row.

[c] Delay = 0.025 sec.

[d] Double row, treated as one row of ten charges.

[e] One-ton charges.

[f] Two-ton charges.

Appendix C
Tables C1 through C31, Airblast Overpressure Data for Buried and Surface Detonations and for IBM Problem M Theoretical Free-Air Burst Calculation

Preceding page blank

Table C1. Sulky, 0.085-kt nuclear, basalt, dry (Ref. 20).

DOB = 90 ft (depth of burst, in ft) | dob = 204.8 ft/kt$^{1/3}$ (scaled depth of burst) | P_0 = 850 mbar (nominal ambient pressure)

Observed data		Observed data scaled to 1.0 kt at P_0 = 1000 mbar		Data from fitted curve		
Distance (ft)	ΔP (psi)	$R_s\left(\frac{ft}{kt^{1/3}}\right)$	ΔP_s (mbar)	$R_s\left(\frac{ft}{kt^{1/3}}\right)$	ΔP_s (mbar)	$f(R_s)$
			A. Ground Shock			
165	0.131	355.5	10.65	400	10.0	0.00935
361	0.0601	778	4.88	600	6.25	0.00950
820	0.0195	1768	1.58	1000	3.40	0.00955
1772	0.0085	3820	0.69	5000	0.51	0.00989
3772	0.0035[a]	8130	0.284	10000	0.22	0.00978
			B. Gas Vent[b]			
165	0.067	355.5	5.44	300	6.5-7.75	0.00431-0.00513
361	0.0294-0.038	778	2.39-3.09	1000	1.79-2.11	0.00503-0.00593
820	0.0095-0.0126	1768	0.772-1.023	10000	0.151-0.178	0.00671-0.00791
1772	0.00425-0.00661	3820	0.345-0.537			
3772	0.00234-0.0028	8130	0.190-0.227			

[a]Corrected for drift.

[b]Estimates of pressure pulse amplitude, pulse barely returned to ambient pressure due to superimposition on negative phase (estimates are based on amplitude above minimum negative pressure, and amplitude above estimated extrapolated negative pressure phase tracing).

Table C2. Palanquin, 4.3-kt nuclear, rhyolite, dry (Refs. 8,9).

DOB = 280 ft dob = 172.2 ft/kt$^{1/3}$ P_0 = 850 mbar

Observed data		Observed data scaled to 1.0 kt at P_0 = 1000 mbar		Data from fitted curve			
Distance (ft)	ΔP (psi)	$R_s\left(\frac{ft}{kt^{1/3}}\right)$	ΔP_s (mbar)	$R_s\left(\frac{ft}{kt^{1/3}}\right)$	ΔP_s (mbar)	$f(R_s)$	f/f_{max}
			A. Ground Shock				
21	0.62-0.74[a]	12.2	50.3-60	20	51	0.00133	0.195
328	0.248	191	20.1	80	29.1	0.00393	0.575
705	0.087	410	7.06	100	25.1	0.00445	0.651
1575	0.0193	917	1.567	200	14.6	0.00597	0.872
3280	0.0079	1910	0.642	300	19.9	0.00656	0.96
7380	0.0053	4295	0.4305	600	4.5	0.00684	1.0
				1000	2.36	0.00661	0.966
				5000	0.341	0.00661	0.966
			B. Gas Vent[b]				
328	0.073	191	5.93	200	5.55	0.00227	0.376
705	0.0307	410	2.49	300	3.60	0.00238	0.394
1575	0.0162	917	1.315	600	1.94	0.00295	0.489
3280	0.0049	1910	0.398	1000	1.24	0.00348	0.577
7380	0.0046	4295	0.3735	2000	0.68	0.00439	0.727
				5000	0.312	0.00603	1.0

[a]True ground-shock overpressure at 21 ft from SGZ; a later overpressure of 5.52 psi was observed at a time corresponding to an anomalous gas vent through a pipe near SGZ.

[b]Superimposed on negative phase.

Table C3. Danny Boy, 0.43-kt nuclear, basalt, dry (ref. 21).

DOB = 110 ft dob = 146 ft/kt$^{1/3}$ P_0 = 838 mbar

Observed data		Observed data scaled to 1.0 kt at P_0 = 1000 mbar		Data from fitted curve		
Distance (ft)	ΔP (psi)	$R_s\left(\frac{ft}{kt^{1/3}}\right)$	ΔP_s (mbar)	$R_s\left(\frac{ft}{kt^{1/3}}\right)$	ΔP_s (mbar)	$f(R_s)$
		A. Ground Shock				
200	0.255	250	21	200	22.2	0.00905
265	0.16	331	13.18	300	16.1	0.01065
350	0.11	438	9.06	600	9.43	0.0144
470	0.12	587	9.88	1000	6.35	0.0178
630	0.075	788	6.18	5000	1.79	0.0347[a]
840	0.045	1050	3.71			
840	0.080 ??	1050	6.59 ??			
1120	0.055	1400	4.53			
3100	0.027	3870	2.22			
		B. Gas Vent				
265	0.04 ?	331	3.3	f-value = 0.00245		
350	0.02 ?	438	1.65	f-value = 0.00173		
470	0.03 ?	587	2.47	f-value = 0.00367		

[a] 0.034 may be high; slope is unrealistically shallow, not consistent with later experiments.

Table C4. Cabriolet, 2.3-kt nuclear, rhyolite, dry (Ref. 1).
DOB = 170.75 ft dob = 129.3 ft/kt$^{1/3}$ P_0 = 840 mbar[a]

Observed data		Observed data scaled to 1.0 kt at P_0 = 1000 mbar		Data from fitted curve			
Distance (ft)	ΔP (psi)	$R_s\left(\frac{ft}{kt^{1/3}}\right)$	ΔP_s (mbar)	$R_s\left(\frac{ft}{kt^{1/3}}\right)$	ΔP_s (mbar)	$f(R_s)$	f/f_{max}
			A. Ground Shock				
3	1.45	2.2	119	10	109	0.00122	0.093
100	0.887	71.6	72.8	30	87	0.00362	0.276
200	0.641	143	52.6	80	66	0.0089	0.68
397	0.244	284	20.04	150	44	0.0127	0.97
800	0.116	572	9.53	300	19.6	0.0130	0.99
1447	0.046	1035	3.78	600	8.6	0.0131	1.0
3300	0.0204	2360	1.675	1000	4.55	0.0128	—
6000	0.0087	4290	0.715	5000	0.6	0.0116	—
			B. Gas Vent				
100	0.115	71.6	9.45	80	9.6	0.00130	0.127
200	0.121	143	9.94	100	9.8	0.00173	0.168
397	0.106	284	8.71	200	9.2	0.00375	0.364
800	0.051	572	4.19	300	8.0	0.00529	0.515
1447	0.028	1035	2.30	600	4.4	0.00670	0.653
3300	0.0135	2360	1.109	1000	2.60	0.00729	0.710
6000	0.0062	4290	0.510	2000	1.30	0.00839	0.816
				5000	0.53	0.01027	1.0

[a]Extrapolation of meteorological observations to Cabriolet SGZ indicates that P_0 ≈ 802 mbar would have been a more appropriate ambient pressure; technically, P_0 at each gage station should be used (we will retain these values).

Table C5. Dugout, 20-ton chemical explosive row charge, five charges of 20 tons each, nitromethane in basalt, dry (Refs. 15, 16, 22).

DOB = 59 ft dob = 217 ft/kt$^{1/3}$ (spacing = 45 ft) P_0 = 850 mbar

Use n = 5 charges in row.

Observed data		Observed data scaled to 1.0 kt at P_0 = 1000 mbar		Data from fitted curve		
Distance (ft)	ΔP (mbar)	$R_s\left(\frac{ft}{kt^{1/3}}\right)$	ΔP_s (mbar)	$R_s\left(\frac{ft}{kt^{1/3}}\right)$	ΔP_s (mbar)	$f(R_s)$
A. Ground Shock ⊥ to row[a]						
171	28.04	597	33	600	30.0	0.0457
351	9.75	1225	11.47	1000	17.5	0.0492
850	5.75	2968	6.77	5000	2.75	0.0533
2300	1.42	8030	1.67	10000	1.22	0.0542
5000	0.52	17450	0.612	15000	0.77	0.0557
B. Ground Shock ∥ to row[b]						
171	11.39	597	13.40	600	13.5	0.0206
354	4.94	1235	5.81	1000	8.0	0.0225
850	1.73	2968	2.035	5000	1.44	0.0279
1510	1.57	5270	1.846	10000	0.70	0.0311
2300	0.94	8030	1.106	15000	0.455	0.033
3410	0.40	11900	0.471			
4600	0.33	16050	0.388			
C. Gas Vent[c] ⊥ to row						
171	9.8	597	11.53	600	11.7	0.01780
351	3.48	1225	4.10	1000	6.5	0.01825
850	1.63	2968	1.917	5000	1.0	0.0194
2300	0.46	8030	0.541	10000	0.45	0.020
5000	0.19	17450	0.224	15000	0.295	0.021
D. Gas Vent ∥ to row[d]						
171	4.58	597	5.39	600	6.6	0.01005
354	2.44	1235	2.87	1000	4.0	0.01124
850	0.772	2968	0.908	5000	0.82	0.0159
1510	0.842	5270	0.99	10000	0.41	0.0182
2300	0.53[e]	8030	0.624	15000	0.275	0.0199
3410	0.215	11900	0.253			
4600	0.188	16050	0.221			

[a]Ground shock f_{max} = 0.0557 ⊥ to row
f_{max} (corrected to single charge) = 0.0557/3.085 = 0.018.

[b]Ground shock f_{max} = 0.033 ∥ to row
f_{max} (corrected to single charge = 0.033/1.495 = 0.022.

[c]Gas vent (superimposed on negative phase)
f_{max} = 0.021 ⊥ to row
f_{max} (corrected to single charge) = 0.021/3.085 = 0.0068.

[d]Gas vent f_{max} = 0.0199 ∥ to row
f_{max} (corrected to single charge) = 0.0199/2.626 = 0.0076.

Note: The above corrections to single-charge values are accomplished using the following relations:

ΔP (row) = $n^{0.7}$ ΔP (single charge) ⊥ to row, ground-shock and gas-vent

ΔP (row) = $n^{0.25}$ ΔP (single charge) ∥ to row, ground-shock overpressures

ΔP (row) = $n^{0.6}$ ΔP (single charge) ∥ to row, gas-vent overpressures.

[e]Gage W-701-2 slightly off; weight W-701-1 more heavily.

Table C6. Buggy I, 1.1-kt nuclear row charge, five devices of 1.1 kt each, basalt, dry medium (Ref. 23).

DOB = 135 ft dob = 130.5 ft/kt$^{1/3}$ P_0 = 846 mbar

Use n = 5 charges in row.

Observed data		Observed data scaled to 1.0 kt at P_0 = 1000 mbar		Data from fitted curve		
Distance (ft)	ΔP (psi)	$R_s\left(\frac{ft}{kt^{1/3}}\right)$	ΔP_s (mbar)	$R_s\left(\frac{ft}{kt^{1/3}}\right)$	ΔP_s (mbar)	$f(R_s)$
		A. Ground Shock ⊥ to Row[a]				
512	0.206	469	16.8	450	18.9	0.0203
1002	0.161	918	13.1	600	16.8	0.0255
2459	0.0493	2250	4.02	1000	11.5	0.0323
4078	0.0389	3740	3.17	5000	2.15	0.0417
5960	0.0229	5450	1.87	10000	1.05	0.0467
6598	0.0152	6040	1.24			
7760	0.0145	7100	1.18			
		B. Ground Shock ∥ to Row[b]				
500	0.073	458	5.96	450	5.95	0.0064
990	0.043	906	3.51	600	5.20	0.0079
1997	0.0266	1827	2.17	1000	3.70	0.0104
3729	0.0171	3415	1.40	5000	0.88	0.0171
7416	0.0091	6790	0.742	10000	0.47	0.0209
9306	0.0065	8520	0.530			
		C. Gas Vent ⊥ to Row[c]				
512	0.095	469	7.75			
1002	0.075	918	6.12	450	7.9	0.0085
2459	0.020	2250	1.63	600	6.95	0.0106
4078	0.0208	3740	1.70	1000	5.2	0.0146
5960	0.0134	5460	1.09	5000	1.27	0.0246
6598	0.0092	6040	0.75	10000	0.59	0.0262
7760	0.0081	7100	0.66			
		D. Gas Vent ∥ to Row[d]				
500	0.061	458	4.98	450	5.0	0.0054
990	0.045	906	3.67	600	4.4	0.0067
1997	0.027	1827	2.20	1000	3.4	0.0095
3729	0.016	3415	1.305	5000	0.97	0.0188
7416	0.0097	6790	0.792	10000	0.50	0.0222
9306	0.0055	8520	0.449			

[a]Ground-shock f_{max} = 0.0467 ⊥ to row
f_{max} (corrected to single-charge) = 0.0467/3.085 = 0.0151.

[b]Ground-shock f_{max} = 0.0209 ∥ to row
f_{max} (corrected to single-charge) = 0.0209/1.495 = 0.0140.

[c]Gas-vent f_{max} = 0.0262 ⊥ to row
f_{max} (corrected to single-charge) = 0.0262/3.085 = 0.00850.

[d]Gas-vent f_{max} = 0.0222 ∥ to row
f_{max} (corrected to single-charge) = 0.0222/2.626 = 0.00846.

Note: The above corrections to single-charge values are accomplished using the following relations:

ΔP (row) = $n^{0.7}$ ΔP (single charge) ⊥ to row, ground-shock and gas-vent

ΔP (row) = $n^{0.25}$ ΔP (single charge) ∥ to row, ground-shock overpressures

ΔP (row) = $n^{0.6}$ ΔP (single charge) ∥ to row, gas-vent overpressures.

Table C7. Schooner, 31-kt nuclear, basalt, partially wet medium (Ref. unpublished).
DOB = 355 ft dob = 113 ft/kt$^{1/3}$ P_0 = 850 mbar

Observed data		Observed data scaled to 1.0 kt at P_0 = 1000 mbar		Data from fitted curve			
Distance (ft)	ΔP (psi)	$R_s\left(\frac{ft}{kt^{1/3}}\right)$	ΔP_s (mbar)	$R_s\left(\frac{ft}{kt^{1/3}}\right)$	ΔP_s (mbar)	f	f/f_{max}
			A. Ground Shock				
21	3.18	6.3	258	10	240	0.00268	0.156
260	1.49	78.4	121	30	180	0.00753	0.435
520	0.685	157	55.6	80	108	0.0147	0.85
1040	0.238	314	19.33	100	85	0.0152	0.89
2080	0.115	628	9.34	300	26.0	0.0172	1.0
3900	0.082	1176	6.66	600	11.0	0.0168	
7800	0.0318	2350	2.58	1000	5.90	0.0166	
15600	0.0094	4700	0.764	5000	0.83	0.0161	
			B. Gas Vent				
1040	1.298	314	105.4	300	120	0.0794	0.520
2080	0.708	628	57.5	600	60	0.0912	0.596
7800	0.2419	2350	19.63	1000	37	0.1040	0.68
15600	0.0970	4700	7.88	2000	19	0.1226	0.8
				5000	7.9	0.153	1.0

Table C8. Sedan, 100-kt nuclear, alluvium, wet (Refs. 19, 24).
DOB = 635 ft dob = 136.9 ft/kt$^{1/3}$ P_0 = 850 mbar

Observed data			Observed data scaled to 1.0 kt at P_0 = 1000 mbar		
Distance (ft)	ΔP (psi)	ΔP_s (mbar)	$R_s\left(\frac{ft}{kt^{1/3}}\right)$	ΔP_s (mbar)	f
		A. Gas Vent Pulse Only			
2960	1.54	106	604	125	0.191
5290	0.74	51	1080	60.1	0.185
7050	0.717	49.5	1440	58.2	0.253
15500	0.035 ?	2.42 ?	3160	2.84 ?	0.032 ?

Note: These results are of questionable accuracy; readers are referred to the Sedan report.

Table C9. Teapot ESS, 1.2-kt nuclear, alluvium, dry (Ref. 10).

DOB = 67 ft dob = 63 ft/kt$^{1/3}$ P_0 = 860 mbar

Observed data		Observed data scaled to 1.0 kt at P_0 = 1000 mbar		
Distance (ft)	ΔP (psi)	$R_s\left(\frac{ft}{kt^{1/3}}\right)$	ΔP_s (mbar)	$f(R_s)$
		A. Ground Shock		
250	0.7 ?	224	56.2	0.0261
300	0.52 ?	268	41.7	0.0240
		B. Gas Vent		
250	14.4	224	1155	0.536
300	14.1	268	1131	0.652
400	11.3	358	907	0.740
600	6.14	537	493	0.653

Table C10. Jangle U, underground Jangle series detonation, 1.2-kt nuclear, alluvium, dry (Ref. 25).

DOB = 17 ft dob = 16 ft/kt$^{1/3}$ P_0 = 12.78 psi = 881 mbar

Observed data		Observed data scaled to 1.0 kt at P_0 = 1000 mbar		Data from fitted curve		
Distance (ft)	ΔP (psi)	$R_s\left(\frac{ft}{kt^{1/3}}\right)$	ΔP_s (mbar)	R_s	ΔP_s (mbar)	f
		A. Gas Vent				
314	32.39	283	2538	450	1120	1.204
498	13.57	449	1064	700	675	1.231
500	14.39	451	1127	1000	450	1.26
680	9.90	613	776	3000	120	1.255
680	10.09	613	790			
920	719	830	564			
1250	5.08	1127	398			
1700	3.26	1534	255			
2300	2.14	2075	167.6			
3100	1.70	2797	133.2			

Table C11. Scooter,[a] 500-ton chemical explosive, alluvium, dry (Ref. 5).

DOB = 125 ft dob = 157.5 ft/kt$^{1/3}$ P_0 = 868 mbar

Observed data		Observed data scaled to 1.0 kt at P_0 = 1000 mbar		Data from fitted curve			
Distance (ft)	ΔP (mbar)	$R_s\left(\frac{ft}{kt^{1/3}}\right)$	ΔP_s (mbar)	$R_s\left(\frac{ft}{kt^{1/3}}\right)$	ΔP_s (mbar)	f	f/f_{max}
			A. Gas Vent				
300	33.8	360	38.9	400	36.2	0.0338	0.546
414	32.4	497	37.3	600	27.2	0.0413	0.67
501	23.7	602	27.3	1000	17.9	0.0502	0.81
575	21.9	692	25.2	2000	9.15	0.0590	0.96
669	18.8	803	21.7	3000	5.90	0.0619	1.0
784	18.0	942	20.7				
1006	12.6	1207	14.5				
1040	11.9	1248	13.7				
1092	11.2	1310	12.9				
1168	10.1	1399	11.65				
1506	8.73	1804	10.05				
1524	8.55	1830	9.85				
1562	7.38	1878	8.50				
1618	8.21	1940	9.46				
2100	5.24	2520	6.04				
2500	5.86	3000	6.76				
536[b]	39.3[b]	644[b]	45.3[b]				
675[b]	30.5[b]	810[b]	35.1[b]				
			B. Ground Shock				
300	11.73	360.5	13.51	300	14.7	0.00973	—
	10.70		12.32	600	8.25	0.01253	—
500	7.59	601	8.74	1000	4.15	0.01163	—
	6.90		7.95	3000	1.24	0.01300	—
1000[c]	2.83	1202	3.26	(3000)	(or 0.98)[d]	(or 0.01027)	
	2.55		2.94				
1500[c]	1.725	1802	1.99				
	1.518		1.75				
2500	0.966	3004	1.113				
	1.311		1.510				

[a]Ground shock—unpublished data, from NOL experiment; courtesy D. N. Montan, LLL.

[b]Elevated (aerial) measurements.

[c]Approximate distance.

[d]Different fit straight line.

Table C12. Pre-Schooner II,[a] 85.5-ton chemical explosive (nitromethane), rhyolite, dry medium (Ref. 26).

DOB = 71 ft dob = 161 ft/kt$^{1/3}$ P_0 = 850 mbar

Observed data		Observed data scaled to 1.0 kt at P_0 = 1000 mbar		Data from fitted curve			
Distance (ft)	ΔP (psi)	$R_s\left(\frac{ft}{kt^{1/3}}\right)$	ΔP_s (mbar)	$R_s\left(\frac{ft}{kt^{1/3}}\right)$	ΔP_s (mbar)	f	f/f_{max}
A. Ground Shock at Ground Level							
0	2.034	0	165	10	164	0.00184	0.0529
75	0.850	162	69	30	141	0.0059	0.1695
150	0.466	323	37.8	80	96	0.0130	0.374
250	0.224	540	18.2	100	86	0.0152	0.437
350	0.161	756	13.1	300	39	0.0258	0.741
500	0.117	1080	9.5	600	20.8	0.0316	0.908
1000	0.062	2155	5.04	1000	12.1	0.0339	0.974
2000	0.028	4300	2.27	2000	5.40	0.0348	1.0
4000	0.0106	8620	0.86	5000	1.69	0.0328	
				7500	1.0	0.0316	

B. Ground Shock, Aerial (from balloon measurements)				
Observed data			Observed data scaled to 1.0 kt at P_0 = 1000 mbar	
Distance (ft)	ΔP (psi)	θ = angle from vertical to gage (deg)	$R_s\left(\frac{ft}{kt^{1/3}}\right)$	ΔP_s (mbar)
190.1	0.531	59	410	43.1
351.6	0.410	33.5	756	33.3
583	0.372	23	1260	30.2
1011.8	0.050	81.25	2177	4.06
1013.9	0.059	72.85	2180	4.79
1039.2	0.040	64.55	2240	3.25
1105.2	0.061	54.6	2380	4.95
1172.3	0.058	48.5	2520	4.71
1291	0.061	40.5	2780	4.95

C. Gas Vent at Ground Level				
Observed data		Observed data scaled to 1.0 kt at P_0 = 1000 mbar		
Distance (ft)	ΔP (psi)	$R_s\left(\frac{ft}{kt^{1/3}}\right)$	ΔP_s (mbar)	f
75	0.537	162	43.6	0.0138
150	0.468	323	38	0.0276

D. Gas Vent, Aerial (from balloon measurements)				
Observed data			Observed data scaled to 1.0 kt at P_0 = 1000 mbar	
Distance (ft)	ΔP (psi)	θ (deg)	$R_s\left(\frac{ft}{kt^{1/3}}\right)$	ΔP_s (mbar)
190.1	0.614	59	410	49.85
583	0.400	23	1260	32.5
1172.3	0.106	48.5	2520	8.6

[a]After careful consideration, the authors decided to use solely nonlimited gage measurements in the Pre-Schooner II airblast investigation. Only the nonlimited observations are included in the table.

Note that the gas-vent ground level measurements contain only two points, both of which are very close to SGZ. For this reason, f_{max} is not well determined. It is certainly larger than these two close-in point f-values would indicate.

Table C13. Buckboard 11, 20-ton chemical explosive,[a] basalt, dry (Ref. 4).

DOB = 25.5 ft dob = 94 ft/kt$^{1/3}$ P_0 = 12.3 psi = 848 mbar

Observed data		Observed data scaled to 1.0 kt at P_0 = 1000 mbar		Data from fitted curve			
Distance (ft)	ΔP (psi)	$R_s\left(\frac{ft}{kt^{1/3}}\right)$	ΔP_s (mbar)	$R_s\left(\frac{ft}{kt^{1/3}}\right)$	ΔP_s (mbar)	f	f/f_{max}
			A. Ground Shock				
108	0.406	376	33.1	400	32.7	0.0306	0.753
129.6	0.329	452	26.8	600	21.7	—	—
163	0.285	568	23.2	700	18.5	0.0339	0.835
207.6	0.242	723	19.7	1000	12.8	0.0359	0.884
264	0.174	920	14.16	2000	6.3	0.0406	1.0
348.3	0.125	1214	10.18				
476.1	0.084	1658	6.84				
			B. Gas Vent				
108	1.39	376	113	300	129	0.0854	0.27
129.6	1.35	452	109.9	600	99.5	0.151	0.478
163	1.28	568	104.2	1000	76	0.213	0.674
207.6	1.08	723	87.9	2000	49	0.316	1.0
264	1.06	920	86.3				
348.3	0.827	1214	67.3				
476	0.639	1658	52.0				

[a]Buckboard: TNT.

Table C14. Buckboard 12, 20-ton chemical explosive, basalt, dry (Ref. 4).
DOB = 42.7 ft dob = 157.5 ft/kt$^{1/3}$ P_0 = 848 mbar

Observed data		Observed data scaled to 1.0 kt at P_0 = 1000 mbar		Data from fitted curve			
Distance (ft)	ΔP (psi)	$R_s\left(\frac{ft}{kt^{1/3}}\right)$	ΔP_s (mbar)	$R_s\left(\frac{ft}{kt^{1/3}}\right)$	ΔP_s (mbar)	f	f/f_{max}
			A. Ground Shock				
110	0.240	383	19.55	400	18	0.0168	0.703
130	0.192	453	15.64	600	12.1	—	—
165	0.155	575	12.62	700	10.3	0.0189	0.791
210	0.109	732	8.38	1000	7.35	0.0206	0.862
265	0.108	923	8.80	2000	3.70	0.0239	1.0
350	0.065	1220	5.29				
480	0.051	1672	4.15				
			B. Gas Vent				
110	0.361	383	29.4	300	34.2	0.0226	0.34
130	0.302	453	24.6	600	22.1	0.0336	0.505
165	0.277	575	22.54	1000	16.0	0.0448	0.674
210	0.240	732	19.54	2000	10.3	0.0665	1.0
265	0.21	923	17.10				
350	0.176	1220	14.32				
480	0.142	1672	11.56				

Table C15. Buckboard 13, 20-ton chemical explosive, basalt, dry (Ref. 4).
DOB = 58.8 ft dob = 217 ft/kt$^{1/3}$ P_0 = 848 mbar

Observed data		Observed data scaled to 1.0 kt at P_0 = 1000 mbar		Data from fitted curve			
Distance (ft)	ΔP (psi)	$R_s\left(\frac{ft}{kt^{1/3}}\right)$	ΔP_s (mbar)	$R_s\left(\frac{ft}{kt^{1/3}}\right)$	ΔP_s (mbar)	f	f/f_{max}
			A. Ground Shock				
59.6	0.504 ??	208	41 ??	600	7.5	0.0114	0.47
79.5	0.465 ??	277	37.8 ??	1000	5.59	0.0157	0.65
159.75	0.097	556	7.9	1500	4.4	0.0201	0.83
214.75	0.079	748	6.43				
298.5	0.068	1039	5.54	(2000)[a]	(3.75)[a]	(0.0242)[a]	(1.0)[a]
430	0.037	1499	3.01				

[a]Extrapolated to R_s = 2000 ft/kt$^{1/3}$ only for purposes of normalizing f/f_{max}. Values at 2000 ft/kt$^{1/3}$ are not to be used.

Table C16. Stagecoach I, 20-ton chemical explosive,[a] desert alluvium, dry (Ref. 3).
DOB = 80 ft dob = 295 ft/kt$^{1/3}$ P_0 = 12.6 psi = 868 mbar

Observed data		Observed data scaled to 1.0 kt at P_0 = 1000 mbar		Data from fitted curve			
Distance (ft)	ΔP (psi)	$R_s\left(\frac{ft}{kt^{1/3}}\right)$	ΔP_s (mbar)	$R_s\left(\frac{ft}{kt^{1/3}}\right)$	ΔP_s (mbar)	f	f/f_{max}
			A. Ground Shock				
80	0.092	282	7.32	300	6.7	0.00444	0.658
110	0.0565	388	4.49	600	3.25	0.00494	0.732
160	0.0270	564	2.15	1000	1.9	0.00532	0.788
270	0.0280	952	2.23	1500	1.23	0.00562	0.833
430	0.0145	1516	1.153	(6000)[b]			(1.0 ?)[b]

[a]For Stagecoach: TNT.

[b]Extrapolated to R_s = 6000 ft/kt$^{1/3}$ only for purposes of normalizing f/f_{max}.

Table C17. Stagecoach II, 20-ton chemical explosive, desert alluvium, dry (Ref. 3).
DOB = 17 ft dob = 62.6 ft/kt$^{1/3}$ P_0 = 868 mbar

Observed data		Observed data scaled to 1.0 kt at P_0 = 1000 mbar			Data from fitted curve			
Distance (ft)	ΔP (psi)	$R_s\left(\frac{ft}{kt^{1/3}}\right)$	ΔP_s (mbar)	f	R_s	ΔP_s (mbar)	f	f/f_{max}
A. Ground Shock								
110	0.68	388	54.1	0.0488	No fitted data because there are only two reliable points			
160	0.42	564	33.4	0.0472				
270	2.58 ??	(952)	(205)?	(0.544)??				
B. Gas Vent								
110	5.15	388	409.5		300	455	0.301	0.350
160	4.37	564	347.5		600	330	0.501	0.583
270	2.82	952	224.0		1000	224	0.628	0.731
430	1.74	1516	138.4		2000	102	0.658	0.766
700	0.95	2470	75.5		4000	45	0.668	0.778
1600	0.34	5640	27.03		6000	28.8	0.694	0.808
3000	0.188	10570	14.95		10000	16.3	0.724	0.843
4700	0.13	16560	10.34		20000	8.4	0.859	1.0

Table C18. Stagecoach III, 20-ton chemical explosive, desert alluvium, dry (Ref. 3).
DOB = 34 ft dob = 125 ft/kt$^{1/3}$ P_0 = 868 mbar

Observed data		Observed data scaled to 1.0 kt at P_0 = 1000 mbar		Data from fitted curve			
Distance (ft)	ΔP (psi)	$R_s\left(\frac{ft}{kt^{1/3}}\right)$	ΔP_s (mbar)	$R_s\left(\frac{ft}{kt^{1/3}}\right)$	ΔP_s (mbar)	f	f/f_{max}
			A. Ground Shock				
110	0.29	388	23.06	300	29.6	0.0196	0.671
160	0.19	564	15.1	600	14	0.0213	0.730
270	0.08	952	6.36	1000	8.2	0.0230	0.788
430	0.06	1516	4.77	3000	2.53	0.0265	0.908
750	0.04	2643	3.18	6000	1.21	0.0292	1.0
1100	0.02	3880	1.59				
1600	0.015	5640	1.19				
			B. Gas Vent				
110	0.70	388	55.6	300	62.5	0.0414	0.271
160	0.58	564	46.1	600	44.5	0.0676	0.442
270	0.36	952	28.6	1000	31.1	0.0871	0.569
430	0.26	1516	20.7	2000	16.6	0.107	0.700
750	0.155	2643	12.33	5000	6.35	0.123	0.804
1100	0.104	3880	8.27	10000	3.10	0.138	0.902
1600	0.073	5640	5.80	20000	1.50	0.153	1.0
5020	0.021	17700	1.67				

Table C19. Pre-Gondola III, Phase I, fourteen chemical explosive devices of 1-ton each in two rows, nitromethane, clay shale, saturated (Ref. 18).

DOB = 19.5 ft dob = 195.0 ft/kt$^{1/3}$ (spacing = 27 ft) $P_0 \approx 930$ mbar

Use n = 7 charges in each row—overpressures caused by charges in one row; interrow spacing = 120 ft = 1200 ft/kt$^{1/3}$; no airblast reinforcement between rows.

Observed data		Observed data scaled to 1.0 kt at P_0 = 1000 mbar			
Distance (ft)	ΔP (psi)	$R_s\left(\frac{ft}{kt^{1/3}}\right)$	ΔP_s (mbar)	f	f[a]
		A. ⊥ to row			
93	0.986	907	73.2	0.183	0.0469
315	0.229	3075	17.0	0.184	0.0471
		B. ∥ to row			
110	0.459	1073	34.1	0.104	0.064
320	0.076	3120	5.64	0.062	0.038?

[a]Corrected to single-charge values. The f-values are corrected to single-charge values using the relations:

ΔP (row) = $n^{0.7}$ ΔP (single charge) ⊥ to row
ΔP (row) = $n^{0.25}$ ΔP (single charge) ∥ to row
} Ground-shock-induced overpressures

Table C20. Pre-Gondola II, five chemical explosive devices (two of 40 tons and three of 20 tons, use mean yield = 28 tons) in a row, nitromethane, clay shale, saturated medium. Overpressures determined from accurately fitted straight lines published in Ref. 18, after measurements made by Vortman.

DOB = 52.6 ft dob = 173.0 ft/kt$^{1/3}$ (spacing = 80 ft) $P_0 \approx 930$ mbar

Use n = 5 charges in the row.

Observed data		Observed data scaled to 1.0 kt at P_0 = 1000 mbar			
Distance (ft)	ΔP (psi)	$R_s\left(\frac{ft}{kt^{1/3}}\right)$	ΔP_s (mbar)	f	f[a]
		A. ⊥ to row			
151	1.0	486	74.2	0.0881	0.0286
3020	0.051	9730	3.78	0.163	0.0529
		B. ∥ to row			
151	0.65	486	48.2	0.0572	0.0383
3020	0.032	9730	2.375	0.102	0.0682

[a]Corrected to single-charge values. The f-values are corrected to single-charge values using the relations:

ΔP (row) = $n^{0.7}$ ΔP (single charge) ⊥ to row
ΔP (row) = $n^{0.25}$ ΔP (single charge) ∥ to row
} Ground-shock-induced overpressures

Table C21. Operation Jangle scaled HE tests, HE-2 and HE-3 buried detonations, 20- and 1.25-ton chemical explosive (TNT), alluvium, dry (Ref. 27).

DOB = 5.73 ft (HE-2) DOB = 6.8 ft (HE-3)

dob = 21.1 ft/kt$^{1/3}$ (HE-2) dob = 63.1 ft/kt$^{1/3}$ (HE-3) P_0 = 12.6 psi = 870 mbar

Observed data		Observed data scaled to 1.0 kt at P_0 = 1000 mbar		Data from fitted curve		
Distance (ft)	ΔP (psi)	$R_s\left(\frac{ft}{kt^{1/3}}\right)$	ΔP_s (mbar)	$R_s\left(\frac{ft}{kt^{1/3}}\right)$	ΔP_s (mbar	f
		A. HE-2 (20 tons) Gas Vent Only				
85.5	21.4	300	1700	300	1700	1.125
148	13.4	520	1063	600	1010	1.535
217	10.1	763	802	1000	575	1.611
378	5.1	1330	405	2000	238	1.535
512	3.3	1800	262	3000	141	1.48
1025	1.35	3600	107			
		B. HE-3 (1.25 tons) Gas Vent				
28.4	4.2	251	334	300	370	0.245
41	4.2	363	334	600	280	0.425
58.8	3.8	520	302	1000	205	0.575
85.5	3.1	757	246	2000	98	0.632
148	2.0	1310	159	5000	32.5	0.630
178	1.4	1575	111			
314	0.73	2780	58			
542	0.43	4800	34.1			
		C. HE-3 Ground Shock (Front Porch)				
28.4	1.2	251	95.3	300	79	0.0523
41	0.82	363	65	600	40.7	0.0619
58.8	0.57	520	45.3	1000	25	0.0700
85.5	0.41	757	32.6			

Table C22. Project Trinidad, close-in airblast measurements for all B-series (single-charge) experiments; aluminized ammonium nitrate slurry explosive (unless otherwise noted) in sandstone and shale, wet medium (Ref. 11).

Altitude ≈ 6200 ft Approximate ambient pressure $P_0 \approx 810$ mbar

	Observed data		Observed data scaled to 1.0 kt at P_0 = 1000 mbar		
	Distance (ft)	ΔP (psi)	$R_s\left(\frac{ft}{kt^{1/3}}\right)$	ΔP_s (mbar)	f
	A. Shot B-4: 1-ton; DOB = 15.9 ft; dob = 159 ft/kt$^{1/3}$.				
Ground shock	350	0.044	3260	3.75	0.0434
	1000	0.015	9321	1.28	0.0523
	2000	0.0063	18642	0.537	0.0502
Gas Vent	350	0.322	3260	27.4	0.317
	1000	0.101	9321	8.61	0.352
	2000	0.0373	18642	3.18	0.298
	B. Shot B-5: 1-ton; DOB = 18.6 ft; dob = 186 ft/kt$^{1/3}$.				
Ground Shock	295	0.057	2750	4.86	0.0459
	810	0.021	7550	1.79	0.0568
	1845	0.007	17200	0.596	0.0508
Gas Vent	295	0.088	2750	7.50	0.0708
	810	0.0335	7550	2.85	0.0903
	1845	0.0123	17200	1.05	0.0896
	C. Shot B-6: 1-ton; DOB = 20.9 ft; dob = 209 ft/kt$^{1/3}$.				
Ground Shock	163	0.0705	1520	6.00	0.0278
	510	0.0260	4750	2.215	0.0403
	1670	0.0079	15560	0.673	0.0507
Gas Vent	163	0.0556	1520	4.74	0.0220
	510	0.0262	4750	2.23	0.0406
	1670	0.0064	15560	0.545	0.0411
	D. Shot B-7: 1-ton; DOB = 22.6 ft; dob = 226 ft/kt$^{1/3}$.				
Ground Shock	275	0.04 ?	2560	3.41 ?	0.0294
	1630	0.00446	15200	0.380	0.0279
Gas Vent	275	0.074	2560	6.30	0.0543
	1630	0.0149	15200	1.27	0.0933
	E. Shot B-8: 1-ton; DOB = 28.1 ft; dob = 281 ft/kt$^{1/3}$.				
Ground Shock	140	0.0528	1305	4.50	0.0174
	460	0.0190	4290	1.62	0.0261
	835	0.0070	7780	0.596	0.0195

Table C22 (continued)

	Observed data		Observed data scaled to 1.0 kt at P_0 = 1000 mbar		
	Distance (ft)	ΔP (psi)	$R_s\left(\frac{ft}{kt^{1/3}}\right)$	ΔP_s (mbar)	f
Gas Vent	140	0.0105	1305	0.895	0.00346
	460	0.0046	4290	0.392	0.00631
	835	0.00133	7780	0.113	0.00371
F. Shot B-10: 1-ton; 3.8 ft above surface; scaled height = 38 $ft/kt^{1/3}$.					
Gas Vent	724	0.55	6750	46.9	
	1840	0.225	17150	19.17	
	3941	0.0615	36750	5.24	
	10620	0.0112	99000	0.954	
	(16350)[a]	(0.0069)[a]	152500	0.588	
G. Shot B-11: 1-ton; 1.9 ft above surface; scaled height = 19 $ft/kt^{1/3}$.					
Gas Vent	759	0.64	7075	54.6	
	1863	0.235	17350	20.0	
	3952	0.070	36800	5.96	
	10645	0.0104	99250	0.886	
	(16375)	(0.0057)	152600	0.486	
H. Shot B-12: 1-ton; at surface.					
Gas Vent	675	0.68	6290	58.0	
	1781	0.274	16600	23.34	
	3871	0.0826	36100	7.04	
	10560	0.0155	98500	1.32	
	(16290)	(0.0073)	151800	0.622	
I. Shot B-13: 1-ton; 1.9 ft below surface; dob = 19 $ft/kt^{1/3}$.					
Gas Vent	792	0.552	7380	47.0	
	1876	0.342	17500	29.1	
	3944	0.075	36800	6.39	
	10655	0.0232	99350	1.376	
	(20790)	(0.00656)	193700	0.559	
J. Shot B-14: 1-ton; DOB = 20.9 ft; dob = 209 $ft/kt^{1/3}$.					
Ground Shock	654	?	6100		
	1741	0.0070	16230	0.596	0.0473
	3816	0.00225	35560	0.1916	0.0390
Gas Vent	654	0.016	6100	1.364	0.0335
	1741	0.0061	16230	0.520	0.0413
	3816	0.00186	35560	0.1585	0.0322

Table C22 (continued)

	Observed data		Observed data scaled to 1.0 kt at P_0 = 1000 mbar		
	Distance (ft)	ΔP (psi)	$R_s\left(\frac{ft}{kt^{1/3}}\right)$	ΔP_s (mbar)	f
K. Shot B-15: 1-ton; DOB = 20.9 ft; dob = 209 $ft/kt^{1/3}$; 14-in. unstemmed hole; unstemmed detonation.					
First Venting Peak	500	0.123 ??	4660	10.48 ??	0.187 ?
	500	0.155	4660	13.20	0.235
	1300	0.0456	12100	3.89	0.218
	2238	0.0299	20850	2.55	0.274
	2238	0.0294	20850	2.51	0.270

[a]Parentheses indicate long-range values.

Table C23. Project Trinidad, close-in airblast measurements for all C-series row-charge experiments; aluminized ammonium nitrate slurry explosive (unless otherwise noted) in sandstone and shale, wet medium (Ref. 11).

Altitude ≈ 6200 ft Approximate ambient pressure $P_0 \approx 810$ mbar

	Observed data		Observed data scaled to 1.0 kt at P_0 = 1000 mbar		
	Distance (ft)	ΔP (psi)	$R_s\left(\frac{ft}{kt^{1/3}}\right)$	ΔP_s (mbar)	f
A. Shot C-1: DOB = 18 ft; dob = 180 ft/kt$^{1/3}$; spacing = 32 ft = 320 ft/kt$^{1/3}$; five-charge row; 1-ton-charges; total yield W = 5 tons.					
Ground Shock					
⊥ to row	392	0.128	3650	10.90	0.144
	1525	0.0134	14200	1.14	0.077
	3360	0.00842	31300	0.718	0.125
∥ to row	302	0.093	2810	7.92	0.0765
	1000	0.027	9321	2.30	0.0941
	3171	—[a]	29580	—	—
Gas Vent					
⊥ to row	392	0.181	3650	15.4	0.204
	1525	0.029	14200	2.48	0.168
	3360	0.0164	31300	1.397	0.244
∥ to row	302	0.152	2810	12.95	0.125
	1000	0.051	9321	4.35	0.178
	3171	—[a]	29580	—	—
B. Shot C-2: DOB = 20.4 ft; dob = 204 ft/kt$^{1/3}$; spacing = 25 ft = 250 ft/kt$^{1/3}$; five-charge row; 1-ton charges; W = 5 tons.					
Ground Shock					
⊥ to row	400	0.137	3730	11.67	0.159
	1515	0.0131	14120	1.116	0.075
	3360	—[b]	31300	—	—
∥ to row	500	0.039	4660	3.32	0.0592
	1350	0.010	12590	0.852	0.0499
	2985	—[c]	27800	—	—
Gas Vent					
⊥ to row	400	0.093	3730	7.92	0.108
	1515	0.0142	14120	1.21	0.0814
	3360	—[b]	31300	—	—
∥ to row	500	0.039	4660	3.32	0.0592
	1350	0.0115	12590	0.98	0.0574
	2985	—[c]	27800	—	—

Table C23 (continued)

	Observed		Observed data scaled to 1.0 kt at P_0 = 1000 mbar		
	Distance (ft)	ΔP (psi)	$R_s\left(\frac{ft}{kt^{1/3}}\right)$	ΔP_s (mbar)	f
C. Shot C-3: DOB = 23.5 ft; dob = 235 ft/kt$^{1/3}$; spacing = 18 ft = 180 ft/kt$^{1/3}$; seven-charge row; 1-ton charges; W = 7 tons.					
Ground Shock					
⊥ to row	349	0.105	3250	8.94	0.103
	1530	0.0175	14250	1.49	0.101
	3360	0.0079	31300	0.673	0.117
∥ to row	461	0.039, 0.063	4300	3.32, 5.37	0.0536, 0.0866
	1160	0.0124, 0.021	10800	1.057, 1.79	0.0516, 0.0873
	2791	0.0048, 0.0067	26000	0.409, 0.571	0.0572, 0.0798
Gas Vent					
⊥ to row	349	0.052	3250	4.43	0.051
	1530	0.0133	14250	1.133	0.077
	3360	0.0049	31300	0.418	0.073
∥ to row	461	0.0291	4300	2.480	0.040
	1160	0.0114	10800	0.971	0.0474
	2791	0.0045 ?	26000	0.383 ?	0.0536 ?
D. Shot C-4: DOB = 20.4 ft; dob = 204 ft/kt$^{1/3}$; spacing = 25 ft = 250 ft/kt$^{1/3}$; five-charge row; 1-ton charges; W = 5 tons; delay = 0.05 sec.					
Ground Shock					
⊥ to row	318	0.032	2960	2.73	0.0282
	1525	0.0052	14200	0.443	0.0299
∥ to starting end of row	500	0.023	4660	1.96	0.0349
	2610	0.0031	24300	0.264	0.0340
∥ to final end of row	1005	0.0107	9365	0.912	0.0375
	3000	—[d]	23000	—	—
Gas Vent					
⊥ to row	318	0.104	2960	8.86	0.0914
	1525	0.0212	14200	1.806	0.122
∥ to starting end of row	500	0.0630	4660	5.36	0.0954
	2610	0.0129	24300	1.10	0.142
∥ to final end of row	1005	0.0399	9365	3.40	0.140
	3000	—[d]	28000	—	—
E. Shot C-5: DOB = 20.4 ft; dob = 204 ft/kt$^{1/3}$; spacing = 25 ft = 250 ft/kt$^{1/3}$; five-charge row; 1-ton charges; W = 5 tons; delay = 0.025 sec.					
Ground Shock					
⊥ to row	400	0.024	3730	2.044	0.0279
	1535	0.0070	14300	0.596	0.0408

Table C23 (continued)

	Observed data		Observed data scaled to 1.0 kt at P_0 = 1000 mbar		
	Distance (ft)	ΔP (psi)	$R_s\left(\frac{ft}{kt^{1/3}}\right)$	ΔP_s (mbar)	f
∥ to starting end of row	500	0.0183	4660	1.56	0.0278
	2430	0.0054	22630	0.46	0.0544
∥ to final end of row	595	0.044	5540	3.75	0.082
	1185	0.0258	11050	2.20	0.110
Gas Vent ⊥ to row	400	0.047	3730	4.00	0.0546
	1535	0.014	14300	1.193	0.0818
∥ to starting end of row	500	0.0346, 0.029	4660	2.95, 2.47	0.0525, 0.0439
	2430	0.0089, 0.0072	22630	0.748, 0.614	0.0897, 0.0727
∥ to final end of row	595	0.042	5540	3.58	0.0784
	1185	0.0274	11050	2.335	0.117
F. Shot C-6: DOB = 20.4 ft; dob = 204 ft/kt$^{1/3}$; spacing = 25 ft = 250 ft/kt$^{1/3}$; ten-charge double row; 1-ton charges; 39 ft between rows; separate contributions from each row not identifiable (use n = 10 charges in the reductions).					
Ground Shock ⊥ to row	485	0.160 ??	4520	13.63	0.234
	1110	0.041	10350	3.49	0.162
	2720	0.0203	25340	1.73	0.235
∥ to row	428	0.080	3990	6.82	0.100
	1690	0.0211	15750	1.80	0.138
	3700	0.0092	34500	0.784	0.154
Gas Vent ⊥ to row	485	0.303 ??	4520	25.8	0.444
	1110	0.098, 0.051	10350	8.35, 4.35	0.387, 0.201
	2720	0.048, 0.028	25340	4.09, 2.39	0.556, 0.325
∥ to row	428	0.147, 0.152	3990	12.5, 13.0	0.184, 0.191
	1690	0.0328, 0.0476	15	2.79, 4.05	0.214, 0.311
	3700	0.0158, 0.0203	34500	1.35, 1.73	0.265, 0.340

[a]Transmitter drift.

[b]Record noisy.

[c]Record lost.

[d]No signal.

Table C24. Project Trinidad, close-in airblast measurements for all D-series row-charge experiments; aluminized ammonium nitrate slurry explosive (unless otherwise noted) in sandstone and shale, wet medium (Ref. 11).

Altitude ≈ 6200 ft Approximate ambient pressures P_0 ≈ 810 mbar

	Observed data		Observed data scaled to 1.0 kt at P_0 = 1000 mbar		
	Distance (ft)	ΔP (psi)	$R_s\left(\frac{ft}{kt^{1/3}}\right)$	ΔP_s (mbar)	f
A. Shot D-1: ANFO (ammonium nitrate fuel oil) explosive; nine-charge row; mean yield = 0.545 tons; total yield W = 4.9 tons; mean dob = 239 ft/kt$^{1/3}$ weighted by individual charge yields; mean spacing = 159 ft/kt$^{1/3}$ weighted by individual yields.[a]					
Ground Shock					
⊥ to row uphill	843	0.084	9620	7.16	0.303
	1482	0.0227	16900	1.935	0.161
⊥ to row downhill	770	0.076	8780	6.48	0.246
	1900	0.0123	21700	1.09	0.123
∥ to row	700	0.0232	7990	1.976	0.0672
	3280	0.0048	37400	0.409	0.0886
Gas Vent					
⊥ to row uphill	843	0.005	9620	0.426	0.0181
	1482	0.0013	16900	0.111	0.0093
⊥ to row downhill	770	0.002	8780	0.170	0.0065
	1900	0.001	21700	0.085	0.0096
∥ to row	700	0.0047	7990	0.401	0.0136
	3280	0.0013	37400	0.111	0.0240
B. Shot D-2: DOB = 17.7 ft; dob = 177 ft/kt$^{1/3}$; spacing = 32 ft = 320 ft/kt$^{1/3}$; five-charge row; 1-ton charges; W = 5 tons.					
Ground Shock					
⊥ to row	1000	0.0606	9321	5.16	0.211
	3210	0.0197	29900	1.68	0.278
∥ to row	1020	0.0460	9510	3.92	0.164
	2240	0.0170	20900	1.45	0.156
	3740	0.0128	34900	1.09	0.217
Gas Vent					
⊥ to row	1000	0.179	9321	15.25	0.624
	3210	0.0411	29900	3.50	0.579
∥ to row	1020	0.0350	9510	2.98	0.125
	2240	0.0135	20900	1.15	0.124
	3740	0.00884	34900	0.753	0.150

Table C24 (continued)

	Observed data		Observed data scaled to 1.0 kt at P_0 = 1000 mbar		
	Distance (ft)	ΔP (psi)	$R_s\left(\frac{ft}{kt^{1/3}}\right)$	ΔP_s (mbar)	f
C. Shot D-3: One-ton row: DOB = 19.1 ft; dob = 191 ft/$kt^{1/3}$; spacing = 35 ft = 350 ft/$kt^{1/3}$. Two-ton row: DOB = 24.4 ft; dob = 194 ft/$kt^{1/3}$; spacing = 35 ft = 278 ft/$kt^{1/3}$. Twelve-charge double row; six 1-ton charges plus six 2-ton charges; 40-ft separation and 0.25-sec delay between rows; no airblast reinforcement; analyze each row separately.					
Ground Shock (1-ton row)					
⊥ to row	1000	0.05	9321	4.26	0.174
	3210	0.0156	29900	1.33	0.220
∥ to row	720	0.0195	6710	1.66	0.046
	2220	0.0067	20700	0.571	0.061
	3815	0.00328	35550	0.279	0.057
Gas Vent (1-ton row)					
⊥ to row	1000	0.0653	9321	5.56	0.228
	3210	0.0210	29900	1.79	0.296
∥ to row	720	0.0526	6710	4.48	0.123
	2220	0.0185	20700	1.576	0.168
	3815	0.0088	35550	0.750	0.153
Ground Shock (2-ton row)					
⊥ to row	1000	—	7400	—[b]	
	3210	—	23750		
∥ to row	720	0.0441	5330	3.76	0.0785
	2220	0.0186	16430	1.585	0.128
	3815	0.00938	28200	0.799	0.123
Gas Vent (2-ton row)					
⊥ to row	1000	0.0579	7400	4.93	0.153
	3210	0.0235	23750	2.00	0.251
∥ to row	720	0.0498	5350	4.24	0.0885
	2220	0.0203	16430	1.73	0.139
	3815	0.01035	28200	0.882	0.136

[a]This weighting was used to overemphasize the larger yield charges but has little effect on the reductions. Weighting is not normally used in most prediction procedures.

[b]Unidentifiable—coincides with first negative phase from 1-ton row.

Table C25. Neptune, 0.115-kt nuclear, tuff and conglomerate, wet (Ref. 28).
DOB = 105 ft dob = 216 ft/kt$^{1/3}$ P_0 = 850 mbar

Observed data		Observed data scaled to 1.0 kt at P_0 = 1000 mbar		
Distance (ft)	ΔP (mbar)	$R_s\left(\frac{ft}{kt^{1/3}}\right)$	ΔP_s (mbar)	f
3500	0.672	6820	0.79	0.0222

Table C26. Distant Plain Events 3 and 5, TNT surface bursts.

	Observed data		Observed data scaled 1.0 kt at P_0 = 1000 mbar	
	Distance (ft)	ΔP (psi)	$R_s\left(\frac{ft}{kt^{1/3}}\right)$	ΔP_s (mbar)
A. Distant Plain, Event 3, 20-ton chemical explosive (TNT) surface burst charge, in shape of sphere half-buried at surface (P_0 = 13.64 psi = 941 mbar) (Ref. 29).				
Surface Burst (final fitted curve; use these values)	8	5500	28.9	403,000
	20	1330	72.2	97,600
	24.8	955	89.6	70,000
	35	600	126.3	44,000
	40	510	144.4	37,400
	60	305	216.7	22,380
	100	130	361	9,540
	150	52	542	3,815
	200	24.8	722	1,819
	250	14.6	903	1,070
	300	9.7	1084	712
	500	4.0	1805	293
	700	2.46	2529	180.5
	1000	1.42	3610	104.1
	1500	0.78	5420	57.2
	2000	0.51	7220	37.4
	3000	0.248	10840	18.1
(sample Canadian pressure gage results—for comparison only—use the above table for better numbers)	106	79	383	5,800
	114	70	412	5,138
	120	75	433	5,500
	133	77	480	5,645
	145	53	524	3,890
	169	50	610	3,670
(sample figures only—use the previous table for more accurate values	200	23	722	1,686
	291	10.2	1050	748
	420	6.6	1515	484
B. Distant Plain, Event 5, 20-ton chemical explosive (TNT) sphere half buried, same configuration as Event 3 above except shot occurred during winter in frozen ground (ambient pressure P_0 = 13.51 psi = 932 mbar) (Ref. 29).				
All results were closely comparable to Event 3, except for one section of the curve, which was slightly higher. Points from this section of the curve are given below:				
Surface Burst Fitted Curve	24.8	1351	89.3	100,000
	35	756	126	56,000

Table C27. Sailor Hat No. 1.1/1.4, two separate surface shots, each of which was 500-ton chemical explosive charge (Refs. 30, 31).

$P_0 \approx 1000$ mbar

Observed data		Observed data scaled to 1.0 kt at P_0 = 1000 mbar	
Distance (ft)	ΔP (psi)	$R_s \left(\frac{ft}{kt^{1/3}}\right)$	ΔP_s (mbar)
A. Event C, Surface Burst			
50	1340 ?	63	92500 ?
105	1000 ?	132	69000 ?
175	430 ?	220	29700 ?
250	178	315	12280
355	83	447	5720
570	30.8	718	2125
957	12.8	1205	884
1738	3.6	2190	248
2568	2.45	3235	169
B. Event D, Surface Burst			
30	1662 ?	38	114600 ?
50	1470 ?	63	101500 ?
175	370 ?	220	25500 ?
250	220	315	15200
355	87	447	6000
570	31	718	2140
957	12	1205	828
2568	2.1	3235	145
4760	0.69	6000	47.6
9000	0.24	11340	16.6

Table C28. Sailor Hat No. 5.2a, three separate surface shots, each of which was 500-ton chemical explosive charge (TNT), in shape of hemisphere at ground surface (Refs. 30, 31).

($P_0 \approx 1000$ mbar)

Observed data		Observed data scaled to 1.0 kt at P_0 = 1000 mbar	
Distance (ft)	ΔP (psi)	$R_s\left(\frac{ft}{kt^{1/3}}\right)$	ΔP_s (mbar)
A. Event B, Surface Burst (gages at ground level)			
980	10.3	1235	711
1450	4.78	1825	330
2290	2.49	2890	172
4460	1.11	5620	76.6
B. Event B, Elevated Gages, Balloon-Supported			
1475	4.8	1860	331
1530	4.2	1930	290
1710	3.4	2150	235
1760	3.6	2220	248
1920	3.5	2420	241
2360	2.3	2970	159
2430	2.2	3060	152
2500	2.14	3150	148
2580	2.04	3250	141
C. Event C, Surface Burst			
957	10.8	1205	746
1738	3.6	2190	248
2568	2.18	3240	150
D. Event D, Surface Burst			
957	10.7	1205	738
1738	2.54	2190	244
2568	1.92	3240	132

Table C29. Prairie Flat,[a] 500-ton chemical explosive (TNT) charge in form of sphere tangent to ground (Refs. 32, 33).

P_0 = 13.79 psi = 952 mbar

Observed data		Observed data scaled to 1.0 kt at P_0 = 1000 mbar	
Distance (ft)	ΔP (psi)	$R_s\left(\frac{ft}{kt^{1/3}}\right)$	ΔP_s (mbar)
A. Surface burst—final fitted curve			
20	6000	24.3	435000
30	3450	36.5	250000
60	2400	73	174000
100	1310	121.6	95000
200	750	243.2	54400
400	175	486.5	12700
500	75	608	5440
700	15.7	852	1140
1000	7.9	1216	572
2000	2.88	2432	209
3000	1.40	3650	101.5
4000	0.84	4865	60.9

[a]All results are questionable due to the presence of several fireball anomalies.

Table C30. ANFO surface burst overpressure data (ABTOAD, smoothed and fitted points), hemispherical charge (Ref. 34).

$P_0 \approx 935$ mbar

Observed data		Observed data scaled to 1.0 kt at P_0 = 1000 mbar	
Distance (ft)	ΔP (psi)	$R_s\left(\frac{ft}{kt^{1/3}}\right)$	ΔP_s (mbar)
A. 20-ton Surface Burst, first shot			
52.4	429	189	31700
85.0	179	306	13200
105.5	116	380	8560
208.6	22.8	751	1680
522.0	3.81	1880	281
825.8	1.83	2970	135
1090.0	1.18	3925	87.1
2463	0.262	8870	19.3
B. 20-ton Surface Burst, second shot			
52.5	386.6	189	28500
79.2	193.9	285	14300
105.3	110.7	379	8170
519.1	3.85	1870	284
817.9	2.02	2945	149
1093	1.32	3935	97.4
2491	0.33	8960	24.4
C. 100-ton Surface Burst			
52.4	945	110.4	69800
91.2	444	192	32800
515.7	9.14	1086	674
800.0	4.05	1685	299
1000.7	2.71	2108	200
1995	0.737	4200	54.4

Table C31. Sample points selected from IBM Problem M Curve[a] (Refs. 35, 36).

(Nuclear free-air burst only)

P_0 = 1000 mbar ambient pressure

T_0 = 300° K temperature

C_0 = 1139 ft/sec sonic velocity

R_m = scaled range, in $ft/kt^{1/3}$

ΔP_m = IBM curve overpressure, in mbar

$R_m\left(\frac{ft}{kt^{1/3}}\right)$	ΔP_m (mbar)
9000	25.5
5000	54
2000	176
1500	262
1000	491
800	731
600	1,310
500	1,930
400	3,070
300	6,210
200	17,800
120	71,000

[a] At distances greater than 9000 $ft/kt^{1/3}$, the IBM Problem M Curve decreases as $R_m^{-1.2}$.

References

1. L. J. Vortman, Project CABRIOLET—Close-in Airblast from the CABRIOLET Event, Sandia Laboratories, Albuquerque, N. Mex., Rept. PNE-951 (1968).
2. D. N. Montan, Source of Airblast from an Underground Explosion, Lawrence Livermore Laboratory, Rept. UCRL-71202 (1968).
3. L. J. Vortman, Project STAGECOACH, Sandia Laboratories, Albuquerque, N. Mex., Rept. SC-4596 (RR) (1962).
4. L. J. Vortman, Project BUCKBOARD, Sandia Laboratories, Albuquerque, N. Mex., Rept. SC-4675 (RR) (1962).
5. J. W. Reed, Project SCOOTER, Sandia Laboratories, Albuquerque, N. Mex., Rept. SC-4602 (RR) (1963).
6. L. J. Vortman, Airblast and Craters from Rows of Two to Twenty-five Buried HE Charges, Sandia Laboratories, Albuquerque, N. Mex., Rept. SC-RR-68-655 (1969).
7. S. M. Johnson, Explosive Excavation Technology, U.S. Army Engineer Explosive Excavation Research Office, Livermore, Rept. NCG-TR-21 (1971).
8. L. J. Vortman, Project PALANQUIN—Close-in Airblast from a Cratering Nuclear Detonation in Rhyolite, Sandia Laboratories, Albuquerque, N. Mex., Rept. PNE-902 (1966).
9. J. W. Reed, Project PALANQUIN—Long-range Airblast, Sandia Laboratories, Albuquerque, N. Mex., Rept. PNE-903F (1969).
10. D. C. Sachs and L. M. Swift, Operation TEAPOT—Project 1.7—Underground Explosion Effects, Stanford Research Institute, Menlo Park, Calif., Rept. WT-1106 (Del.) (1959).
11. L. J. Vortman, Airblast from Project TRINIDAD Detonations, Sandia Laboratories, Albuquerque, N. Mex., Rept. SC-RR-710056 (1971).
12. J. W. Reed, Climatology of Airblast Propagations from Nevada Test Site Nuclear Airblasts, Sandia Laboratories, Albuquerque, N. Mex., Rept. SC-RR-69-572 (1969).
13. J. W. Reed, Acoustic Wave Effects Project: Airblast Prediction Techniques, Sandia Laboratories, Albuquerque, N. Mex., Rept. SC-M-69-332 (1969).
14. J. W. Reed, "Airblast from Cratering Explosives," in Engineering with Nuclear Explosives, Third Plowshare Symposium, April 21, 22, and 23, 1964, (University of California, Davis, 1964), Rept. TID-7695.
15. L. J. Vortman, Project DUGOUT—Close-in Airblast from a Row Charge in Basalt, Sandia Laboratories, Albuquerque, N. Mex., Rept. PNE-608F (1965).
16. L. J. Vortman, Comparison of Airblast from Two Sizes of Row Charges, Sandia Laboratories, Albuquerque, N. Mex., Rept. SC-RR-66-415 (1966).
17. C. A. Rappleyea, Crater, Ejecta, and Airblast Studies from Five High-Explosive Charges in a Horizontal Array, Sandia Laboratories, Albuquerque, N. Mex., Rept. SC-RR-66-480 (1967).

18. J.P. Cress, J.E. Lattery, J.B. Andrews, and F.F. Warden, Project Pre-GONDOLA III, Phase I—Summary Report, U.S. Army Engineer Explosive Excavation Research Office, Livermore, Rept. PNE-1114 (1970).
19. L.J. Vortman, Project SEDAN—Close-in Airblast from a Nuclear Event in NTS Desert Alluvium, Sandia Laboratories, Albuquerque, N. Mex., Rept. PNE-211F (1964).
20. L.J. Vortman, Project SULKY—Close-in Airblast from a Relatively Deep Low-yield Nuclear Detonation in Basalt, Sandia Laboratories, Albuquerque, N. Mex., Rept. PNE-711F (1965).
21. L.J. Vortman, Project DANNY BOY—Project 1.1b—Close-in Airblast from a Nuclear Detonation in Basalt, Sandia Laboratories, Albuquerque, N. Mex., Rept. POR-1810 (1962).
22. L.J. Vortman, Close-in Airblast from Buried Row Charges, Sandia Laboratories, Albuquerque, N. Mex., Rept. SC-DC-68-24-67 (1968).
23. L.J. Vortman, Close-in Airblast from the BUGGY I Event, Sandia Laboratories, Albuquerque, N. Mex., Rept. PNE-320 (1970).
24. M.D. Nordyke and M.M. Williamson, The SEDAN Event, Lawrence Livermore Laboratory, Rept. PNE-242F (1965).
25. W.J. Howard and R.D. Jones, Operation JANGLE—Project 1.4—Free Air Pressure Measurements, Sandia Laboratories, Albuquerque, N. Mex., Rept. WT 306 (1952).
26. J.W. Reed and L.J. Vortman, Project Pre-SCHOONER II, Airblast Measurements, Sandia Laboratories, Albuquerque, N. Mex., Rept. PNE-512F (1967).
27. E.B. Doll and V. Salmon, Scaled HE tests—Operation JANGLE Project 1(9)-1 Final Report, Stanford Research Institute, Stanford, Calif., Rept. DA-49-129-eng-119, WT-377 (1952).
28. A.V. Shelton, M.D. Nordyke, and R.H. Goeckermann, The NEPTUNE Event, A Nuclear Explosive Cratering Experiment, Lawrence Livermore Laboratory, Rept. UCRL-5766 (1960).
29. J.H.B. Anderson, Canadian Airblast Measurements from Operation "DISTANT PLAIN" Events 3 and 5 Defence Research Establishment Suffield, Ralston, Alberta, Suffield Technical Note No. 214 (1968).
30. J.F. Pittman, Operation SAILOR HAT—Free-field Airblast Measurements, U.S. Naval Ordnance Laboratory, White Oak, Silver Spring, Md., Rept. POR-4056 (1966).
31. R.E. Reisler, R.J. Raley, D.P. LeFevre, Operation SAILOR HAT—Airblast Measurements Recorded by Standard and Developmental Instrumentation, Aberdeen Proving Ground, Md., Rept. POR-4050 (1967).
32. J.H.B. Anderson and A.M. Patterson, Canadian Airblast Measurements from Operation PRAIRIE FLAT, Defence Research Establishment Suffield, Ralston, Alberta, Suffield Memorandum No. 129/68 (1969).

33. G.A. Coulter and R.L. Peterson, Operation PRAIRIE FLAT—Blast Fill Time of a One-room Structure, Aberdeen Proving Ground, Md., Rept. POR-2102 (1969).
34. J.H.B. Anderson and A.M. Patterson, AN/FO Trials Carried Out at DRES, DRES, Ralston, Alberta, Suffield Technical Note No. 268 (1970).
35. C.D. Broyles, IBM Problem M Curves, Sandia Laboratories, Albuquerque, N. Mex., Rept. SC-TM-268-56-51 (1960).
36. B.C. Hughes, Nuclear Construction Engineering Technology, U.S. Army Engineer Explosive Excavation Research Office, Livermore, Rept. NCG TR-2 (1968).